# CHARACTERIZING DEGRADATION OF NANO-ENABLED MATERIALS AND ENGINEERED NANOMATERIAL RELEASE FOLLOWING NATURAL AND ARTIFICIAL WEATHERING

*By*
Ronald S. Lankone

A dissertation submitted to Johns Hopkins University in conformity with the requirements for the degree of Doctor of Philosophy

Department of Chemistry
The Johns Hopkins University
Baltimore, Maryland
July, 2018

**Abstract**

Engineered nanocomposite materials are increasingly utilized in consumer products. Nanocomposite degradation is inevitable and therefore must be studied as degradation is likely to cause nanomaterial release, resulting in nanomaterial exposure to humans and the environment. To address existing knowledge gaps, a two-tiered investigative strategy that characterized both nanocomposite degradation and resulting nanomaterial release following either accelerated or natural weathering is described herein. To that end, this body of work had two primary focuses: a) Determine how the initial nanoparticle content within a polymer nanocomposite impacted said nanocomposite's photodegradation following accelerated weathering; b) Identify the impact of local climate in driving nanomaterial release from a nano-enabled consumer product following natural weathering. Overall, data from these studies described the interplay of nanoparticle, composite matrix, and weathering conditions in regulating nanocomposite degradation and subsequent nanomaterial release. This information is crucial in the development of adequate and accurate risk assessments of products and materials composed of nanocomposites.

The first investigative strategy focused on the lab-based accelerated weathering and photodegradation of carbon nanotube polymer nanocomposites (CNT-PNCs) with a span of initial CNT concentrations (0 – 5% w/w). A point of emphasis in this study was the extensive characterization of the CNT-PNCs surface throughout the photodegradation process. Data obtained details the CNT-PNCs' changing surface chemical composition, molecular structure, and morphology as a function of photodegradation. In addition to characterizing CNT-PNCs as they photodegraded, single particle inductively coupled

plasma mass spectrometry was used to simultaneously quantify the concentration and characterize the form (individual CNTs vs. aggregates of CNTs embedded in polymer fragments) of released CNTs. Combined, characterization data of both the CNT-PNC and released material served as the foundation for developing mechanistic insight that described how increasing concentrations of CNTs within CNT-PNCs mitigated the rate and magnitude of polymer nanocomposite photodegradation.

The second investigative strategy required the installation and coordination of outdoor weathering stations in five distinct locations across the continental United States with the explicit goal of measuring both nanomaterial release and local weather conditions at each location. Lab prepared carbon nanotube and silver nanoparticle polymer nanocomposites (CNT-PNCs & Ag-PNCs) were weathered during the first phase of this study and commercially available pressure treated lumber (containing copper nanoparticles) was weathered during the second phase. Throughout the study, all samples were secured in custom designed outdoor sample holders and set out to weather and release naturally. Nanomaterial release in the accumulated rain runoff was collected monthly and quantified with inductively coupled plasma mass spectrometry or inductively couple plasma optical emission spectrometry. The total nanomaterial release measured was analyzed in tandem with site specific weather data to determine which climate factors are most important in regulating nanomaterial release in the natural environment. Additionally, information from these studies was used to inform more accurate life cycle assessment models. At the conclusion of phase one of this study, it was found that after a year of weathering, polymer nanocomposites released less than 5% of their originally embedded nanoparticulate mass, irrespective of climate conditions.

Following the conclusion of phase two, it was determined that the most important factor in regulating copper release from pressure treated lumber is rainfall. It was also found, however, that drier climates led to wood cracking, which in turn led to sustained and increased copper release into the second year of weathering.

Prof. D. Howard Fairbrother (Advisor)

Prof. H.J. Silverstone (Reader)

Prof. J.D. Tovar (Reader)

**Acknowledgements**

Any and all success I've found during my ten year trek through higher education (and life for that matter) can be attributed to the love and support of my parents and brother, Ron, Debbie, and Joe, as much as it can be attributed to me. Without their unwavering commitment to my success, I doubt I would have made it this far. So thank you, you guys – I know I haven't called as much as I should and I was probably a bit more ornery when talking about my struggles than I needed to be, but you always listened and never once let doubt in myself take hold.

I would also like to thank my advisor, Prof. Howard Fairbrother. I suspect I may have been a bit more of an unconventional graduate student than anticipated when I joined, but Howard was steadfast in his commitment to helping me grow as a chemist. I've learned quite a bit working for Howard but I think the most important thing he taught me is that in all research, we should always strive to attain true knowledge. I could not have wished for a better advisor and I hope to take with me not just the skills I've learned as his student, but also his passion for doing science uncompromisingly well. And so again, thank you Howard – both for your guidance towards success, but perhaps more importantly, your patience in helping me navigate through failure.

I would be remiss to not also thank Prof. James Ranville and his students Rob Reed, Angie Barber, Jingjing Wang, and Katie Challis. While Jim and his group may be 2/3 across the country in lovely Golden, CO, (home of Woody's Pizza Buffet) they've been excellent collaborators and wonderful people to work with – I consider myself fortunate to have worked with them and despite all the low quality/dropped Skype calls

we've had to endure, it really has been a pleasure to work on all the various projects we've had together.

In no particular order, I would also like to thank Prof. Leanne Gilbertson, Dr. Dave Durkin, and Dr. Dave Goodwin. They have been tremendous role-models in how to be a successful scientist. I'd also like to thank my labmate Mike Barclay for all the hard work he puts into keeping our instruments humming along and for always taking my call (even once on a gorgeous Saturday he was out sailing that happened to also be his birthday) when I needed help troubleshooting an issue. I'd also like to include a big thank you to Boris as well for going above and beyond the call of Building Manager. And thank you to all my labmates, past and present, for always being there to lend helpful advice and occasionally providing of an example of exactly what not to do.

Last and certainly least, I'd like to thank my friends who been there to both celebrate the good times and help survive the bad – Justin, Ben, Suz, Cody, Mark, Matt, Pbtrick [sic], Matt Henry, Guy, Justin, Kristen, Anna, Digs, Zach, Ken, Reid, Julie, Josh, Ashleigh, the Streifels, Oz, and the zone…I'm sure I'm forgetting plenty, but they know who's been good to them.

Table of Contents

**Figure List**

**Table List**

# **Chapter 1.** Introduction

## Nanoparticles – A brief definition, perspective on their growth

Nanoparticles are generally and least exhaustively defined as particles with at least one dimension that is less than 100nm in size,[1] roughly equivalent to one one-millionth the width of a human hair. Due to their small size, nanoparticles possess a high surface area to volume ratio which results in unique optical, electronic, and material properties.[2-3] Notable examples of such properties include the brilliant ruby color of suspended gold nanoparticles first observed by Michael Faraday in 1857,[4] quantum dots exhibiting a tunable size-dependent photoluminescence spectrum,[5-6] silver and copper nanoparticles' antimicrobial activity,[7-10] and multiwalled carbon nanotubes demonstrating a tensile strength comparable to or greater than steel.[11-13] To realize these and other useful properties, nanoparticles are commonly incorporated into a given matrix (e.g. polymer, textile, wood) in order to confer the desired property(ies) to the newly formed nanocomposite material.[14] Such nanocomposites are not just intellectual curiosities whose efficacy in a given application is restricted to the laboratory scale. Rather, a wide variety of nanocomposites are currently available on the market for consumer purchase and use – such as skis composed of carbon nanotubes (La Sportiva), clothing imbedded with silver nanoparticles (nanosilvɘr [sic]), television displays enhanced with quantum dots (Samsung), or wood that is pressure treated with copper nanoparticles (YellaWood). These and other commercially available nano-enabled products are simply nanocomposite materials which have made it to the consumer market due to the cost-effective nature of their production.[15-16]

The field of nanotechnology is one that is rich with interest and continuous growth. This growth was recently highlighted in a report released by *bbcResearch* which projected the global market for nanocomposites to grow from $2.0 billion in 2017 to $7.3 billion by 2022.[17] While this surge in the interest and development of various nanotechnologies has led to the production of many useful nano-enabled products, an equal effort to examine the risk of various nanotechnologies has lagged behind. That is not to say the proliferation of nanotechnology poses an unspoken existential threat to civilization, as once mused in the late nineteen eighties.[18] Rather, the overall usefulness of a given nanocomposite in a specific application will be improved by better understanding the potential risks it poses to its user – and more broadly humans and the environment –during its life-cycle. That being said, it is unlikely a nanocomposite will reach consumers if it poses an obvious risk to their health. However, following nanocomposite use and/or disposal, previously embedded and potentially hazardous nanoparticles may become exposed and/or liberated. Therefore, it is necessary to examine the processes through which a nanocomposite can be expected to wear, degrade, and eventually release its embedded nanomaterial. With a sound description of these degradation and release processes – as this body of work sought to contribute to and develop – a more thorough understanding of nanocomposites' risk to humans and the environment can be crafted.

**Assessing nanoparticle risk**

The risk of a nanomaterial is defined as the product of the nanomaterial's inherent hazard (i.e. toxicity) and the likelihood of human/environmental exposure.[19] One of the earliest studies to address the risk of nanoparticles was published in 1990 and focused on

the pulmonary toxicity of $Al_2O_3$ and $TiO_2$. The authors found that nano- $Al_2O_3$ and nano-$TiO_2$ penetrated more easily into rat lungs and were more toxic than their micron sized counterparts.[20-21] Since then, numerous other toxicity studies have been carried out on an assortment of other nanoparticles, such as carbon nanotubes,[22-25] silver nanoparticles,[26-29] graphene oxide,[30-32] and quantum dots.[33-35] The modes of nanoparticle toxicity on biological life are complex and our understanding of nanoparticle-cellular interactions is continually improving. However, to fully assess a nanoparticle's risk – as it is formally defined – its likelihood of exposure to humans and the environment must also be better understood. In particular, special attention must be given to quantifying the release of potentially hazardous nanomaterial from nano-enabled products, as it presents one of the more direct route towards nanomaterial-human/environmental exposure.[36-37]

Nanomaterial release is a process by which embedded nanoparticles are released from their surrounding matrix. Because nanoparticles themselves may transform (e.g. chemically, morphologically, surface functionalization) during the release process, remaining nano in size but no longer resembling the initially embedded nanoparticle,[19, 38] it is often more apropos to describe released material as nanomaterial, rather than strictly defining it to be the originally embedded nanoparticle. There are two general pathways through which release may occur – passively (e.g. desorption, dissolution, or and/or diffusion),[39] or as the result of degradation of the surrounding matrix (e.g. mechanical abrasion, photodegradation, thermal degradation, and/or hydrolysis).[40] While release is relatively straightforward to categorize, nanomaterial release from nanocomposites is far more challenging to characterize.

There exist two principal hurdles to accurately studying nanocomposite degradation and nanomaterial release: the first is designing an experiment that accurately reproduces realistic nanocomposite use and degradation conditions on an experimentally accessible timescale; the second is to accurately quantify and characterize the released nanomaterial. However, by overcoming both of these challenges, accurate nanocomposite degradation and nanomaterial release data may be obtained to be used in tandem with existing toxicology data in order to develop a more thorough assessment of a given nano-enabled product's risk.

**The lifecycle of a nanocomposite**

To better contextualize the significance and necessity of quantifying nanomaterial release from nanocomposites, it useful to also consider the life cycle of a given nanocomposite utilized in a nano-enabled product. The life cycle of a nano-enabled product can be broken down into four general stages: 1) Materials acquisition (i.e. mining the raw materials required to produce the required nanoparticles). 2) Materials processing (i.e. the physical manufacturing and production of nanoparticles and resulting nanocomposite). 3) Use. 4) End-of-Life (i.e. disposal following use).[41]

Presently, there is relatively little ambiguity regarding nanomaterial exposure to humans and the environment during the first two stages of a nanocomposite's lifecycle. During stage one, the nanoparticle is not yet formed, so while there are hazards inherently associated with activities such as mining, there is not a risk posed that is specific to the nanoparticle itself. Entering stage two, raw materials are transformed into nanoparticles and their exposure to humans and the environment becomes a possibility. But, due to the rather confined nature of nanoparticle manufacturing facilities and the obvious potential

for human exposure, workplace exposure scenarios have been well studied to the extent that human exposure to nanoparticles during nanoparticle/nanocomposite manufacturing is reasonably accounted for if not outright quantified.[42-43]

Nanomaterial release and exposure to humans and the environment during the Use and End-of-Life (EoL) phases, however, is far less well quantified. This is in large part due to the open-ended nature of the use phase: nano-enabled products will be subject to wear/degradation associated with their intended application but they may also endure unanticipated wear/degradation due to misuse and/or neglect. The general unpredictability of nanocomposite degradation leads to uncertainty surrounding the extent of nanomaterial release, which ultimately prevents accurate estimations of release without direct measurements of specific systems. The uncertainty regarding nanomaterial release during a nano-enabled product's use also compounds the difficulty of assessing nanomaterial release during its EoL. Without accurate measurements of nanomaterial release during use, the quantity of nanomaterial remaining in a nano-enabled product following its disposal can only be estimated. Such estimations are extremely simplified to the point that often times, one just assumes zero or one hundred percent release when crafting their risk assessment of a given nanocomposite.[44-46]

This perspective of a nano-enabled product's life-cycle reinforces the necessity of accurately quantifying nanomaterial release – release during the use phase is the remaining unknown preventing a complete description of nanomaterial exposure to humans and the environment during a nano-enabled product's life-cycle. But, what also becomes clear is that to fill in this knowledge gap, the most useful studies of

nanomaterials will be those which replicate scenarios that reasonably reflect a given nano-enabled product's use phase.

**Nano-enabled product use and degradation scenarios**

As stated above, nanomaterial release can occur passively[39] or as the result of active nanocomposite degradation.[40] Intuitively, it is obvious that the use of a given nanocomposite (or any consumer product for that matter) for some application will result in some degree of wear/degradation. Because of the inherent wear associated with use, many experimental approaches seek to reproduce wear/degradation conditions. One of the challenges in assessing nanocomposite degradation and subsequent nanomaterial release during the use phase, however, is designing an experimental approach that accurately represents use scenarios. There does not exist a single experimental method that encapsulates all use phase conditions and this fact is observed by the number of experimental methods and procedures applied to represent different use phase conditions (i.e. wear and degradation scenarios), primarily: lab-based abrasion testing,[47-49] thermal stability/flame retardant testing,[50-53] and simulated/accelerated weathering. [54-61]

While the specific procedures used to simulate use phase conditions vary greatly from study to study, as highlighted in a comprehensive review of nanocomposite degradation,[62] one overarching goal remains constant: expose the nanocomposite(s) of interest to well-controlled laboratory conditions that accurately represent conditions that would be found in the real-world, but are accelerated in such a manner that nanocomposite degradation and subsequent nanomaterial release will occur on an experimentally accessible timescale.

**Nanocomposite weathering**

Of all use phase degradation scenarios, weathering is arguably the most ubiquitous and frequently occurring – especially for nano-enabled products designed for outdoor use. [63-66] As such, it is the principal degradation pathway examined within the body of work detailed in the following chapters.

There are two experimental approaches one may take to assess the degradation of a nanocomposite following weathering. As mentioned above, one may employ a lab based approach in which specific weathering conditions are reproduced and magnified to accelerate the degradation process. Alternatively, a second approach is to simply place the nanocomposite(s) of interest outside to weather naturally. Each approach has its own set of advantages and disadvantages, with the main tradeoff in selecting one over the other being realism vs. precise variable control and completing experiments on a reasonable time scale.

In designing accelerated weathering studies, the principal goal is to recreate exposure conditions a nanocomposite could experience during natural weathering but in a very controlled and well defined manner. This goal is perhaps no more fully realized and accomplished than by the National Institute of Standards and Technology (NIST) integrated weathering device, the SPHERE (Simulated Photodegradation via High Energy Radiant Exposure). The SPHERE is a spherical weathering chamber approximately two meters in diameter in which samples may be exposed to precisely set ultraviolet irradiation, temperature, and relative humidity.[56] With the SPHERE system, the accelerated weathering of numerous nanocomposite materials have been studied, such as those composed of graphene oxide-polyurethane,[67] multiwalled carbon nanotubes-

epoxy,[68] and silica nanoparticle-epoxy.[69] In each of these studies, a regimented characterization scheme was utilized before and after exposure to track changes to the nanocomposite. Characterization included atomic force microscopy, scanning electron microscopy, X-ray photoelectron spectroscopy, and attenuated total internal reflectance FTIR. Findings from these studies provided some of the earliest evidence of two behaviors that are widely observed in studies of the weathering of nanocomposites: a) the addition of nanoparticles impacted the rate/extent of photodegradation of the surrounding matrix and b) as the surrounding matrix degrades, previously embedded nanoparticles will become exposed and in some instances, accumulate on the surface.[70]

For outdoor weathering studies, the exposure conditions are less controlled, with the only real control over exposure being the selection in location and time of day/year a nanocomposite is set outside to weather. Additionally, degradation as a result of natural weathering proceeds at a much slower rate than the rate achieved with laboratory based simulated weathering approaches. As a result, studies which utilize natural weathering tend not to observe accumulation of embedded nanoparticles on the surface of weathered nanocomposites simply because natural weathering did not result in a sufficient degree of matrix degradation over the experimental timespan to expose embedded nanoparticles.[71]

Despite being prolonged by the time it takes to observe extensive degradation, natural weathering studies are a powerful tool for examining the degradation of nanocomposites because they are completely realistic. Specifically, data collected from the natural weathering of a nanocomposite (e.g. spectroscopic and morphological) can be utilized to provide valuable benchmarks for establishing the rate at which lab-based simulated weathering studies accelerate degradation, and more importantly, confirming

the degradation pathways observed in lab-based testing are consistent with the degradation pathways that occur in the real world. Presently, however, few studies of nanocomposites have taken this comparative approach.[72] As the field of study of nanocomposite weathering matures, greater emphasis should be given to examining nanocomposites that are weathered naturally to ensure knowledge gained from lab-based degradation studies reflects real world processes, albeit at an accelerated rate.

**Characterizing nanomaterial release**

As stated above, nanomaterial release during the use phase is poorly defined – this lack of data prevents a complete description of a given nanocomposite's risk to humans and the environment, as quantifying released nanomaterial is necessary to establish potential nanomaterial exposure. Because the degradation of nanocomposites during the use phase will lead to nanomaterial release, the study of different degradation scenarios – especially weathering due to its ubiquitous nature – is requisite to characterizing nanomaterial release. Therefore, once sound natural or accelerated weathering experiments that degrade nanocomposites are developed, the resulting nanomaterial release that occurs as a result of degradation can then be characterized and used to inform the likelihood that a given nanocomposite will result in human/environmental nanomaterial exposure.

The characterization (i.e. quantification and/or identification of released nanomaterial form) of nanomaterial is easier stated than accomplished. This is almost entirely because of the small size and low concentration of released nanomaterial resulting in their being below the detection limit of many conventional analytical techniques.[73] As a result, inductively coupled plasma mass spectrometry (ICP-MS) or

ICP-optical emission spectrometry (ICP-OES) is generally utilized to quantify the concentration of released and dissolved metallic nanomaterials (e.g. silver or gold nanoparticles), because of their low detection limits (i.e. parts-per-million sensitivity).[74]

Single-particle ICP-MS (spICP-MS) has recently emerged a powerful technique to more definitively characterize released particulate nanomaterial – capable of both quantifying low concentrations of release nanomaterials as well as characterizing the form (i.e. aggregate vs. individual particle vs. dissolved ion) of released nanomaterial.[75] spICP-MS achieves this ability through its use of millisecond (<10ms) dwell times, with dwell time defined as the time per reading over which the mass spectrometer measures signal. By using such short dwell times, compared to the hundreds of milliseconds used in conventional ICP-MS, spICP-MS is able to distinguish dissolved analyte signal (i.e. background signal) from discrete pulses of ions produced by individual nanoparticles as they enter the plasma.[76] This pulse data is used to determine particle mass (as pulse intensity is directly proportional to the quantity of atoms present in a given particle) and particle mass can then be used in turn to calculate particle size, assuming the particle is spherical.[77] With this information, particle concentration and particle size distribution in a given sample can then be determined.

The facile operation of spICP-MS permits such characterization to be achieved with relatively little sample preparation and in a short amount of time, especially when compared to alternative methods of measuring particle size such as imaging a statistically relevant number of samples with electronic microscopy.[78] Less time intensive spectroscopic methods may also be applied to characterize nanomaterial quantities in solution, such as ultra-violet visible spectroscopy[79] or near infrared fluorescence

spectroscopy,[80-81] however both techniques are easily confounded if the sample of interest contains environmental sources of impurities (e.g. suspended solids or natural organic matter). As a result, ICP-MS and ICP-OES remain the two most reliable methods for determining nanomaterial concentration in environmental samples, with the development of spICP-MS presenting a tractable alternative for improved sample characterization, as described in the following chapters.

**Relevance and outline of the work described herein**

The body of research detailed in the following chapters developed a thorough description of weather-driven nanocomposite degradation processes and how those processes impacted and regulated nanomaterial release. This was achieved through the accelerated weathering of polymer nanocomposites (Chapter 2) and the natural weathering of polymer nanocomposites and pressure treated lumber (Chapters 3 and 4). Broadly, knowledge gained from these studies may in turn be used to inform accurate assessments of nanomaterial exposure during the nanocomposites' use phase, as depicted in Figure 1-1. Additionally, this knowledge underpins a complete description of a given nanocomposite's risk. So while this work did not seek to fully examine the risk of released nanomaterials (e.g. by also studying released nanomaterial toxicity), the relationship between weather-driven degradation and release (red arrow, Figure 1-2) described herein may be used tandem with such toxicity studies to fully understand the risk associated with a variety of nanocomposite materials.

Toward that end – describing the relationship between nanocomposite degradation and nanomaterial release – the principle work of this dissertation is organized into the three self-contained subsequent chapters. Chapter 2 focuses on the accelerated

weathering, via accelerated photodegradation, of carbon nanotube polymer nanocomposites (CNT-PNCs) composed of a span of initial carbon nanotube concentrations. In addition to meticulous characterization of the photolyzed CNT-PNCs following discrete periods of photodegradation, the released material was also captured for analysis with spICP-MS. With spICP-MS, not only was the concentration of released CNTs measured, but their form (individual CNT vs. CNT aggregated) was also explicitly monitored. By combing data from the CNT-PNCs' chemical, structural, and morphological characterizations with spICP-MS release data, a mechanistic description of the role of initial CNT concentration in regulating CNT-PNC degradation and release was developed. Chapters 3 & 4 both moved outside of the laboratory and made use of

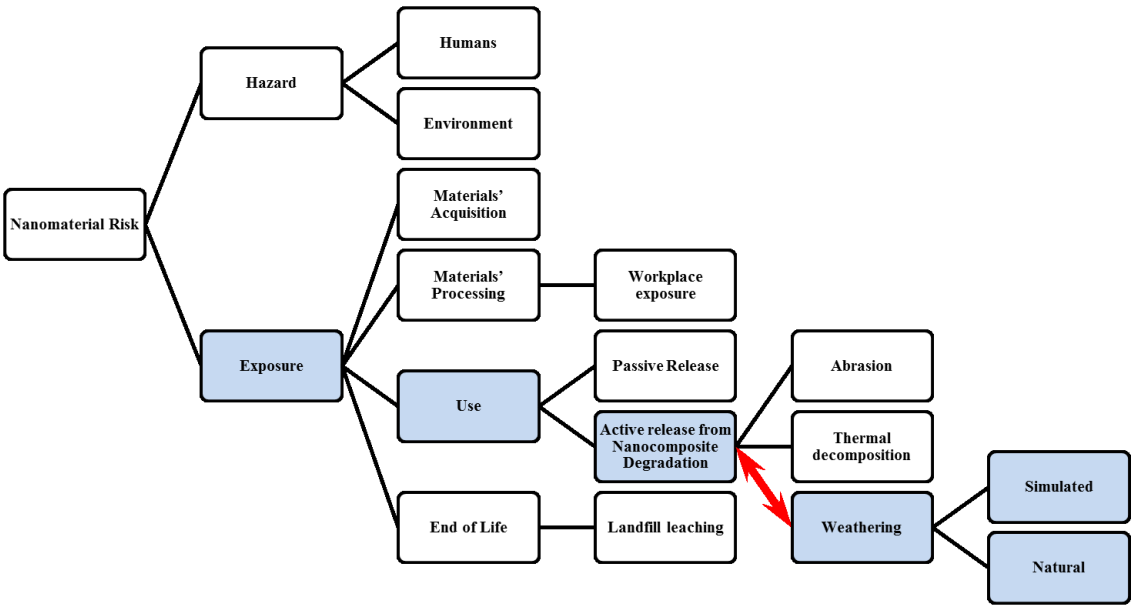


**Figure 1-1**: A simplified flowchart describing the relationship among various components necessary for a complete assessment of a nanocomposite's risk. Highlighted in blue are the compartments examined in this body of work in order to better understand the relationship among weathering, nanocomposite degradation, and nanomaterial release. Highlighted in red is the relationship between weathering and nanocomposite degradation – a process that was studied in detail for various nanocomposite materials.

natural weathering to study nanocomposite degradation and nanomaterial release. As detailed in Chapter 3, an original methodology was developed in order to permit the study of natural weathering of a wide variety of materials. Two crucial components of this methodology were the capture of rainwater runoff from samples as they weathered and the recording of site-specific local weather conditions. Combined, these data enabled the examination of which weather factors are most important in driving nanocomposite degradation and release. In Chapter 4, this methodology is implemented in order to study the natural weathering of pressure treated lumber (which contains copper nanoparticles) in five locations, with different climates, across the country. Release and weather data from this study were used to determine the extent to which local climate impacts the magnitude and rate of copper release from pressure treated lumber.

## References


1. Strambeanu, N.; Demetrovici, L.; Dragos, D.; Lungu, M., Nanoparticles: Definition, Classification and General Physical Properties. In *Nanoparticles' Promises and Risks: Characterization, Manipulation, and Potential Hazards to Humanity and the Environment*, Lungu, M.; Neculae, A.; Bunoiu, M.; Biris, C., Eds. Springer International Publishing: Cham, 2015; pp 3-8.
2. Wang Zhong, L., Characterization of Nanophase Materials. *Particle & Particle Systems Characterization* **2001,** *18* (3), 142-165.
3. Dan, G.; Guoxin, X.; Jianbin, L., Mechanical properties of nanoparticles: basics and applications. *Journal of Physics D: Applied Physics* **2014,** *47* (1), 013001.
4. Faraday, M., LIX. Experimental relations of gold (and other metals) to light.—The bakerian lecture. *The London, Edinburgh, and Dublin Philosophical Magazine and Journal of Science* **1857,** *14* (96), 512-539.
5. Fauchet, P. M., Light emission from Si quantum dots. *Materials Today* **2005,** *8* (1), 26-33.
6. Kim, T. Y.; Park, N. M.; Kim, K. H.; Sung, G. Y.; Ok, Y. W.; Seong, T. Y.; Choi, C. J., Quantum confinement effect of silicon nanocrystals in situ grown in silicon nitride films. *Applied Physics Letters* **2004,** *85* (22), 5355-5357.
7. Le Ouay, B.; Stellacci, F., Antibacterial activity of silver nanoparticles: A surface science insight. *Nano Today* **2015,** *10* (3), 339-354.
8. Cervantes, C.; Gutierrez-Corona, F., Copper resistance mechanisms in bacteria and fungi. *FEMS Microbiology Reviews* **1994,** *14* (2), 121-137.
9. Ren, G.; Hu, D.; Cheng, E. W. C.; Vargas-Reus, M. A.; Reip, P.; Allaker, R. P., Characterisation of copper oxide nanoparticles for antimicrobial applications. *International Journal of Antimicrobial Agents* **2009,** *33* (6), 587-590.
10. Hajipour, M. J.; Fromm, K. M.; Akbar Ashkarran, A.; Jimenez de Aberasturi, D.; Larramendi, I. R. D.; Rojo, T.; Serpooshan, V.; Parak, W. J.; Mahmoudi, M., Antibacterial properties of nanoparticles. *Trends in Biotechnology* **2012,** *30* (10), 499-511.
11. Yu, M.-F.; Lourie, O.; Dyer, M. J.; Moloni, K.; Kelly, T. F.; Ruoff, R. S., Strength and Breaking Mechanism of Multiwalled Carbon Nanotubes Under Tensile Load. *Science* **2000,** *287* (5453), 637.
12. Chang, C.-C.; Hsu, I. K.; Aykol, M.; Hung, W.-H.; Chen, C.-C.; Cronin, S. B., A New Lower Limit for the Ultimate Breaking Strain of Carbon Nanotubes. *ACS Nano* **2010,** *4* (9), 5095-5100.
13. Bernholc, J.; Brenner, D.; Buongiorno Nardelli, M.; Meunier, V.; Roland, C., Mechanical and Electrical Properties of Nanotubes. *Annual Review of Materials Research* **2002,** *32* (1), 347-375.
14. Schmidt, G.; Malwitz, M. M., Properties of polymer–nanoparticle composites. *Current Opinion in Colloid & Interface Science* **2003,** *8* (1), 103-108.
15. Tamayo, L.; Azócar, M.; Kogan, M.; Riveros, A.; Páez, M., Copper-polymer nanocomposites: An excellent and cost-effective biocide for use on antibacterial surfaces. *Materials Science and Engineering: C* **2016,** *69*, 1391-1409.
16. Roes, A. L.; Marsili, E.; Nieuwlaar, E.; Patel, M. K., Environmental and Cost Assessment of a Polypropylene Nanocomposite. *Journal of Polymers and the Environment* **2007,** *15* (3), 212-226.
17. McWilliams, A. *Nanocomposites, Nanoparticles, Nanoclays and Nanotubes: Global Markets to 2022*; bcc Research 2018.
18. Drexler, K. E., *Engines of Creation*. Anchor Books: 1986; p 312.
19. Hristozov, D.; Malsch, I., Hazards and Risks of Engineered Nanoparticles for the Environment and Human Health. *Sustainability* **2009,** *1* (4).
20. Ferin, J.; Oberdörster, G.; Penney, D. P.; Soderholm, S. C.; Gelein, R.; Piper, H. C., Increased pulmonary toxicity of ultrafine particles? I. Particle clearance, translocation, morphology. *Journal of Aerosol Science* **1990,** *21* (3), 381-384.
21. Oberdörster, G.; Ferin, J.; Finkelstein, J.; Wade, P.; Corson, N., "Increased pulmonary toxicity of ultrafine particles? II. Lung lavage studies.". *J Aerosol Science* **1990,** *21*.

22. Cimbaluk, G. V.; Ramsdorf, W. A.; Perussolo, M. C.; Santos, H. K. F.; Da Silva De Assis, H. C.; Schnitzler, M. C.; Schnitzler, D. C.; Carneiro, P. G.; Cestari, M. M., Evaluation of multiwalled carbon nanotubes toxicity in two fish species. *Ecotoxicology and Environmental Safety* **2018,** *150*, 215-223.
23. Lanone, S.; Andujar, P.; Kermanizadeh, A.; Boczkowski, J., Determinants of carbon nanotube toxicity. *Advanced Drug Delivery Reviews* **2013,** *65* (15), 2063-2069.
24. De Marchi, L.; Neto, V.; Pretti, C.; Figueira, E.; Chiellini, F.; Morelli, A.; Soares, A. M. V. M.; Freitas, R., Toxic effects of multi-walled carbon nanotubes on bivalves: Comparison between functionalized and nonfunctionalized nanoparticles. *Science of The Total Environment* **2018,** *622-623*, 1532-1542.
25. Bhattacharya, K.; Andón, F. T.; El-Sayed, R.; Fadeel, B., Mechanisms of carbon nanotube-induced toxicity: Focus on pulmonary inflammation. *Advanced Drug Delivery Reviews* **2013,** *65* (15), 2087-2097.
26. Abramenko, N. B.; Demidova, T. B.; Abkhalimov, E. V.; Ershov, B. G.; Krysanov, E. Y.; Kustov, L. M., Ecotoxicity of different-shaped silver nanoparticles: Case of zebrafish embryos. *Journal of Hazardous Materials* **2018,** *347*, 89-94.
27. Choi, Y.; Kim, H.-A.; Kim, K.-W.; Lee, B.-T., Comparative toxicity of silver nanoparticles and silver ions to Escherichia coli. *Journal of Environmental Sciences* **2018,** *66*, 50-60.
28. Šiller, L.; Lemloh, M.-L.; Piticharoenphun, S.; Mendis, B. G.; Horrocks, B. R.; Brümmer, F.; Medaković, D., Silver nanoparticle toxicity in sea urchin Paracentrotus lividus. *Environmental Pollution* **2013,** *178*, 498-502.
29. Moreno-Garrido, I.; Pérez, S.; Blasco, J., Toxicity of silver and gold nanoparticles on marine microalgae. *Marine Environmental Research* **2015,** *111*, 60-73.
30. An, W.; Zhang, Y.; Zhang, X.; Li, K.; Kang, Y.; Akhtar, S.; Sha, X.; Gao, L., Ocular toxicity of reduced graphene oxide or graphene oxide exposure in mouse eyes. *Experimental Eye Research* **2018,** *174*, 59-69.
31. Lv, X.; Yang, Y.; Tao, Y.; Jiang, Y.; Chen, B.; Zhu, X.; Cai, Z.; Li, B., A mechanism study on toxicity of graphene oxide to Daphnia magna: Direct link between bioaccumulation and oxidative stress. *Environmental Pollution* **2018,** *234*, 953-959.
32. De Marchi, L.; Pretti, C.; Gabriel, B.; Marques, P. A. A. P.; Freitas, R.; Neto, V., An overview of graphene materials: Properties, applications and toxicity on aquatic environments. *Science of The Total Environment* **2018,** *631-632*, 1440-1456.
33. Li, J.; Zhang, Y.; Xiao, Q.; Tian, F.; Liu, X.; Li, R.; Zhao, G.; Jiang, F.; Liu, Y., Mitochondria as target of Quantum dots toxicity. *Journal of Hazardous Materials* **2011,** *194*, 440-444.
34. Hu, L.; Zeng, G.; Chen, G.; Huang, Z.; Wan, J.; Chen, A.; Yu, Z.; Yang, J.; He, K.; Qin, L., Bioaccumulation and toxicity of CdSe/ZnS quantum dots in Phanerochaete chrysosporium. *Colloids and Surfaces B: Biointerfaces* **2017,** *159*, 303-311.
35. Sharma, V. K.; McDonald, T. J.; Sohn, M.; Anquandah, G. A. K.; Pettine, M.; Zboril, R., Assessment of toxicity of selenium and cadmium selenium quantum dots: A review. *Chemosphere* **2017,** *188*, 403-413.
36. Nanomaterials https://echa.europa.eu/regulations/nanomaterials (accessed August 22).
37. Reviewing New Chemicals under the Toxic Substances Control Act (TSCA). https://www.epa.gov/reviewing-new-chemicals-under-toxic-substances-control-act-tsca/control-nanoscale-materials-under#regs.
38. Reidy, B.; Haase, A.; Luch, A.; Dawson, K. A.; Lynch, I., Mechanisms of Silver Nanoparticle Release, Transformation and Toxicity: A Critical Review of Current Knowledge and Recommendations for Future Studies and Applications. *Materials* **2013,** *6* (6), 2295-2350.
39. Duncan, T. V.; Pillai, K., Release of Engineered Nanomaterials from Polymer Nanocomposites: Diffusion, Dissolution, and Desorption. *ACS Applied Materials & Interfaces* **2015,** *7* (1), 2-19.
40. Duncan, T. V., Release of Engineered Nanomaterials from Polymer Nanocomposites: the Effect of Matrix Degradation. *ACS Applied Materials & Interfaces* **2015,** *7* (1), 20-39.

41. Gilbertson, L. M.; Wender, B. A.; Zimmerman, J. B.; Eckelman, M. J., Coordinating modeling and experimental research of engineered nanomaterials to improve life cycle assessment studies. *Environmental Science: Nano* **2015,** *2* (6), 669-682.
42. van Broekhuizen, P.; van Broekhuizen, F.; Cornelissen, R.; Reijnders, L., Workplace exposure to nanoparticles and the application of provisional nanoreference values in times of uncertain risks. *Journal of Nanoparticle Research* **2012,** *14* (4), 770.
43. Kuhlbusch, T. A. J.; Asbach, C.; Fissan, H.; Göhler, D.; Stintz, M., Nanoparticle exposure at nanotechnology workplaces: A review. *Particle and Fibre Toxicology* **2011,** *8* (1), 1-18.
44. Walser, T.; Demou, E.; Lang, D. J.; Hellweg, S., Prospective Environmental Life Cycle Assessment of Nanosilver T-Shirts. *Environmental Science & Technology* **2011,** *45* (10), 4570-4578.
45. Hicks, A. L.; Gilbertson, L. M.; Yamani, J. S.; Theis, T. L.; Zimmerman, J. B., Life Cycle Payback Estimates of Nanosilver Enabled Textiles under Different Silver Loading, Release, And Laundering Scenarios Informed by Literature Review. *Environmental Science & Technology* **2015,** *49* (13), 7529-7542.
46. Eckelman, M. J.; Mauter, M. S.; Isaacs, J. A.; Elimelech, M., New Perspectives on Nanomaterial Aquatic Ecotoxicity: Production Impacts Exceed Direct Exposure Impacts for Carbon Nanotoubes. *Environmental Science & Technology* **2012,** *46* (5), 2902-2910.
47. Masood, M. T.; Heredia-Guerrero, J. A.; Ceseracciu, L.; Palazon, F.; Athanassiou, A.; Bayer, I. S., Superhydrophobic high impact polystyrene (HIPS) nanocomposites with wear abrasion resistance. *Chemical Engineering Journal* **2017,** *322*, 10-21.
48. Kanokwijitsilp, T.; Traiperm, P.; Osotchan, T.; Srikhirin, T., Development of abrasion resistance SiO2 nanocomposite coating for teak wood. *Progress in Organic Coatings* **2016,** *93*, 118-126.
49. Naderizadeh, S.; Athanassiou, A.; Bayer, I. S., Interfacing superhydrophobic silica nanoparticle films with graphene and thermoplastic polyurethane for wear/abrasion resistance. *Journal of Colloid and Interface Science* **2018,** *519*, 285-295.
50. Vahabi, H.; Saeb, M. R.; Formela, K.; Cuesta, J.-M. L., Flame retardant epoxy/halloysite nanotubes nanocomposite coatings: Exploring low-concentration threshold for flammability compared to expandable graphite as superior fire retardant. *Progress in Organic Coatings* **2018,** *119*, 8-14.
51. Gu, L.; Qiu, J.; Yao, Y.; Sakai, E.; Yang, L., Functionalized MWCNTs modified flame retardant PLA nanocomposites and cold rolling process for improving mechanical properties. *Composites Science and Technology* **2018,** *161*, 39-49.
52. Zhang, Z.; Han, Y.; Li, T.; Wang, T.; Gao, X.; Liang, Q.; Chen, L., Polyaniline/montmorillonite nanocomposites as an effective flame retardant and smoke suppressant for polystyrene. *Synthetic Metals* **2016,** *221*, 28-38.
53. Khobragade, P. S.; Hansora, D. P.; Naik, J. B.; Chatterjee, A., Flame retarding performance of elastomeric nanocomposites: A review. *Polymer Degradation and Stability* **2016,** *130*, 194-244.
54. Hirth, S.; Cena, L.; Cox, G.; Tomović, Ž.; Peters, T.; Wohlleben, W., Scenarios and methods that induce protruding or released CNTs after degradation of nanocomposite materials. *Journal of Nanoparticle Research* **2013,** *15* (4), 1-15.
55. Vilar, G.; Fernández-Rosas, E.; Puntes, V.; Jamier, V.; Aubouy, L.; Vázquez-Campos, S., Monitoring migration and transformation of nanomaterials in polymeric composites during accelerated aging. *Journal of Physics: Conference Series* **2013,** *429* (1), 012044.
56. Chin, J. E., Ned ; Garver, J.; Dickens, B.; Finn, T.; Martin, J. W., Accelerated UV weathering device based on integrating sphere technology. *Review of scientific instruments* **2004,** *75* (11), 8.
57. Petersen, E. J.; Lam, T.; Gorham, J. M.; Scott, K. C.; Long, C. J.; Stanley, D.; Sharma, R.; Alexander Liddle, J.; Pellegrin, B.; Nguyen, T., Methods to assess the impact of UV irradiation on the surface chemistry and structure of multiwall carbon nanotube epoxy nanocomposites. *Carbon* **2014,** *69*, 194-205.
58. Nguyen, T. V.; Nguyen Tri, P.; Nguyen, T. D.; El Aidani, R.; Trinh, V. T.; Decker, C., Accelerated degradation of water borne acrylic nanocomposites used in outdoor protective coatings. *Polymer Degradation and Stability* **2016,** *128*, 65-76.
59. Kaynak, C.; Sarı, B., Accelerated weathering performance of polylactide and its montmorillonite nanocomposite. *Applied Clay Science* **2016,** *121–122*, 86-94.

60. Froggett, S. J.; Clancy, S. F.; Boverhof, D. R.; Canady, R. A., A review and perspective of existing research on the release of nanomaterials from solid nanocomposites. *Particle and Fibre Toxicology* **2014,** *11* (1), 1-28.
61. Al-Kattan, A.; Wichser, A.; Vonbank, R.; Brunner, S.; Ulrich, A.; Zuin, S.; Nowack, B., Release of TiO2 from paints containing pigment-TiO2 or nano-TiO2 by weathering. *Environmental Science: Processes & Impacts* **2013,** *15* (12), 2186-2193.
62. Pandey, J. K.; Raghunatha Reddy, K.; Pratheep Kumar, A.; Singh, R. P., An overview on the degradability of polymer nanocomposites. *Polymer Degradation and Stability* **2005,** *88* (2), 234-250.
63. Lee, J.; Mahendra, S.; Alvarez, P. J. J., Nanomaterials in the Construction Industry: A Review of Their Applications and Environmental Health and Safety Considerations. *ACS Nano* **2010,** *4* (7), 3580-3590.
64. Vapor Nano. http://www.sportiva.com/products/ski/skis/vapor-nano (accessed 2016-03-14).
65. Zyvex technologies. http://www.zyvextech.com/sports/ (accessed 2016-03-16).
66. Khanna, V.; Bakshi, B. R., Carbon Nanofiber Polymer Composites: Evaluation of Life Cycle Energy Use. *Environmental Science & Technology* **2009,** *43* (6), 2078-2084.
67. Bernard, C.; Nguyen, T.; Pellegrin, B.; Holbrook, R. D.; Zhao, M.; Chin, J., Fate of graphene in polymer nanocomposite exposed to UV radiation. *Journal of Physics: Conference Series* **2011,** *304* (1), 012063.
68. Nguyen, T.; Pellegrin, B.; Bernard, C.; Gu, X.; Gorham, J. M.; Stutzman, P.; Stanley, D.; Shapiro, A.; Byrd, E.; Hettenhouser, R.; Chin, J., Fate of nanoparticles during life cycle of polymer nanocomposites. *J Phys: Conf Ser* **2011,** *304*.
69. Nguyen, T.; Pellegrin, B.; Bernard, C.; Rabb, S.; Stuztman, P.; Gorham, J.; Gu, X.; Yu, L.; Chin, J., Characterization of surface accumulation and release of nanosilica during irradiation of polymer nanocomposites by ultraviolet light. *J Nanoscience and Nanotechnology* **2012,** *12*.
70. Nguyen, T.; Pellegrin, B.; Mermet, L.; Shapiro, A.; Gu, X.; Chin, J., Network aggregation of CNTs at the surface of epoxy/MWCNT composite exposed to UV radiation. *Nanotechnology* **2009,** *1*, 90-93.
71. Rabea, A. M.; Mohseni, M.; Mirabedini, S. M.; Tabatabaei, M. H., Surface analysis and anti-graffiti behavior of a weathered polyurethane-based coating embedded with hydrophobic nano silica. *Applied Surface Science* **2012,** *258* (10), 4391-4396.
72. Miklečić, J.; Blagojević, S. L.; Petrič, M.; Jirouš-Rajković, V., Influence of TiO2 and ZnO nanoparticles on properties of waterborne polyacrylate coating exposed to outdoor conditions. *Progress in Organic Coatings* **2015,** *89*, 67-74.
73. Petersen, E. J.; Flores-Cervantes, D. X.; Bucheli, T. D.; Elliott, L. C. C.; Fagan, J. A.; Gogos, A.; Hanna, S.; Kägi, R.; Mansfield, E.; Bustos, A. R. M.; Plata, D. L.; Reipa, V.; Westerhoff, P.; Winchester, M. R., Quantification of Carbon Nanotubes in Environmental Matrices: Current Capabilities, Case Studies, and Future Prospects. *Environmental Science & Technology* **2016,** *50* (9), 4587-4605.
74. Lankone, R.; Challis, K.; Bi, Y.; Hanigan, D.; Reed, R. B.; Zaikova, T.; Hutchison, J.; Westerhoff, P.; Ranville, J. F.; Fairbrother, H.; Gilbertson, L., Methodology for Quantifying Engineered Nanomaterial Release from Diverse Product Matrices Under Outdoor Weathering Conditions and Implications for Life Cycle Assessment. *Environmental Science: Nano* **2017**.
75. Reed, R. B.; Goodwin, D. G.; Marsh, K. L.; Capracotta, S. S.; Higgins, C. P.; Fairbrother, D. H.; Ranville, J. F., Detection of single walled carbon nanotubes by monitoring embedded metals. *Environmental science. Processes & impacts* **2013,** *15* (1), 204-13.
76. Wang, J.; Lankone, R. S.; Reed, R. B.; Fairbrother, D. H.; Ranville, J. F., Analysis of single-walled carbon nanotubes using spICP-MS with microsecond dwell time. *NanoImpact* **2016,** *1*, 65-72.
77. Pace, H. E.; Rogers, N. J.; Jarolimek, C.; Coleman, V. A.; Higgins, C. P.; Ranville, J. F., Correction to Determining Transport Efficiency for the Purpose of Counting and Sizing Nanoparticles via Single Particle Inductively Coupled Plasma Mass Spectrometry. *Analytical Chemistry* **2012,** *84* (10), 4633-4633.
78. Vilar, G.; Fernández-Rosas, E.; Puntes, V.; Jamier, V.; Aubouy, L.; Vázquez-Campos, S., Monitoring migration and transformation of nanomaterials in polymeric composites during accelerated aging. *J Phys: Conf Ser* **2013,** *429*, 012044.

79. Attal, S.; Thiruvengadathan, R.; Regev, O., Determination of the Concentration of Single-Walled Carbon Nanotubes in Aqueous Dispersions Using UV−Visible Absorption Spectroscopy. *Analytical Chemistry* **2006,** *78* (23), 8098-8104.
80. Schierz, A.; Parks, A. N.; Washburn, K. M.; Chandler, G. T.; Ferguson, P. L., Characterization and Quantitative Analysis of Single-Walled Carbon Nanotubes in the Aquatic Environment Using Near-Infrared Fluorescence Spectroscopy. *Environmental Science & Technology* **2012,** *46* (22), 12262-12271.
81. Schierz, A.; Espinasse, B.; Wiesner, M. R.; Bisesi, J. H.; Sabo-Attwood, T.; Ferguson, P. L., Fate of single walled carbon nanotubes in wetland ecosystems. *Environmental Science: Nano* **2014,** *1* (6), 574-583.

**Chapter 2.** Photodegradation of polymer-CNT nanocomposites: Effect of CNT loading and CNT release characteristics

Reproduced from

Lankone, R. S.; Wang, J.; Ranville, J. F.; Fairbrother, D. H., Photodegradation of polymer-CNT nanocomposites: effect of CNT loading and CNT release characteristics. Environmental Science: Nano 2017, 4 (4), 967-982.

**Abstract**

Information is currently lacking on the effect that carbon nanotubes (CNTs) have on the mechanism and extent of polymer photodegradation as well as the quantity, kinetics, and form of CNTs released. To address this, the photodegradation of a photolabile CNT-polymer nanocomposite (CNT-PNC) composed of single walled CNTs and polycaprolactone was followed in detail. Analysis of released CNT-containing fragments was accomplished with single particle inductively coupled plasma mass spectrometry (sp-ICP-MS). The mechanism of polymer photodegradation remained unchanged upon CNT inclusion, although polymer mass loss decreases systematically as CNT loading increases. This inhibitory effect is due to the light absorption and scattering properties of CNTs, which reduces the depth of photolysis and consequently the extent of CNT-PNC mass loss. Preferential CNT retention in the polymer during photodegradation results in CNT release at lower quantities than predicted based on their mass loading. The form of the released CNTs depends on CNT loading and evolves as the CNT-PNC photodegradation process proceeds. For CNT-PNCs with higher CNT loadings, multiple CNTs are initially released embedded within polymer fragments; as CNT-PNC degradation slows, released fragments contain predominantly isolated CNTs. For sufficiently long irradiation times, a dense CNT-mat forms at the surface, stabilizing the CNT-PNC towards further polymer or CNT loss. Extrapolating these findings to other CNT-PNC systems suggests that the quantity and form of released CNTs, as well as the extent of CNT-PNC photodegradation, will be influenced by the CNT loading and will evolve over the course of the CNT/PNC photodegradation process.

## Introduction

Polymer nanocomposites (PNCs), particularly those containing carbon nanotubes (CNT-PNCs), are being utilized in a growing variety of commercial products such as sporting equipment, shoe soles, bicycles, and wind turbine blades[1] and applications in highly-engineered materials such as the wingtip fairings of Lockheed Martin's F-35 Joint Strike Fighter.[2] With the increased use of CNT-PNCs, the potential for CNT release into the environment and exposure to different ecosystems (aquatic, terrestrial, human) will inevitably increase as well. Release is an important factor to consider because it is the precursor to exposure, which along with hazard determines the risk posed by a material.[3] Extensive research has already been conducted to explore the toxicity (hazard) of CNTs.[4-7] In contrast, far less information is available on nanoparticle (NP) release from consumer products, especially the factors that control release from products. For the case of CNT-PNCs, this includes the influence that CNTs have on the polymer photodegredation and release mechanism(s), the kinetics of CNTs release, the quantity and overall fraction of incorporated CNTs released, and the form of the released CNTs (dispersed vs. embedded in polymer fragments). Without such information, well-informed risk assessments of PNC products are difficult to develop.

The release of CNTs from PNC-CNTs as a result of photochemical weathering can occur during PNC-CNT use or end of life phases and as such represents an important release scenario.[8]Previous studies have shown that nanomaterial release from polymer nanocomposites occurs as a consequence of the photodegradation of the surrounding polymer matrix.[9-10] As highlighted in a review by Kingston *et al.,* PNCs composed of a variety of polymer matrices, such as epoxy, polyamide, polyurethane, and polycarbonate,

are found to be susceptible to nanomaterial release through polymer photodegradation .[11] However, polymer photodegredation is slow and one of the difficulties in studying polymer photodegradation in the natural environment is that it may take months or more typically years for measureable degradation to occur. Consequently, CNT-PNC weathering is often examined using conditions that accelerate the degradation process, although specific methods vary. Such accelerated degradation approaches include the NIST SPHERE (Simulated Photodegradation via High Energy Radiant Exposure) [12-13] and standardized accelerated weathering tests, such as ISO 3892-2:2006[14] or ISO 4892/06. [15] Accelerated degradation is not an approach that is restricted to studying the weathering of CNT-PNCs weathering. For example, Pillai *et al.* submerged quantum dot (QD)-low density polyethylene PNCs in either water or 3% acetic acid, and heated the system to 75 $^{0}$C for up to 15 days to accelerate release in a manner similar to the protocol developed by the FDA to study the migration of components from food contact materials. [16] By using conventional ICP-MS to detect dissolved elements (Cd, Se, Zn, and S) indicative of released QDs, they were able to determine release mechanisms and identify that release in this system is driven largely by particle dissolution and impacted by QD size.[16]

The extent of CNT release during weathering of CNT/PNCs has been reported to vary considerably depending on the details of the release scenario, as defined by both the CNT-PNC and the environmental conditions to which it is exposed. Thus, Wohlleben *et al.* did not find any evidence for the spontaneous release of CNTs following the weathering of CNT-polyurethane nanocomposites.[17] However, using radiolabelled CNTs ($^{14}$C-CNT), Rhiem *et al.* estimated that following a UV dose equivalent to three years of

natural exposure in Florida, 64 mg CNT/$m^2$ released from a polycarbonate polymer nanocomposites and that photodegraded polymers were more likely to release CNTs at the end-of-life disposal scenarios.[18] In a review of over a dozen studies on the weathering of CNT-PNCs[19], Schlagenhauf *et al*. found that the quantification of released CNTs was left largely unaddressed. However, four of these studies did attempt to monitor CNT release through characterization of released material with TEM imaging[20] or analytical ultracentrifugation[14, 17, 21] and in two studies, it was concluded that CNT release was unlikely to have occurred based on SEM imaging of the surrounding sample holder[10] or AFM scratch lithography of the weathered PNC surface.[13] Wohlleben *et al.* provided a more quantitative assessment in a review of 27 different nanocomposite materials weathered under the ISO 4892 protocol and found their release rates (mg/MJ of UV) to span five orders of magnitude.[22] Regarding CNT-PNCs specifically, release rates spanned roughly 0.05mg/MJ (CNT – cross-linked polyurethane) to 8mg/MJ (CNT – epoxy).

A constant challenge that pervades CNT release studies is that CNTs are released from CNT-PNCs at concentrations at or below the CNT detection limit of most analytical techniques. As a result, CNT release is often expressed in qualitative terms without quantification of released CNTs or the form of the released CNTs (embedded within polymer fragments or purely as CNTs) identified. As highlighted in a recent review [23], while many techniques currently exist that are capable of detecting CNTs, each technique has its own unique set of limitations. For example, although UV-Vis spectroscopy is an inexpensive and readily available analytical method to measure the concentration of suspended CNTs[24], it lacks both the sensitivity needed to detect the low concentrations of CNTs expected to be released from CNT-PNCs and the selectivity to distinguish CNTs

from other naturally occurring environmental particles. In contrast, although transmission electron microscopy has the requisite sensitivity to identify released engineered nanomaterials and can directly image and confirm the presence of CNTs[25] as well as resolve their form (individual tubes vs. embedded in polymer fragments), it is costly, time consuming, and not an intrinsically quantitative technique. Near infrared fluorescence is both quantitative and can detect CNTs in environmental matrices, but it requires CNTs that are both well dispersed and of a specific chirality (semi-conducting). [26-27] Scintillation counting of $^{14}$C-labelled carbon nanotubes may also be used to quantify CNT release following weathering[18], however $^{14}$C-labelled-CNTs are inherently expensive, difficult to synthesize and require specialized apparatus to be detected . One approach that combines sensitivity with selectivity for CNT detection involves the use of ICP-MS to measure metal nanoparticles, intimately bound to the CNTs, as a means to quantify CNT release. For example, following the abrasion of 1% (w/w) CNT-epoxy samples, Schlagenhauf *et al.* collected submicron sized fragments ($PM_1$), submerged them in dilute nitric acid, and measured the dissolved metal ion concentration with ICP-MS as a route to quantify protruding and free standing CNTs, under the assumption that only exposed CNTs would lead to their bound metal nanoparticles being available for dissolution. From their findings, they estimate that for every one gram of material abraded, $PM_1$ particles produced will have 40 μg of MWCNTs protruding from epoxy fragments and just 0.4 μg of MWCNTs will be free standing.[28]

The present study focuses on developing a detailed, mechanistic understanding of CNT-PNC photodegradation. A key experimental component of the present study was the use of single particle inductively coupled plasma mass spectrometry (sp-ICP-MS) to

analyze released CNTs through the use of metal nanoparticles, residual from CNT synthesis, as proxies for CNT detection.[29-30] This novel approach to analysis of released CNT distinguishes itself from the characterization techniques discussed above due to the fact that it can simultaneously quantify the concentration and characterize the form of released CNTs from data collected during a single analysis of a given sample. In order to develop a more fundamental mechanistic understanding of how CNTs influence the photodegradation of CNT-PNCs and CNT release characteristics, CNT-PNCs composed of SWCNTs and poly-ε-caprolactone (PCL) with UVC light were selected to photodegrade; 254 nm irradiation was used to accelerate the rate of photodegradation because it is close to the absorption maximum in the ester's n to π* band (Figure 2-1). SWCNTs were selected, as opposed to more commercially relevant MWCNTs, due to the presence of residual yttrium nanoparticle catalysts remaining intimately bound to the SWCNTs. These Y nanoparticles act as proxies for the SWCNTs and allow for their detection and quantification with sp-ICP-MS.[30] Additionally, because SWCNTs and MWCNTs produced from a variety of different methods all share similar extinction coefficients[31], the light attenuating behavior of the SWCNTs utilized in this study will likely be similar to other CNT-PNCs. PCL was chosen because it is both photolabile and because CNT-PNCs can readily be prepared with well-defined properties via solution blending. PCL also possesses characteristic spectral features in both infrared (IR) and X-ray photoelectron (XP) spectroscopies that allow for the extent of its degradation to be accurately monitored. A particular point of emphasis in this study was to elucidate the role that CNT loading plays in regulating the extent of CNT release and polymer degradation during weathering. Indeed, although CNT-PNCs contain a range of different

CNT loadings (typically in the range of 0.1 - 5% wt), there is a surprising lack of information on the role that CNT loading plays in determining the kinetics of CNT-PNC photodegradation as well as CNT release. To address this issue, photodegradation on CNT-PNCs prepared with a range of CNT loadings (0 - 5 wt %) was studied. By monitoring changes to the polymer on both the macroscopic level (mass loss) and molecular level (IR and XPS), and acquiring information on released fragments during CNT-PNC photodegradation, it was possible to compare the extent of polymer degradation to the magnitude and rate of CNT release. Collectively, this information on released material and the remaining photolyzed nanocomposite enabled the identification of the mechanism by which CNTs influence the rate and extent of polymer photodegradation, as well the dependence of CNT release characteristics on initial CNT loading and irradiation time.

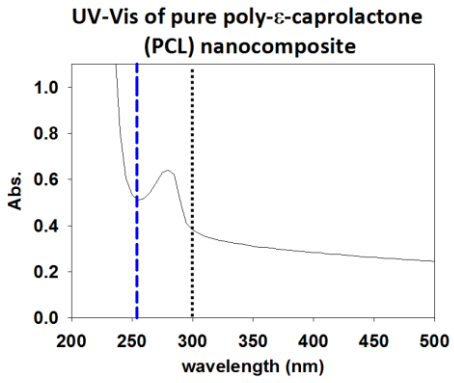


**Figure 2-1**: Low pressure mercury lamps used in this study have an intense emission at 254nm (blue dashed line). The ester functionality of PCL is photoexcited with light below 300nm (black dashed line) and photodegrades by means of a Norish type II reaction.

## Experimental Methods

### Chemicals

Chloroform and tetrahydrofuran (Fisher Scientific) were used without further purification or drying. HPLC grade water was purchased from VWR International. Ethyl cellulose (EC), poly-ε-caprolactone (PCL) and sodium deoxycholate (SDC) was purchased from Sigma Aldrich; for PCL, the manufacturer reports the number-average molecular weight (Mn 45,000). Single-walled carbon nanotubes (SWCNTs) were purchased from Carbon Solutions, Inc (Product number: AP-SWNT). The AP-SWNT sample is described by the manufacturer to be "as prepared" and not purified. They were used as received and characterized with TEM imaging and EDX spectra (Figure 2-2) and Raman spectroscopy. Raman spectra (Figure 2-3) of the SWCNTs is dominated by the G band, indicating a high level of SWCNT purity and a relative lack of damage to the sidewalls. Raman spectra also contain two well defined radial breathing modes at 155$cm^{-1}$ and 176$cm^{-1}$ (with a third mode potentially at 188$cm^{-1}$), corresponding to a SWNCT tube diameter of 1.4nm – 1.6nm. [32]

### Nanocomposite Preparation

All CNT-PNCs were prepared via solution blending.[33] This technique allows for both a high degree of SWCNT dispersion and batch to batch consistency between composites. Characterization using SEM found no signs of SWCNT clumping or aggregation at the surface (Figure 2-7). In addition to CNT-free PCL, nanocomposite samples were prepared at three SWCNT mass loadings (% w/w): 0.25% SWCNT, 1.5% SWCNT, and 5.0% SWCNT. Nanocomposites were prepared by first weighing out the

required mass of SWCNT powder and adding it to a 50 mL Erlenmeyer flask. Next, 21 mL of THF, 21 mL of chloroform, and 31.5 mg of EC were added. EC is required to create well dispersed SWCNTs in the nanocomposites; 31.5 mg was sufficient to disperse all SWCNT masses used in this study and prevented any visible SWCNT aggregation in the suspensions.

To create a uniform SWCNT dispersion the flask containing the mixture of SWCNT, EC, chloroform and THF was sealed with a septa, partially submersed in a low power (70W) bath sonicator (Branson 1800) and sonicated for 3 hours. PCL (420 mg) was then added to this solution and the PCL/SWNCT mixture sonicated for an additional hour. The final solution was poured, in 6 mL portions, into 7 separate Fisherbrand Disposable Aluminum Dishes which were then covered with a cardboard box, and allowed to dry overnight at room temperature. Circular nanocomposite samples, referred to as coupons (approximately 30 μm thick and 40 mm in diameter), were formed as the solvent mixture evaporated. All nanocomposites were allowed to dry for at least one additional day in a desiccator prior to characterization and UV irradiation. Examples of CNT-PNCs with different CNT loadings are shown in Figure 2-4. The average starting mass of the nanocomposite samples used in this study was 31.0 mg (+/-2.3 mg). Hereafter, PCL samples free of CNTs are referred to as PCL/EC, while PCL samples free of CNTs and EC are referred to as PCL.

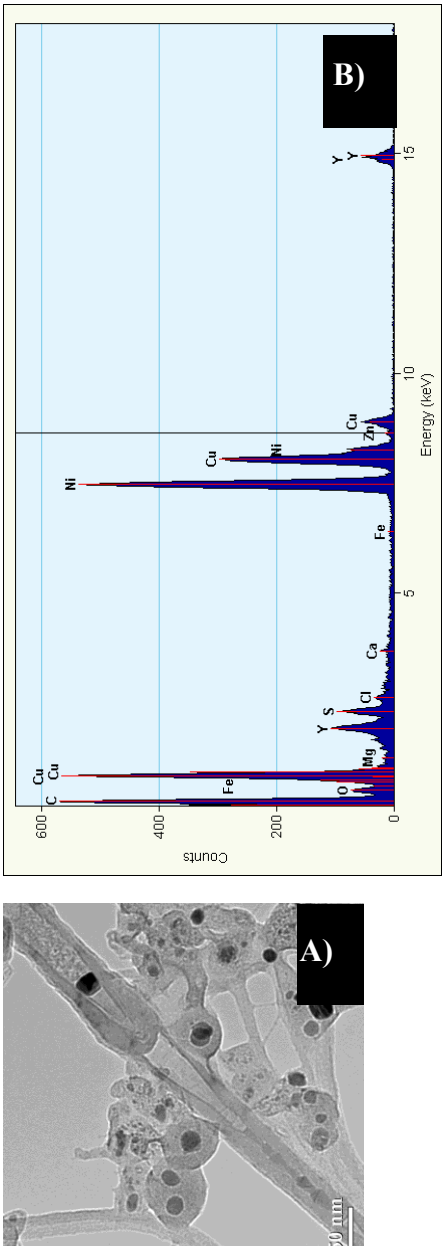


**Figure 2-2:** A) TEM imaging as received SWCNTs, highlighting their residual metal nanoparticles. B) EDX confirms presence of yttrium and nickel, residual from synthesis. Manufacturer reports a metal content < 30% (via TGA). Copper is measured due to the Cu grid.

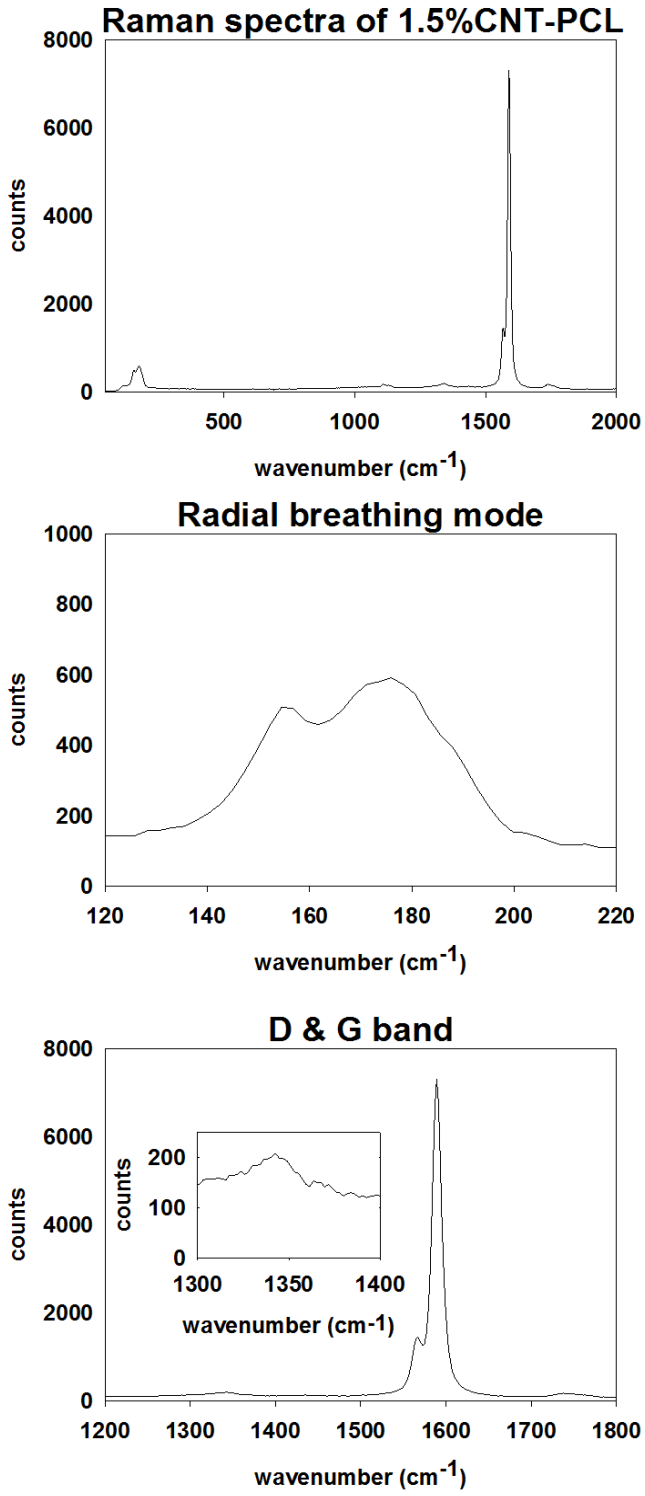


**Figure 2-3**: Raman spectra of the as received SWCNTs within a 1.5%CNT-PCL sample.

UV Irradiation of Polymer Nanocomposites

Polymer nanocomposites were irradiated in a RPR-100 Rayonet photochemical reactor by 16 cylindrically oriented low pressure mercury lamps (purchased from The Southern New England Ultraviolet Co.). To accelerate photodegredation, irradiation was performed principally at 254 nm (UVC) with the fluence = 1.62 x $10^{17}$ photon/second, as determined by actinometry[34]. Additionally, 300 nm (UVB) was used in some comparative control studies to assess photodegradation in more environmentally relevant conditions. During irradiation, the temperature in the reactor was maintained at ≈ 30 $^{0}$C by an internal fan. To prepare CNT-PNC samples for irradiation, individual nanocomposite samples were weighed and bound to a glass slide by thin strips of Teflon tape. These samples were then placed upright in a 15 mL quartz test tube (Figure 2-4).

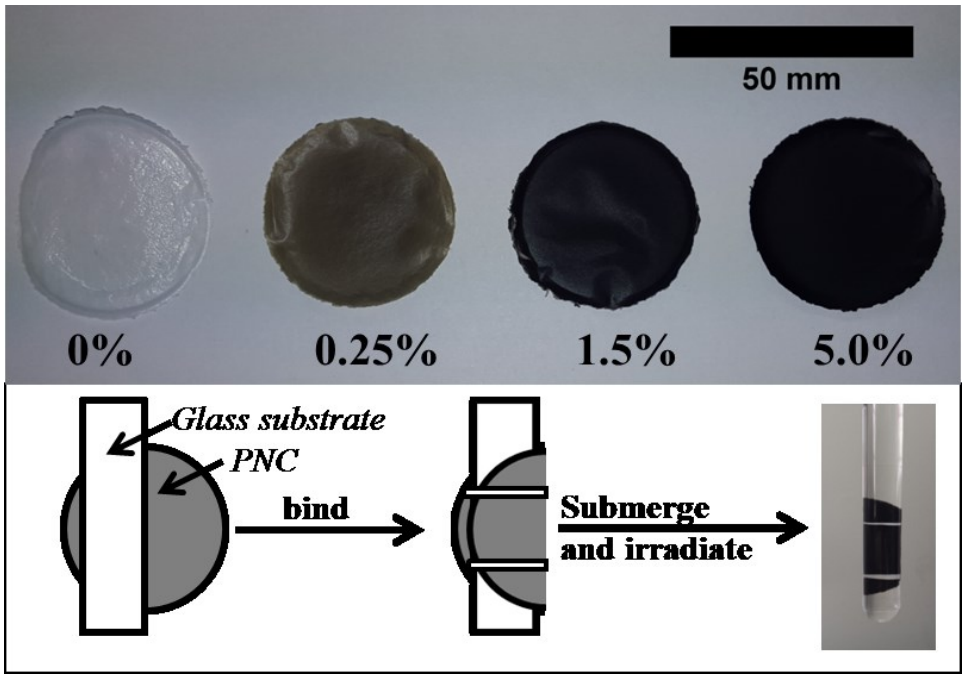


**Figure 2-4**: Figure (Top) Polymer nanocomposites (PNC) prepared by solution blending with a poly-ε-caprolactone (PCL) polymer matrix and 0 – 5% (by weight) SWCNT nanoparticle filler. (Bottom) Samples are bound to a glass slide using teflon tape, submerged in water, and irradiated in a quartz test tube.

Each test tube was subsequently filled with 12 mL of HPLC grade water and sealed with septa to prevent supernatant evaporation; the septa was wrapped with aluminum to prevent its photodegradation. Samples were submersed in water for the entire period of irradiation to ensure that all released nanomaterial is captured for subsequent sp-ICP-MS analysis. Up to 12 samples, each in individual test tubes could be irradiated simultaneously in a rotating carousel. Samples used in this study were continuously irradiated for time periods ranging from 0 hours up through, and including 125 days.

Supernatant Collection

Two different methods were used to determine SWCNT release from irradiated nanocomposites.

i) Incremental SWCNT release

This approach was adopted for the PCL/EC, 0.25% CNT-PCL, and 5.0% CNT-PCL samples which were irradiated for 20, 40, 80, and 125 days. Four samples at each CNT loading (a total of 12 individual coupons) were studied with this incremental sampling scheme. During the initial 20 day period of irradiation, the supernatant from all 12 samples were collected and fully replenished every 5 days (days 5, 10, 15 and 20). On each sampling day, the nanocomposite samples were removed from the test tube. 100 μL of 2% SDC was then added to the solution remaining in the test tube before the contents were transferred into a clean glass vial. The empty test tube was then cleaned with soapy water and rinsed vigorously before the glass slide containing the nanocomposite sample was returned. At this stage the test tube was refilled with 12 mL of HPLC grade water, resealed and irradiation resumed for another five day period. The addition of SDC surfactant to the supernatant prior to collection was done to ensure that all of the released

SWCNTs and SWCNT-containing polymer fragments were dispersed into solution. Due to volume requirements, release supernatants generated from the 0-5 day and 6-10 day irradiation periods were combined, as were the supernatants collected from 11-15 days and 16-20 days.

After 20 days of irradiation had elapsed, one nanocomposite from each SWCNT loading (PCL/EC, 0.25% CNT-PCL, and 5.0% CNT-PCL) was removed from the photochemical reactor, dried for one day in a desiccator, weighed, and then characterized by scanning electron microscopy (SEM) and X-ray photoelectron spectroscopy (XPS). These remaining samples were exposed to a total of 40, 80, or 125 days of irradiation. For these longer periods of irradiation, the supernatant was not periodically collected and replenished, as it was for the first 20 days, but instead collected at the conclusion of sample exposure. At the end of 40, 80, or 125 days one nanocomposite from each SWCNT loading was removed from the photochemical reactor, dried, weighed and characterized. The release supernatant from each nanocomposite was analyzed by single particle inductively coupled mass spectrometry (sp-ICP-MS).

ii) Cumulative SWCNT release

A different sampling approach was used for 1.5% SWCNT-PCL nanocomposite samples. In these experiments 14 samples were irradiated for a total of 2, 5, 10, 20, 40, 80, or 125 days (duplicate samples for each time point) and the supernatant was allowed to accumulate for the entire duration of exposure. At the end of each exposure time, two nanocomposites were removed from their glass substrates, dried, weighed and then characterized. The release supernatant remaining in the test tubes after each time point

was collected in a glass vial and analyzed for SWCNT by sp-ICP-MS analysis after the addition of 2% SDC, following the same procedure described in i).

Determination of CNTs in "Release Supernatants" by single particle ICPMS (sp-ICPMS)

Prior to sp-ICP-MS analysis, 1 wt% of surfactant was added to each "release supernatant" along with a 30 min period of sonication to ensure that all released CNTs were suspended. Samples were then diluted to a concentration suitable for spICP-MS analysis. After each dilution, solutions were placed in 15 mL polypropylene centrifuge tubes and sonicated (Fisher FS60H bath sonicator, Pittsburgh, PA) for 15-20 minutes.

Single particle ICP-MS analysis was performed to determine the SWCNT content of the release supernatants using $^{89}Y$ pulses as surrogates for SWCNT detection, as detailed in Reed *et al*.[29]. All sp-ICP-MS analyses were performed in triplicate using a NexION 300Q ICP-MS (Perkin Elmer, Waltham, MA). Data collection used a dwell time of 0.1 ms, with 60 second total acquisition time. The sample introduction flow rate was 0.3 mL/min. To determine the background $^{89}Y$ signal Nanopure water was analyzed by sp-ICP-MS at the beginning of each experiment. Data collection and sp-ICP-MS calculations were performed using the SyngistixTM (version 1.0) Nano Application Module, with additional data processing being performed using EXCEL. The Syngistix software was used to determine the background counts, and any readings that were greater than 3 sigma above this background were considered to be a possible CNT entering the plasma. To discriminate these readings from random noise they were further examined, and only those that were part of two or more consecutive readings greater than 3 sigma above the background were considered part of a pulse generated by a CNT. All

consecutive readings that occurred above background intensity were combined to provide the total intensity of that CNT.

The ICP-MS was tuned daily with Perkin Elmer NexION Setup solution (1% $HNO_3$, 10 µg/L Be, Ce, Fe, In, Li, Mg, Pb, U, Perkin Elmer, Waltham, MA). Dissolved Au calibration solutions (0, 2, 5, 10 µg/L) were prepared using Claritas PPT (SPEX Certiprep, Metuchen, NJ) ICP-MS standards and 2% hydrochloric acid (Optima, Fisher Chemical, Fair Lawn, NJ). A gold NP standard (56 nm, National Institute of Standards and Technology (NIST) RM 8013, Gaithersburg, MD) was diluted to 500 ng/L from the stock 50 mg/L (~2.98 ± 0.04 x $10^{13}$ particles/mL) solution with 18.2 MΩ $cm^{-1}$ Nanopure water (Barnstead Nanopure Diamond, Lake Balboa, CA) and analyzed to determine transport efficiency.[35] Similarly, dissolved yttrium ion calibration solutions (0, 1, 2, 5

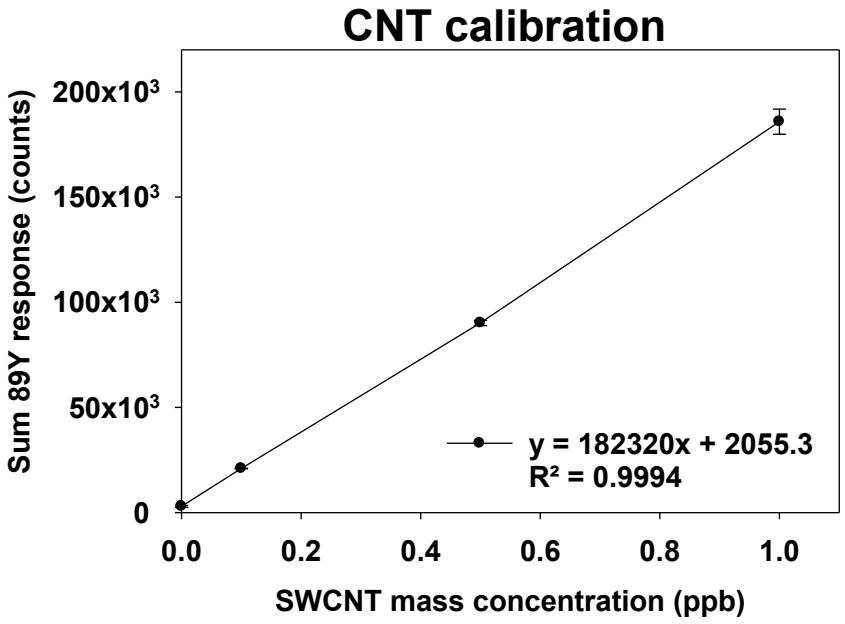


**Figure 2-5**: Calibration curve constructed from SWCNT suspensions of increasing concentration. 89Y response to CNT concentration established from this plot is used to determine CNT concentration in release supernatants.

μg/L) were prepared using Claritas PPT ICP-MS standards and 2% nitric acid (Optima, Fisher Chemical, Fair Lawn, NJ) to establish instrument sensitivity to $^{89}Y$ and to allow the total NP mass in each pulse to be determined.

To directly establish the relation of the sum of $^{89}Y$ response determined by sp-ICPMS with CNT mass concentration, CNT solutions (0, 100, 500, 1000 ng/L) were prepared by suspending a known mass of SWCNTs in a known volume of ultrapure water (HPLC grade) containing 1 wt% sodium deoxycholate (Sigma-Aldrich, Saint Louis, MO). A bath Branson 1510 ultrasonicator (Danbury, CT) was used to suspend CNTs overnight. Because this suspension was not immediately characterized following its preparation, the dilutions prepared from it were sonicated for 30 minutes immediately prior to sp-ICP-MS analysis to debundle any CNTs that may have aggregated. This ensures that particle number measurements from the sample are accurate. A calibration curve was constructed between the known CNT mass in suspension and the $^{89}Y$ response (Figure 2-5) so that release supernatants containing an unknown CNT concentration could be measured and quantified.

Characterization of Nanocomposites

*Surface Chemical Characterization:*

i) X-ray photoelectron spectroscopy (XPS)

Surface analysis of CNT-PNC samples was performed before and after periods of irradiation by XPS using a PHI 5600 with Mg Kα X-ray (1253.6 eV) radiation. Prior to analysis, samples were dried overnight in a desiccator and were cut to size and affixed to a sample stub by copper tape. Quantitative analysis of the carbon (C(1s)) and oxygen (O(1s)) regions was completed using a pass energy of 58.7 eV, 10 sweeps, and a step size

of 0.125eV. XPS data analysis was performed with CasaXPS. Survey scans were also collected to ensure samples were free of contamination.

ii) Attenuated total internal reflectance – infrared spectroscopy (ATR-FTIR)

ATR-FTIR was performed on select nanocomposite samples before and after specific periods of irradiation. Spectra were collected with a Nicolet iS5 FT-IR Spectrometer, equipped with a diamond window. Prior to analysis, all samples were dried overnight in a desiccator. The manufacturer reports a sampling depth of approximately two microns for the diamond window. Samples were analyzed at a resolution of 0.482$cm^{-1}$, with 32 scans. Each ATR-FTIR was referenced to the ambient atmosphere.

*Morphological Characterization:*

iii) Scanning Electron Microscopy (SEM)

SEM was performed using a Jeol 6700F, FESEM. Nanocomposite samples were dried overnight in a desiccator and mounted on a conductive metal stub with copper tape prior to imaging. To minimize charging, all samples were sputter coated with platinum for 300 seconds, at a rate of 2 nm/minute. For each sample imaged, four locations on the surface were randomly selected and imaged at increasing magnifications.

**Results and Discussion**

Effect of Photolysis on CNT Polymer Nanocomposites

*Mass loss*

Figure 2-6 displays the percent mass loss of SWCNT-PCL composites with different SWCNT loadings (PCL/EC, 0.25%, 1.5%, 5%) as a function of the irradiation time. Regardless of the SWCNT loading, the dependence of mass loss on irradiation time follows a qualitatively similar trend. All nanocomposites exhibit their most significant period of mass loss during the first 20 days of irradiation. For periods of irradiation in

excess of 20 days the rate of mass loss slows and after day 40, no significant additional nanocomposite mass loss occurs. Although the qualitative trend in mass loss was similar for the various nanocomposites studied, the absolute magnitude of mass loss observed was strongly attenuated as the SWCNT loading increases. Thus, following 20 days of UVC exposure, PCL/EC, 0.25% CNT, 1.5% CNT, and 5.0% CNT samples lost 35.3%, 16.8%, 7.3%, and 4.5% of their mass, respectively. The final mass loss for the four loadings after 125 days irradiation is measured to be 44.9%, 23.9%, 10.6%, and 7.4%, respectively, (with the absolute measured mass loss shown in Appendix Figure 5-1).

In experiments using a longer wavelength of light more representative of sunlight, PCL/EC irradiated with UVB light also showed photodegradation and mass loss albeit at decreased magnitude and rate, as compared to PCL/EC irradiated with UVC.

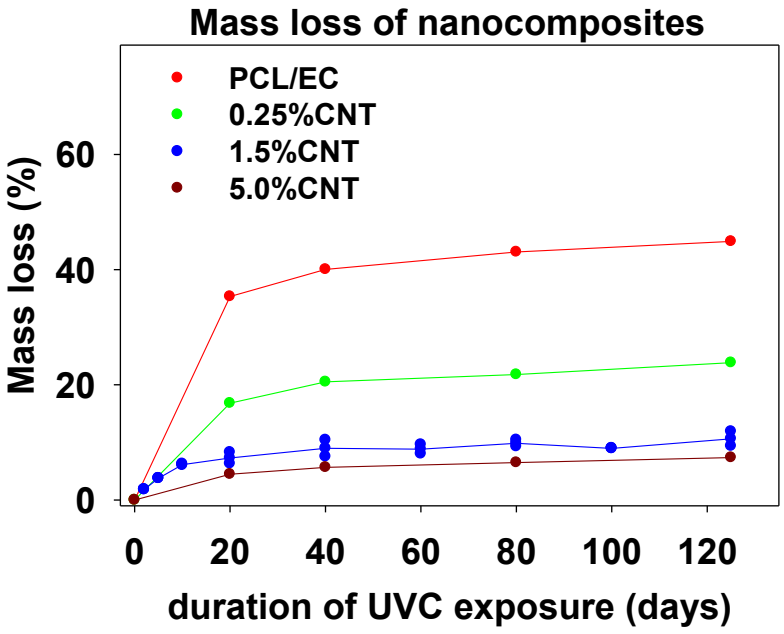


**Figure 2-6**: Mass loss of SWCNT-PCL nanocomposites with varying SWCNT loading (%w/w) following incremental periods of irradiation with 254nm light. The average initial mass of all samples used in the study is 31.0mg (+/-2.3mg).

Specifically, UVB irradiation of PCL/EC following 20 and 40 days of exposure produces a mass loss of 3.18% and 6.44%, respectively. In contrast, following 20 and 40 days of UVC exposure, PCL/EC has lost 35.3% and 40.0% of its mass, respectively.

*Nanocomposite Characterization*

A comprehensive suite of characterization techniques was employed to track the surface composition (XPS), chemical structure (ATR-FTIR), and morphology (SEM) of the nanocomposites as they photodegraded. Previous studies have utilized spectroscopic characterization of the polymer matrix following increasing periods of exposure to both track degradation of the polymer structure[10, 13, 36] and the accumulation of embedded nanoparticles at the surface[10, 13]; spectroscopic characterization was utilized to monitor polymer degradation as a function of both irradiation time and initial CNT loading.

*Surface Morphology*

Figure 2-7 shows how the surface morphology of 0.25% CNT and 5.0% CNT nanocomposite samples evolve after 0, 20, and 125 days of UVC irradiation. All of the samples exhibited nearly identical initial surface morphology: smooth and lacking any defining features, including the absence of any observable SWCNTs (see Figure 2-7 and Figure 2-8A). Following 20 days of UVC exposure, the surface morphology of each sample has changed. On the surface of the 5.0% CNT sample, SWCNTs have accumulated to form a dense mat. While SWCNTs dominate the surface morphology, a small number of somewhat smoother regions devoid of SWCNTs are also observed. Such CNT mat formation has been observed previously by Nguyen *et al.* [10, 21, 37], Ging *et al.* [38], and Hirth *et al.* [39] following UV exposure of CNT-epoxy PNCs. The accelerated weathering of CNT- polyoxymethylene also found CNTs on the surface of the PNC.[21] In

contrast to the behavior of the 5.0% CNT samples, on the surface of the PCL, PCL/EC (Figure 2-8 B,C), and 0.25% CNT samples, bulbous spherical structures approximately 500 nm in diameter have formed and are distributed across the sample. SWCNTs, however, are not observed on the surface of the irradiated 0.25% CNT sample. Higher magnification SEM images of the 0.25%CNT sample confirm the absence of CNTs at the surface (Figure 2-9).

Following 125 days of irradiation, the dense and continuous CNT mat persists on the surface of the 5.0% CNT nanocomposite, with no signs of fragmentation or perforation. The PCL/EC and 0.25% CNT samples also retain a similar surface morphology to that observed following 20 days of irradiation. Additionally, the surface morphology of the 1.5% CNT sample, not shown, was found to be similar to the PCL/EC and 0.25% CNT samples following 0, 20, and 125 days of irradiation. An absence of observable CNTs at the surface following photolysis of CNT-PNCs has been previously documented by Schlagenhauf *et al.,* in the study of 1% CNT-epoxy composites. [40]

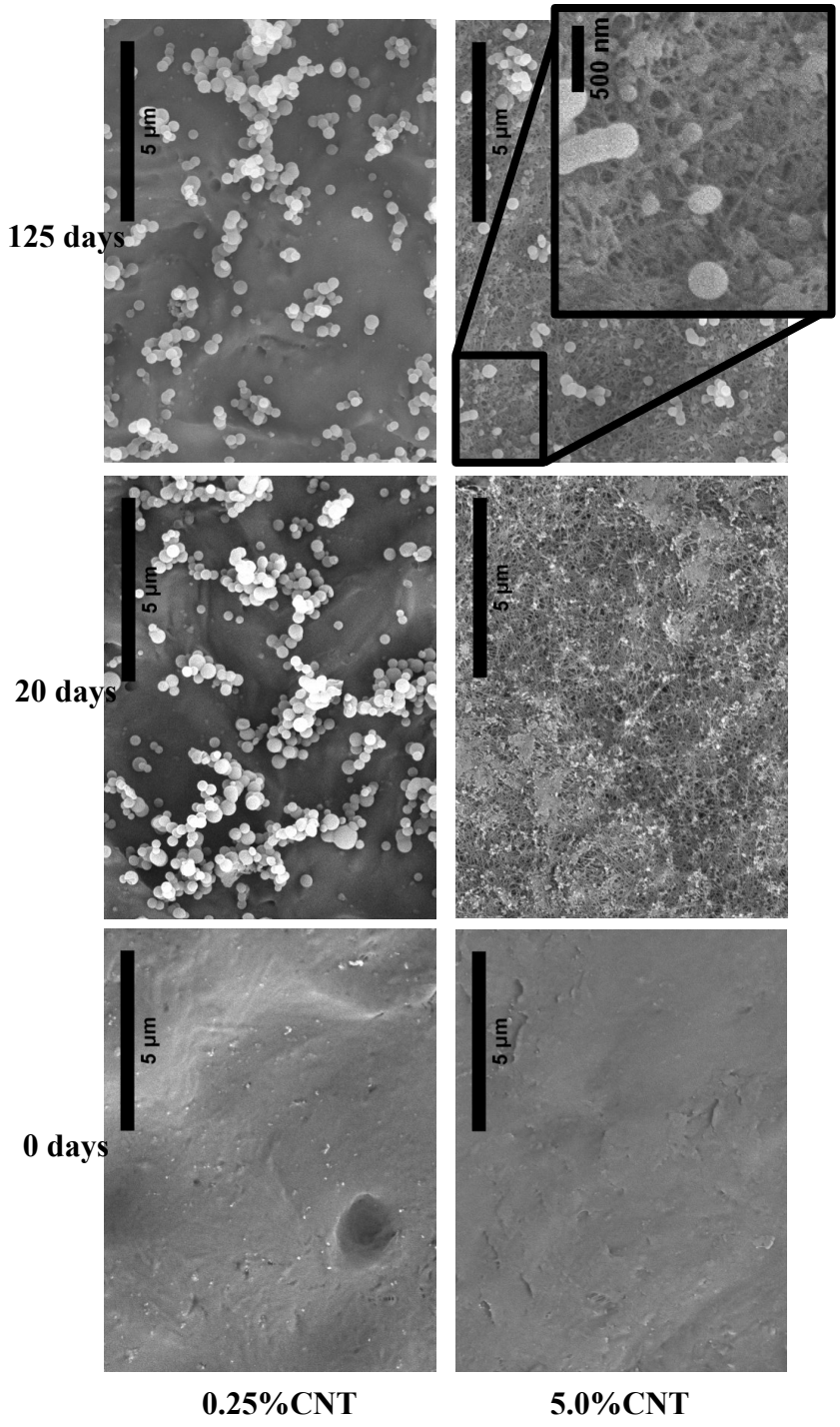


**Figure 2-7**: SEM imaging shows CNT accumulation on the surface of 5.0%CNT sample following UVC exposure. Lower CNT loading samples do not show visible SWCNT accumulation.

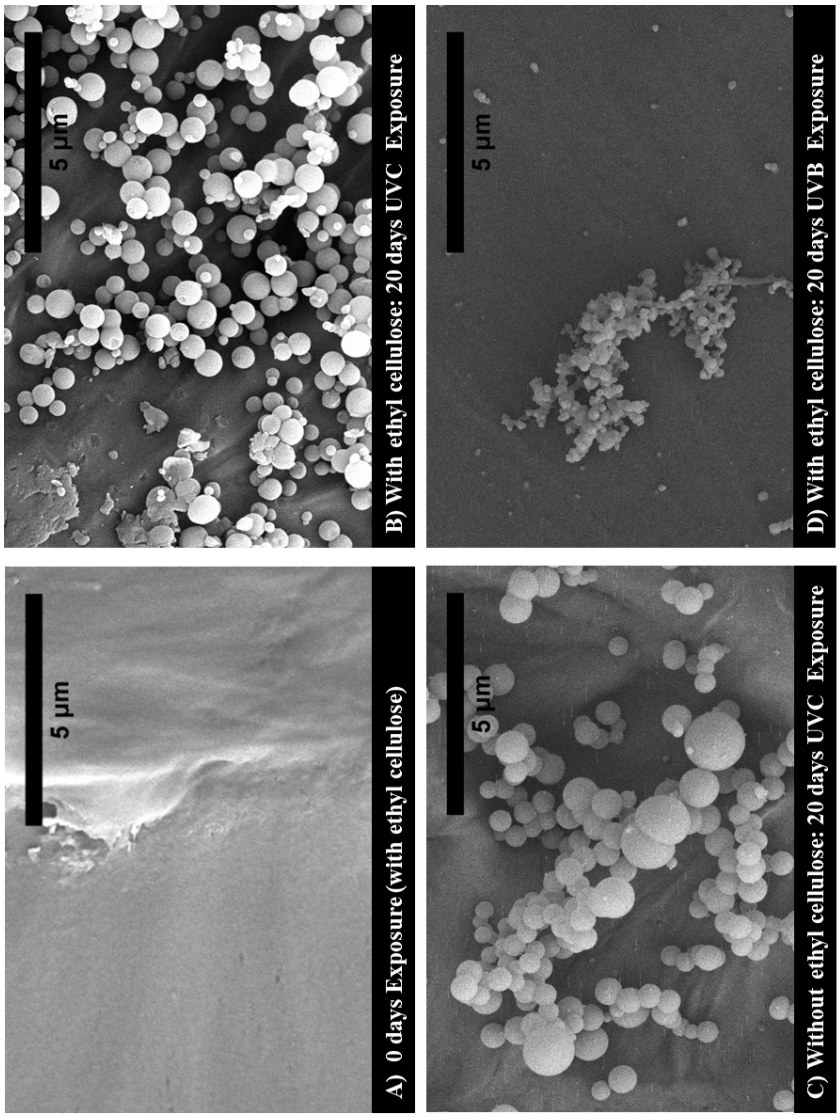


**Figure 2-8**: SEM imaging of Pure PCL with and without ethyl cellulose shows the formation of bulbous like features following UVC exposure (B and C, respectively). Pure PCL samples with ethyl cellulose show the formation of the smaller bulbous features following UVB exposure (D).

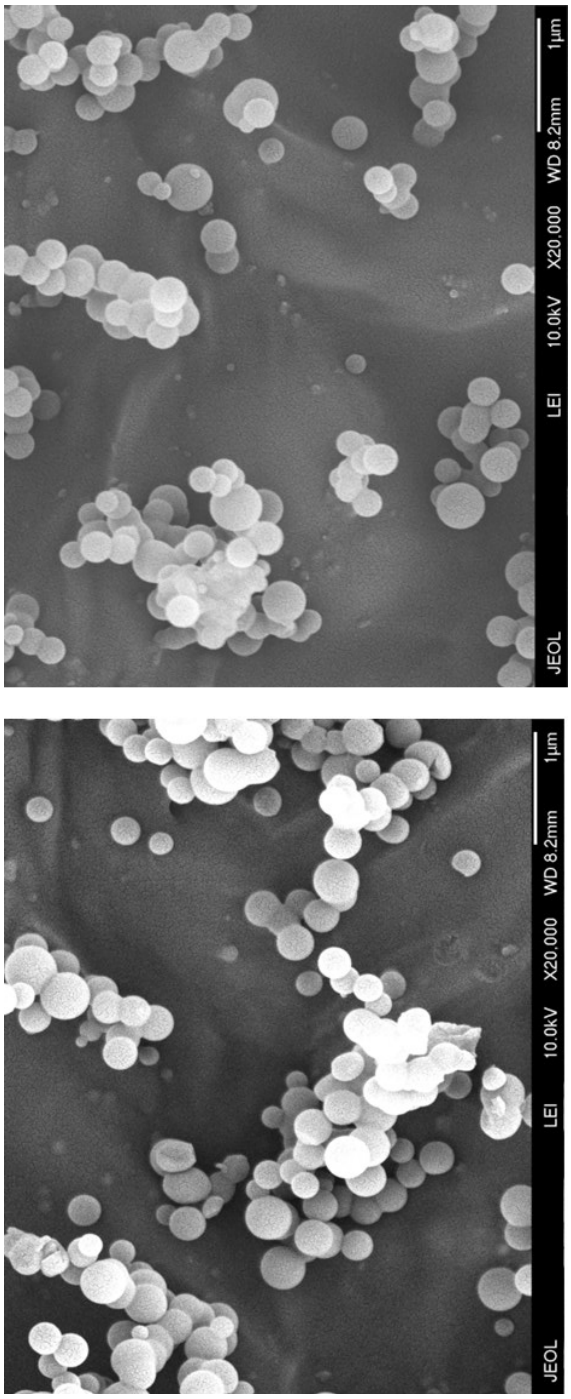


**Figure 2-9**: SEM images of 0.25%CNT-PCL sample following 20 days of UVC Exposure, (left) and 0.25%CNT-PCL sample following 125 days of UVC Exposure (right)

*Surface Chemistry*

Figure 2-10A shows XPS data, demonstrating how the C(1s) region of the 1.5% CNT nanocomposite changes as a function of UVC exposure. The corresponding XPS data for the PCL, PCL/EC, and other nanocomposite samples are shown in Figure 2-11 and Figure 2-12, respectively. Inspection of Figure 2-10A reveals that the intensity of the ester peak observed at 288.5 eV decreases rapidly during the initial period of UVC exposure followed by little to no change for days 20 through 125. This behavior is similar to the changes observed for PCL (compare Figure 2-11A to 2-11C), PCL/EC (compare Figure 2-11A to 2-11B) and all other nanocomposites (Figure 2-12), with all samples showing a rapid decrease in the ester peak over the first ≈ 20 days of irradiation but little to no change thereafter. Figure 2-10B depicts the O:C ratio, as measured by XPS, of the 1.5%CNT nanocomposite samples as a function of irradiation time, which decreases by ≈ 50% through the first 40 days of irradiation before remaining constant thereafter.

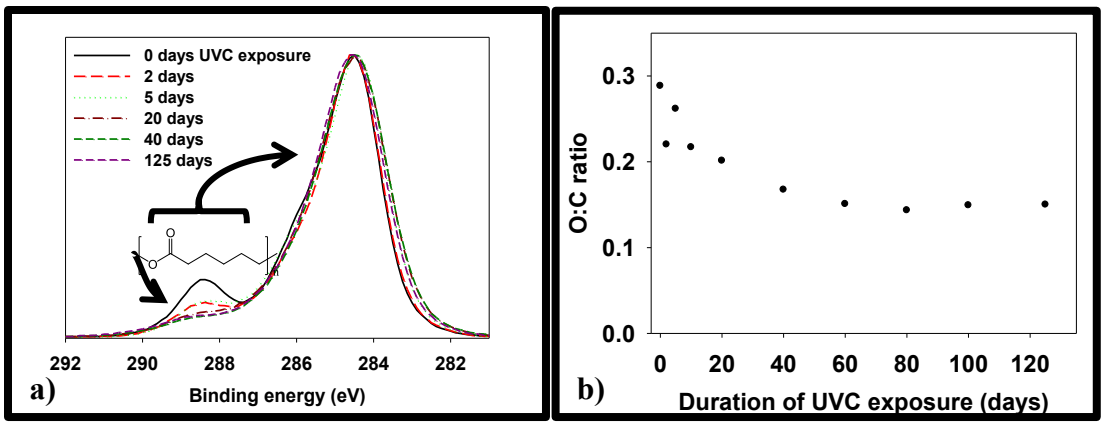


**Figure 2-10**: Transformations in (a) the C(1s) region and (b) O:C ratio of the 1.5%CNT composites as a function of UVC irradiation. The largest changes are seen to occur during the by first 20 – 40 days with little change in either the C(1s) region or the O:C ratio thereafter.

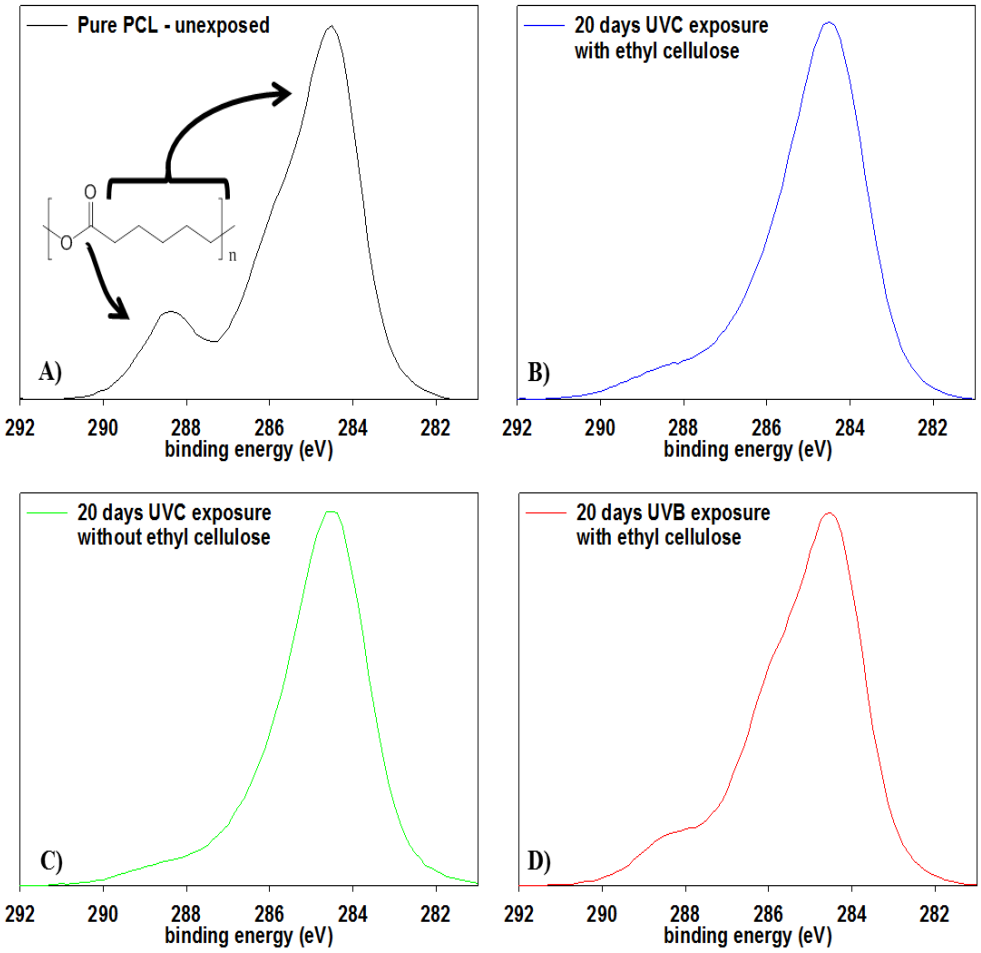


**Figure 2-11**: XPS characterization of Pure PCL with and without ethyl cellulose both lose the ester peak following UVC exposure (compare B and C to A). Pure PCL with ethyl cellulose show a diminished ester peak following UVB exposure (compare D to A).

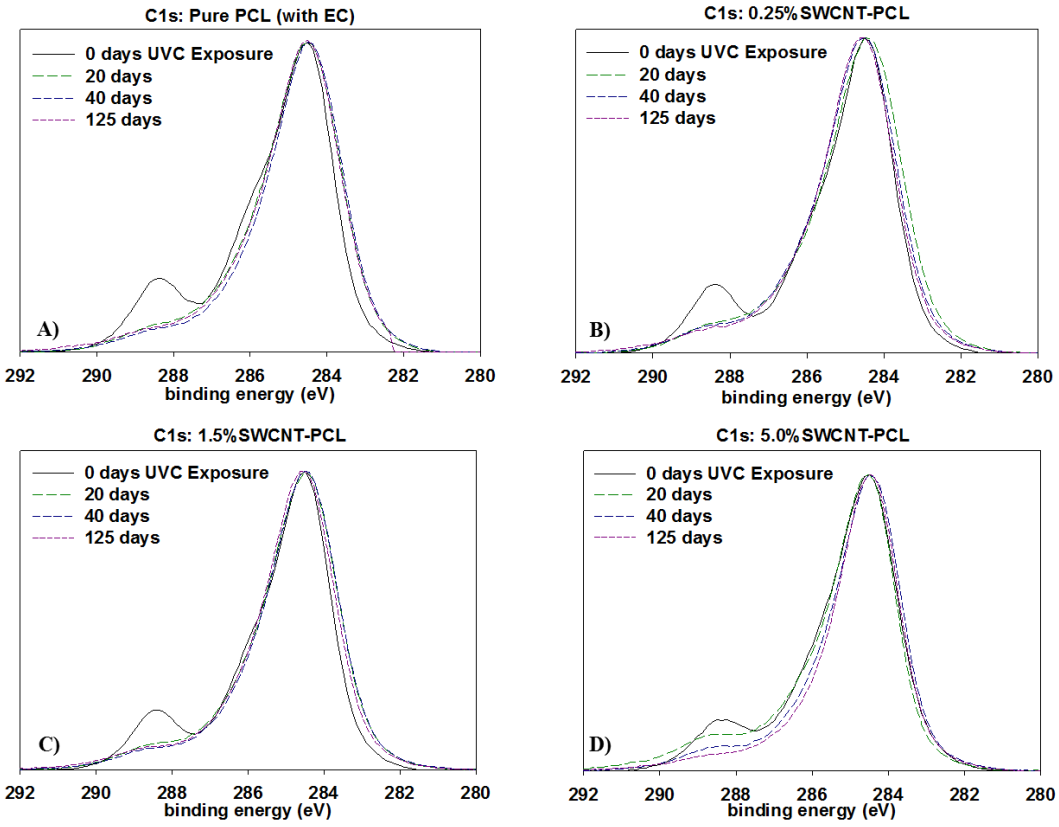


**Figure 2-12**: XPS characterization of nanocomposites shows consistent loss of ester peak within the first 20 days of UVC exposure for the three lower loadings; the 5%CNT samples appears to lose ester by day 40.

ATR-FTIR was used to probe changes that occur to the chemical bonding within the near surface region (~2 μm) of the PNCs as a result of UVC irradiation. Pure PCL, PCL/EC, and all nanocomposite samples were analyzed prior to UVC exposure and then again following 125 days of irradiation, as shown in Figure 2-13A. Prior to irradiation, the ATR-FTIR of each sample was identical to literature spectra of PCL[41] with absorption bands at 2866 $cm^{-1}$ and 2942 $cm^{-1}$ due to the symmetric and asymmetric C-H stretching modes of the alkyl carbon atoms. In addition to the characteristic fingerprint region of PCL < 1500 $cm^{-1}$, each sample also exhibits a sharp and intense ester stretch at 1720 $cm^{-1}$ due to the ester group.[41] No spectroscopic signature of CNTs was observed. Following 125 days of irradiation, the IR intensity in the C-H stretching region is relatively unchanged following irradiation regardless of CNT loading, with each sample still exhibiting an absorption band at 2866 $cm^{-1}$, although subtle changes to the spectral envelope have occurred. Specifically, two small new bands appear at 2959 $cm^{-1}$ and 2925 $cm^{-1}$, replacing the band originally observed at 2942 $cm^{-1}$. No other new features or absorption bands are observed as a consequence of photolysis. Although the C-H stretching region remains relatively unchanged after 125 days irradiation, inspection of Figure 2-13A reveals that the intensity of the ester peak and signatures of PCL in the fingerprint region decrease for all samples. However, as the CNT loading increases the extent to which these spectral features decrease in intensity decreases significantly.

Figures 2-13B and 2-13C quantify the relationships between CNT loading, mass loss, and the depletion of the ester groups in the near surface region, the latter measured by ATR-FTIR. It is observed that the mass loss of PNCs and the fractional decrease in the ester group's concentration in the near surface region, following 125 days of UVC exposure,

both decrease with increasing CNT loading [42](Figure 2-13B). Moreover, Figure 2-13C demonstrates that there is a linear relationship ($R^2 = 0.98$) between the fractional decrease in the ester group's near surface concentration and the extent of polymer mass loss.

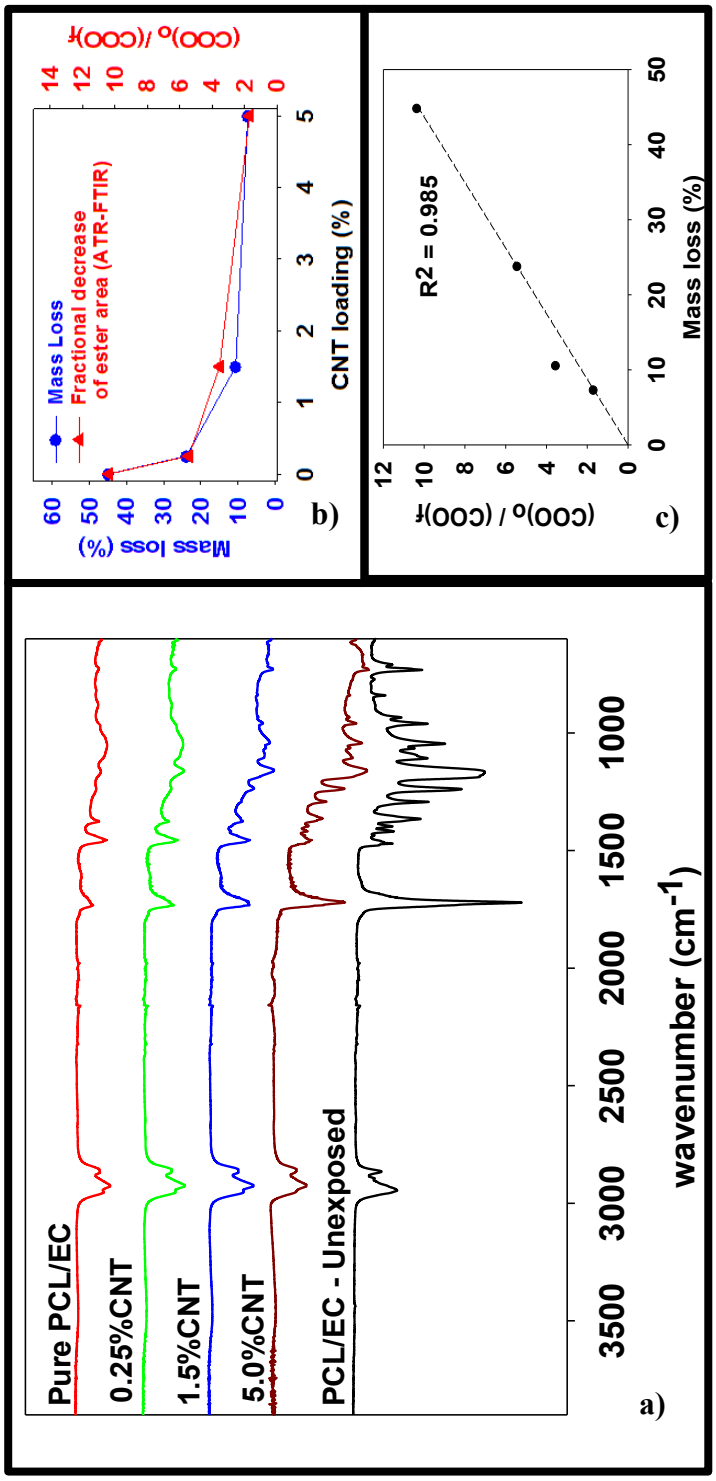


**Figure 2-13**: (a) ATR-FTIR analysis of the nanocomposites shows a reduction in intensity of the ester peak (1720cm$^{-1}$) following 125 days irradiation. (b) Following 125 days of exposure, the final mass loss and fractional decrease of ester band area show a similar dependence on CNT loading. (c) mass loss increases linearly with the fractional decrease in ester band area

Carbon nanotube release and detection

Figure 2-14A is an additional representative TEM image of the SWCNTs used in this study. Residual metal nanoparticles, left over from the fabrication process, are clearly observed attached to the SWCNTs, with most appearing to be fully encapsulated by carbonaceous material. The manufacturer reports a total metal content of < 30%, by mass. In all images captured, no free metal nanoparticles were observed. The nanoparticles are roughly spherical with an average diameter of 15-20 nm, although the number of nanoparticles per nanotube is very heterogeneous.

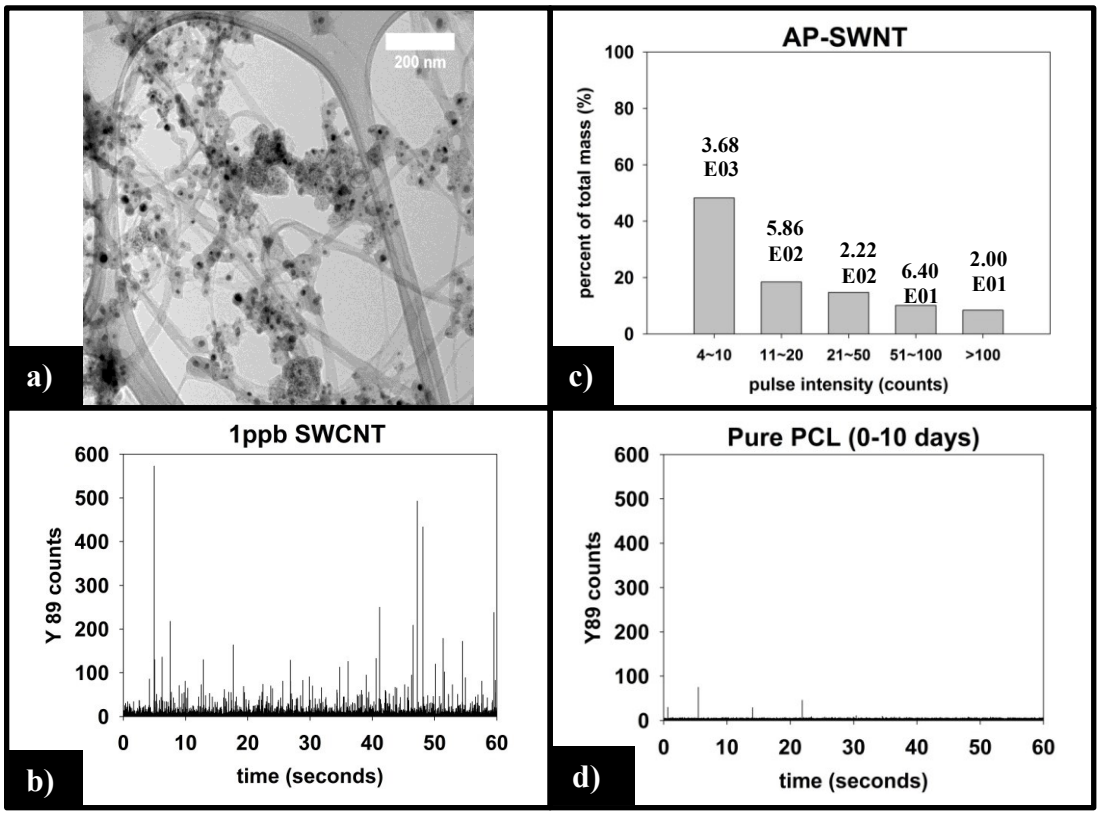


**Figure 2-14**: (a) TEM of SWCNTs shows embedded residual yttrium and nickel catalyst nanoparticles. (b) sp-ICP-MS analysis of 1ppb SWCNT suspension prepared with 2% SDC. (c) Y mass distribution for SWCNT suspension, with the corresponding number of particles detected noted above each bin. (d) sp-ICP-MS of supernatant generated by 10 day irradiation of Pure PCL is absent of $^{89}Y$ response (i.e. no CNT release or interference from the polymer matrix).

*sp-ICP-MS analysis of Carbon Nanotubes*

The yttrium sp-ICP-MS signal, obtained for a suspension of 1ppb SWCNTs, is shown in Figure 2-14B. For such dilute suspensions of CNTs, sp-ICP-MS data display discrete pulses in element intensity. The generation of each pulse is a result of metal nanoparticle containing CNTs entering the ICP-MS and being ablated. In this study, the signal and pulses utilized for sample analysis are generated by the yttrium nanoparticles associated with CNTs. Each $^{89}Y$ pulse is a result of a single CNT, a CNT bundle, or a polymer fragment containing multiple CNTs. This view, that $^{89}Y$ pulses are associated with CNTs is supported by both the lack of free metal nanoparticles observed by TEM and by the magnitude of the pulses observed by sp-ICP-MS. Based on the dissolved $^{89}Y$ calibration curve a yttrium nanoparticle < 20 nm should produce a pulse of 2-4 counts per dwell time, with a small variation in pulse intensity.[30] In contrast, most pulses observed for the CNT suspensions have intensities greater than what would be expected from the individual metal catalysis NPs observed in the TEM images. However, due to the variability in the size and number of attached yttrium particles, the $^{89}Y$ pulse intensity varies considerably between SWCNTs. Each pulse contains the intensities in consecutive, non-background dwell times. In order to better interpret the data, all pulses are collected into bins and divided by the total intensity for that sample. Following this convention, the resulting fractional mass distribution for the data shown in Figure 2-14B, is given in Figure 2-14C, which reveals that of 4572 pulses detected, 48% of the total mass of yttrium measured is from 3680 nanoparticles with pulse intensities of 4-10 $^{89}Y$ counts. Only 20 SWCNTs were measured to have pulse intensities greater than 100 $^{89}Y$ counts,

and they accounted for less than 0.5% of the total measured mass. Only two pulses were detected that resulted in intensities greater than 300 $^{89}$Y counts.

*sp-ICP-MS analysis of the "release supernatant" generated from PCL/EC during photodegredation*

The sp-ICP-MS signal obtained for the supernatant of PCL/EC following 10 days of UVC exposure is shown in Figure 2-14D; the lack of pulses indicate that pure PCL does not release nanoparticulate yttrium, as expected. Thus, out of 600,000 total dwell times recorded, 98.5% are 0 – 3 counts. Only 10 total pulses are measured to be greater than 10 counts (false positive detections), are not of statistical relevance, and attributed to trace amounts of yttrium found in the sample or solution.

*sp-ICP-MS analysis of the "release supernatant" generated from CNT-PNCs during photodegradation*

*(i) Measured vs. predicted SWCNT mass release*

Integration of the $^{89}$Y signal allows the total mass of SWCNTs released to be determined using the calibration curve obtained with the SWCNT dispersions (Figure 2-5). Figure 2-15A displays the cumulative SWCNT mass released from each nanocomposite into solution during different periods of photolysis. Figure 2-15B depicts the predicted cumulative CNT release mass assuming that as polymer mass is lost, CNTs release proportionally with the polymer based on the initial CNT loading. A summary of the measured and predicted/proportional mass loss of SWCNTs from 0.5%, 1.5% and 5% CNTs during different stages of photolysis is provided in Table 2-1. It is noted that the error depicted in Figure 2-15A and shown in Table 2-1 for the 0.25%CNT and 5.0%CNT samples was calculated by the summation of the samples' independent uncertainties.[43] In separate control experiments the extent of CNT release from nanocomposite samples that

were not irradiated but were submerged in water under the same conditions used for the photolysis experiments was assessed. For all nanocomposite samples, submersion resulted in < 0.1µg CNT release. Consequently, all of the SWCNT released in this study are a result of PNC photodegredation.

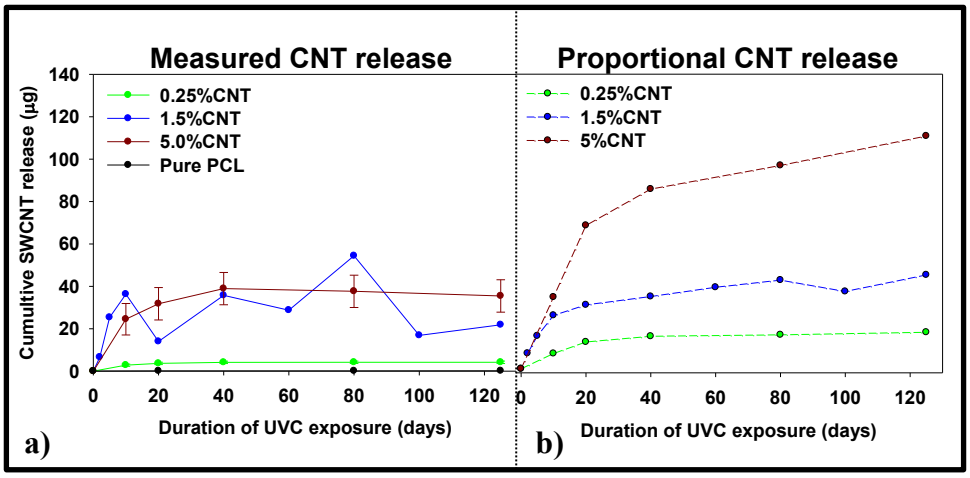


**Figure 2-15**: Left) Cumulative CNT release plateaus within the first 40 days of exposure and is less than the predicted release of CNTs (Right), assuming CNTs are lost at the same rate as the polymer.

| | 0 - 20 days | | 0 - 125 days | |
|---|---|---|---|---|
| | Measured | Predicted | Measured | Predicted |
| 0.25% CNT | 3.66 (+/- 0.56) | 13.76 | 4.19 (+/- 0.56) | 18.63 |
| 1.5% CNT | 13.97 | 32.55 | 21.88 | 47.78 |
| 5.0% CNT | 31.79 (+/- 7.63) | 73 | 35.46 (+/- 7.63) | 118.5 |

**Table 2-1**: Cumulative release of SWNCTs measured by sp-ICP-MS shown in Figure 7, from PCL/CNTs with different CNT loadings. Measured values are compared to the values predicted assuming that the rate of CNT mass loss is equal to the rate of polymer mass loss. Units are µg of SWCNTs released into solution.

From knowledge of the PNC mass, the CNT loading and the SWCNT mass released the fraction of SWCNTs released at different stages of the photodegradation process can also be determined. This analysis reveals that, for the same period of photolysis, the fraction of SWCNTs released decreases as the CNT loading increases. Thus, the 0.25%CNT sample lost 3.9% of its total CNTs during the first ten days of exposure, 1.1% from days 11 – 20, and 0.7% of initial CNTs during the last 21 – 125 days of exposure. In contrast, during the same intervals of irradiation, the 5.0%CNT sample lost 1.6%, 0.5%, and 0.4% of the CNTs initially present, respectively.

*(ii) Functional form of SWNCT released*

Figure 2-16 displays the raw and processed sp-ICP-MS data collected for the 5.0% CNT nanocomposite during the initial (0-10 days), intermediate (11-20 days), and final (21-125 days) irradiation intervals. The data are binned by increasing $^{89}Y$ pulse intensity (i.e. particle mass) and plotted as the fractional mass distribution of the SWCNTs detected in those intervals. During the first 10 days of irradiation (Figure 2-16A), the largest number of yttrium pulses, as well as the most intense pulses, are detected. During the subsequent periods of irradiation, the pulse number and intensity steadily decrease, as shown in Figures 2-16B and 2-16C. It should be noted that the lack of any increase in the background signal (0-4 counts) during PNC-CNT photolysis indicates that $^{89}Y$ is not being released from the CNT-polymer matrix as ions or as individual 20 nm yttrium NPs (both of which would increase the background signal rather than be detected as a discrete pulse), but rather as multiple NPs still attached to the SWCNTs.

Figure 2-17 displays the sp-ICP-MS data collected for the 0.25% CNT nanocomposite during the same initial (0-10 days), intermediate (11-20 days), and final (21-125 days) irradiation intervals described above for the 5.0% CNT samples, as well as the mass distribution of the SWCNTs detected from those intervals. Unlike the 5.0% CNT sample, in which a large number of particle detection events (pulses) are detected during each period of exposure, the 0.25% CNT samples released substantially less particles: during the initial, intermediate, final irradiation intervals; only 1021, 653, and 632 total particles are detected, respectively.

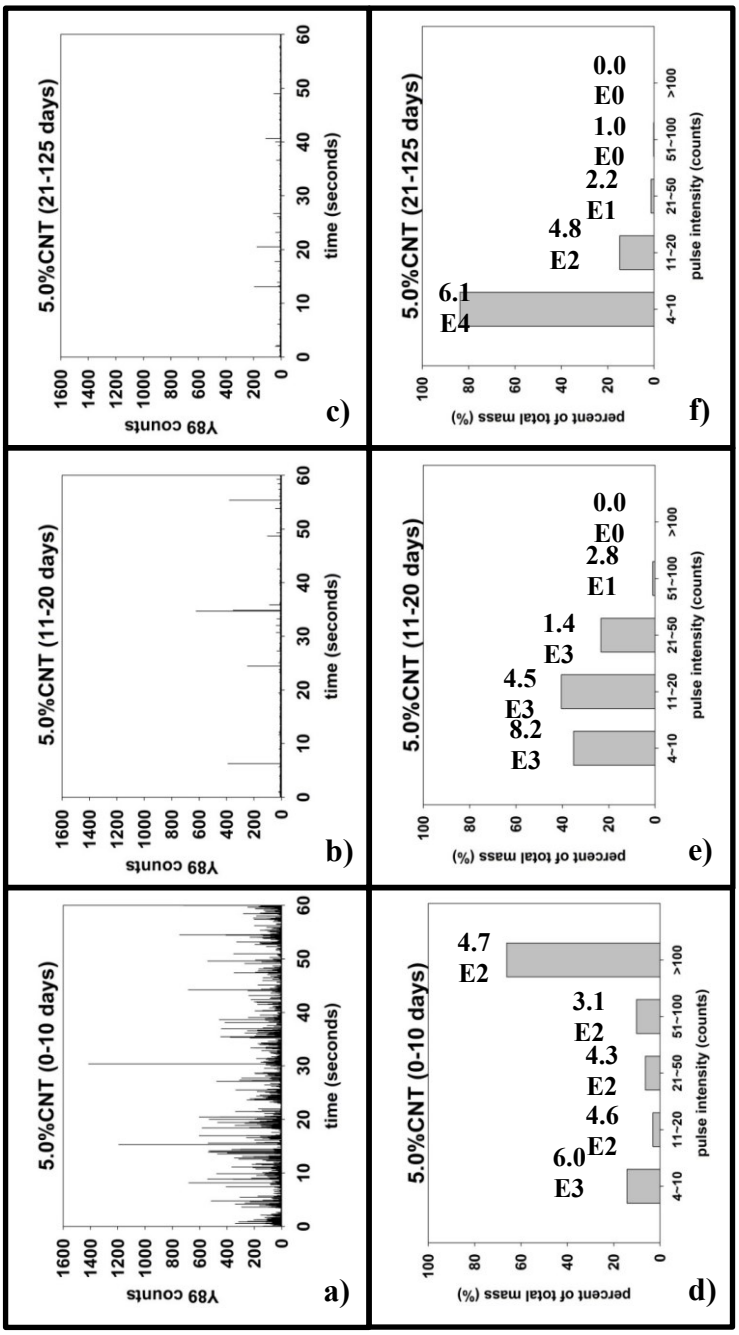


**Figure 2-16**: (a), (b), (c) Raw sp-ICP-MS data collected for 5.0%CNT nanocomposites with increasing duration of UVC exposure. (d), (e), (f) Y mass distribution for each period of exposure, with the corresponding number of particles detected noted above each bin.

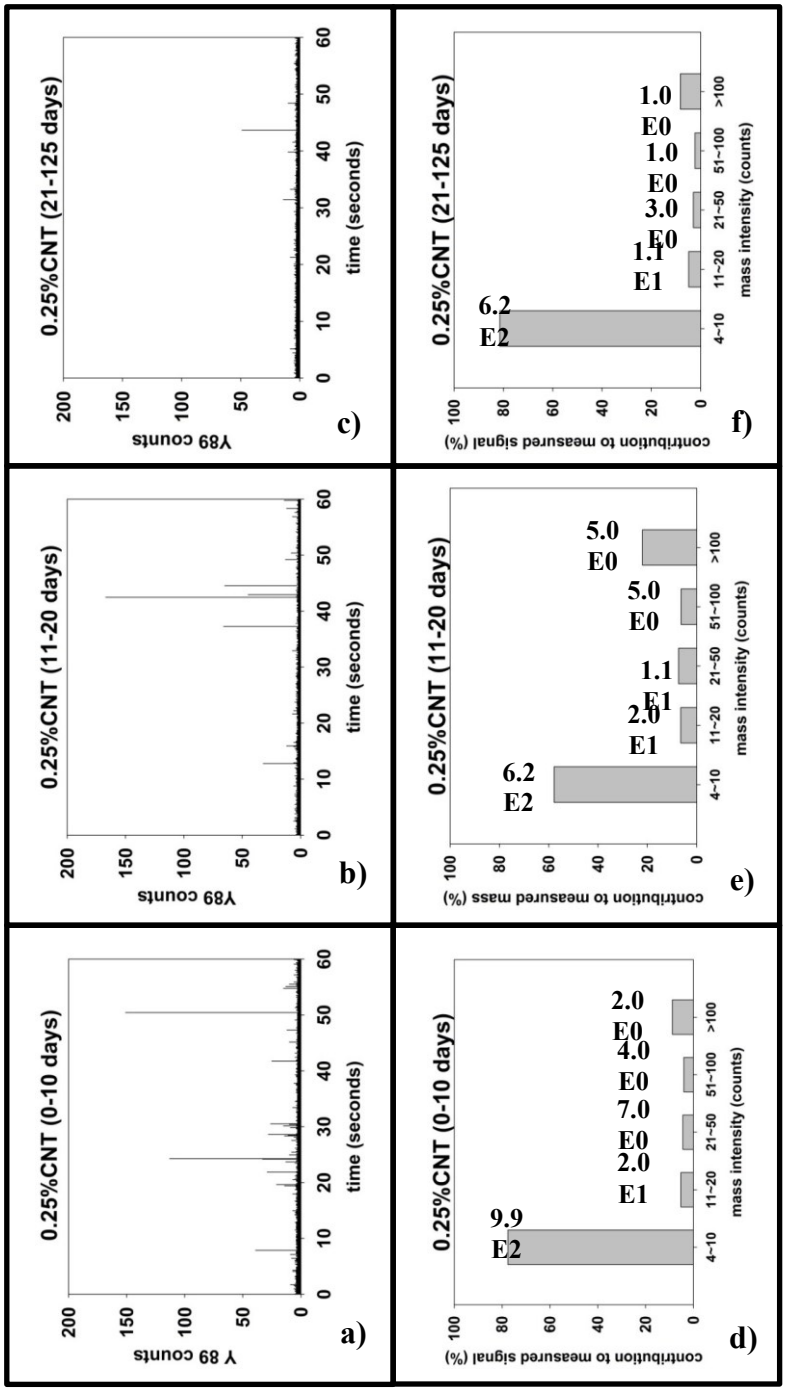


**Figure 2-17**: (a), (b), (c) Raw sp-ICP-MS data collected for 0.25%CNT nanocomposites with increasing duration of UVC exposure. (d), (e), (f) Y mass distribution for each period of exposure, with the corresponding number of particles detected noted above.

Described above was a detailed description of CNT-PNCs' changing surface morphology, structure, and composition as well as explicit characterization of released CNT material. With this information in hand, outlined below is a thorough discussion regarding how the addition of CNTs to a polymer matrix impacts rate and magnitude of photodegradation and CNT release.

Control Studies for PCL Photodegradation

(i) Ethyl cellulose (EC): EC was used as a natural surfactant to stabilize the CNTs in solution during nanocomposite preparation. Although EC was present in all of the nanocomposites, the weight percentage (7.5% w/w) was held constant regardless of the SWCNT loading, so that the effect of SWCNT loading could be isolated. To verify that the addition of EC had no measureable impact on the photodegradation process, control studies were conducted on PCL coupons prepared with and without EC (7.5% w/w). Results from these studies demonstrate that the addition of ethyl cellulose did not significantly alter the rate of photodegradation, with only a 5% difference in mass loss during the first 20 days of irradiation between PCL/EC and PCL samples (35.6% vs. 40.8%, respectively). Moreover, the photodegradation pathway, as determined by XPS (compare 2-11A to 2-11B and compare to 2-11C), ATR-FTIR, and SEM (Figure 2-8B and 2-8C), reveals that the same chemical and structural changes occurred following irradiation, irrespective of the presence of EC.

(ii) 300 nm vs. 254 nm Irradiation: Studies were also carried out in which PCL/EC samples were irradiated with 300 nm light (UVB). 300 nm light is on the edge of the ester group's absorption band (Figure 2-1) and also constitutes a small but measureable flux of photons (approximately 1.2%) reaching the earth[44], although the absolute flux reaching

the surface depends on the local climate . It was observed that PCL/EC photodegraded at 300 nm by cleavage and loss of the ester functionality (Figure 2-12D), albeit at a slower rate than at 254 nm, as found by mass loss measurements. Irradiation with 300 nm light also produced qualitatively similar changes in surface morphology to those observed following irradiation with 254 nm light (compare Figure 2-11B and 2-11D), although the spheres were smaller (< 200 nm in diameter), and far fewer were observed. These results support the idea that the use of 254 nm represents a form of accelerated photodegradation, mimicking the same degradation process that the polymer would experience in the natural environment.

Comparing power data collected by the UV-B Monitoring and Research Program[45], it was estimated that at 300nm the photochemical reactor used in this study accelerates photodegradation by a factor of approximately 100. Since experimental data indicates that the use of 254nm rather than 300nm light accelerates photodegradation by an addition factor of 10, it is estimated that an accelerated photodegradation rate on the order of $10^3$ as compared to "natural" outdoor conditions was produced.

PCL Photodegradation in the absence of CNTs

Poly-ε-caprolactone (PCL) $[-(CH_2)_5COO-]_n$ was selected as the polymer matrix because of its ability to form well dispersed CNT composites and its relative ease of photodegradation, the latter a consequence of its molecular composition, specifically the presence of photolabile ester groups. Additionally, PCL's ester group provides characteristic spectral features in both ATR-FTIR and XPS that allow for the extent of photodegradation to be quantified spectroscopically.

*Kinetics and Mechanism of Photodegradation*

To evaluate the effect of CNT inclusion, it is first necessary to understand the photodegradation of PCL in the absence of CNTs. Direct photoexcitation into the ester's n to $\pi^*$ band initiates PCL photodegradation and results in a 35% mass loss during the first 20 days of exposure (Figure 2-6). However, only 5% more mass loss was observed in the following 20 days of irradiation. For irradiation times in excess of 40 days, very little additional mass loss was observed, reaching a plateau of approximately 45% mass loss following 125 days of photolysis (Figure 2-6). XPS characterization of PCL/EC samples, measured as a function of irradiation time, reveal that the rate of mass loss is correlated with the relative concentration of ester groups in the near surface region, consistent with a Norrish Type II reaction (compare 2-11A to 2-11B, and observe spectral profile change in 2-12A ).[46] It is believed that the species lost during PCL photodegradation are hydrophilic carboxylic acid capped polymer fragments which have been previously identified as photoproducts in Norrish Type II photodegradation of PCL[46]; consistent with this assertion, gelatinous yellow polymeric material was observed to have been released into solution during the first 20 days of PCL photodegradation.

The depletion of the ester groups in the near surface region is even more convincingly demonstrated by the ATR-FTIR spectra shown in Figure 2-13A. This shows that following 125 days of irradiation the carbonyl stretching band associated with the ester group in PCL, along with peaks in the fingerprint region below 1500 $cm^{-1}$, are both greatly diminished in intensity. In contrast, the C-H stretching region stretching intensity remains nearly unchanged. Close inspection of C-H stretching region (Figure 2-18) suggests the formation of alkene bonds following UVC exposure, an expected product of

the Norrish Type II reaction.[46] However, the change in peak profile is subtle and definitive absorption band assignment is not possible. Inspection of the difference spectra of each photodegraded sample (Figure 2-18), with respect to the unexposed PCL/EC spectrum makes the changes in the C-H stretching region more apparent and provides further evidence of alkene bond formation in the surface region following irradiation. In addition to mass loss and changes to the chemical bonding in the near surface region (< 2 μm), SEM imaging shows that photodegradation transforms the initially smooth PCL surface (Figure 2-8A) into one with a high concentration of spherical structures (Figure 2-8B).

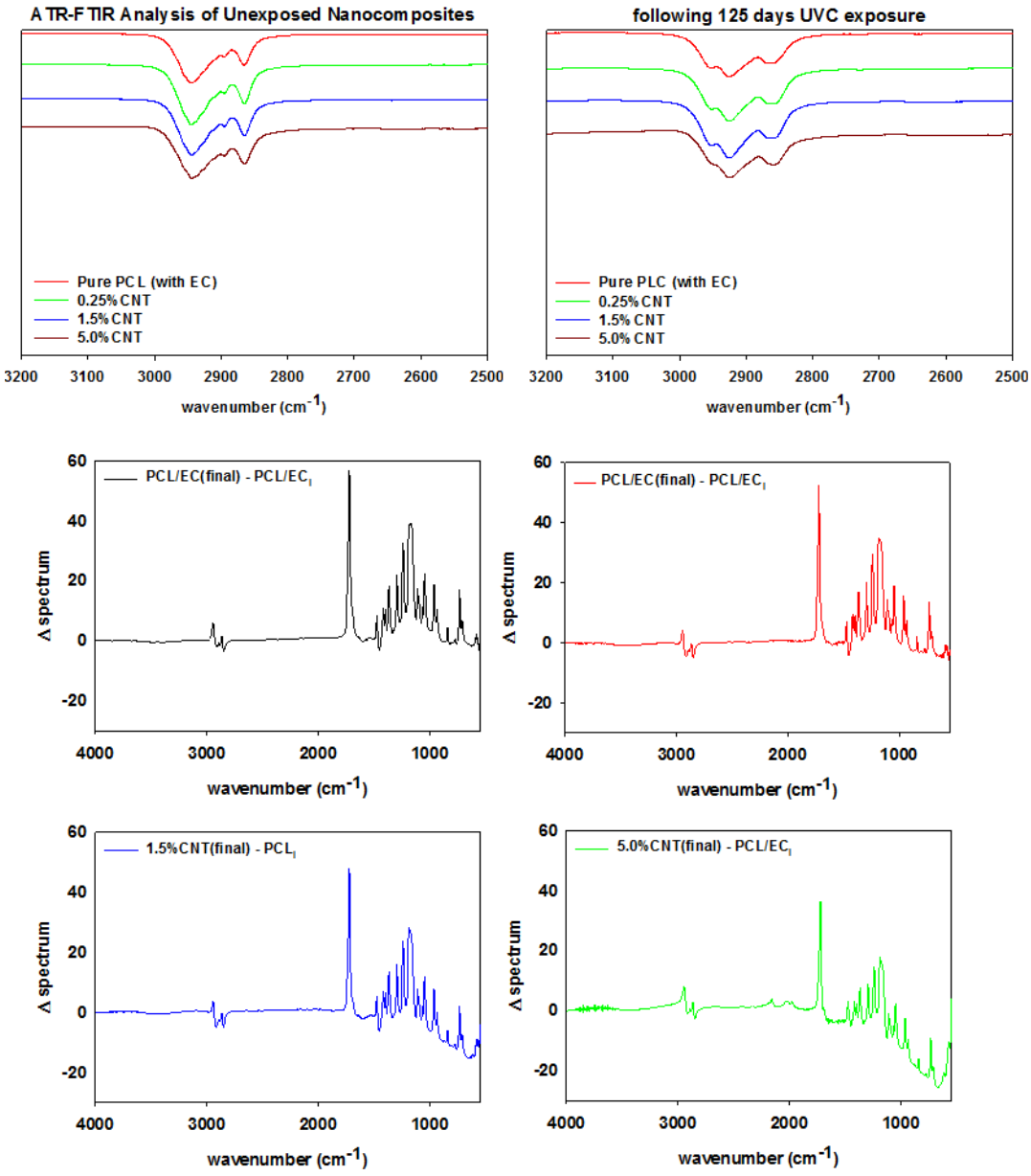


**Figure 2-18**: ATR-FTIR of all composites before and after exposure highlights similarity of finer spectral features among the nanocomposites (Top). Difference IR spectra for each exposed nanocomposite sample. Spectra is calculated by subtracting the unexposed PCL/EC spectra from the spectra collected after 125 days of UVC exposure, for each sample (bottom).

The combination of mass loss, XPS, and ATR-IR data supports the idea that the photodegradation of PCL/EC occurs through direct excitation and bond cleavage within the ester chromophore, leading initially to a rapid mass loss. As the photodegradation process proceeds, however, the ester group concentration in the near surface region decreases and a residual hydrocarbon rich layer builds up at the interface as the hydrophilic carboxylic acid capped fragments are released into solution. It is believed that the spherical nodules observed by SEM are a manifestation of these residual hydrocarbon structures, as the alkene end would experience a hydrophobic interaction and preferentially form a sphere with other hydrophobic fragments. The thickness of this hydrocarbon layer increases as the photolysis continues, leading to in a decrease in the concentration of ester groups within the near surface region that can be accessed/photolyzed by the incident irradiation. Ultimately, the hydrocarbon layer reaches a thickness that is comparable to the penetration depth of the light and at this stage, the photodegradation process and mass loss stop. This process of rapid initial polymer/PCL mass loss followed by the accumulation of a hydrocarbon layer is depicted pictorially in Figure 2-19.

Effect of CNT Incorporation on Photodegradation

To examine the impact of SWCNTs on the photodegradation process, SWCNT-PCL nanocomposites (PNCs) were produced with a range of SWCNT loadings (0.25%, 1.5%, and 5.0%, w/w). Analysis of the mass loss kinetics as well as the XPS and ATR-FTIR data reveals that at least qualitatively, similar changes occur to the SWCNT-PCL and PCL samples during photolysis. For example, XPS analysis of the 1.5% CNT sample (Figure 2-10) reveals that there is a rapid reduction in the ester groups present at the

surface during the first 20 days of exposure (Figure 2-10A). Thereafter, the concentration of ester groups in the near surface region (< 5nm) has been depleted and there is little subsequent change in surface composition (Figure 2-10B) and little to no additional mass loss (Figure 2-6). A similar depletion of ester groups at the surface within the first 20 days was observed for all nanocomposite samples (Figure 2-12), although XPS data indicates that the 5.0% CNT nanocomposite retained ester groups in the near surface (topmost 5 nm or so) layers for at least 40 days of irradiation (Figure 5-12D). Thus, the experimental data points towards a photodegradation process that still proceeds through a Norrish Type II pathway, regardless of the presence of CNTs, mediated by the photolabile ester groups in the near surface region.

Although the photodegradation mechanism is insensitive to the presence of CNTs, the extent of photodegradation is highly sensitive to the presence of CNTs. As seen in Figure 2-6, the addition of just 0.25% CNT reduces the total mass loss of the nanocomposite to half that of the CNT-free polymer. Similarly, for higher CNT loadings of 1.5% CNT and 5.0% CNT, the extent of polymer mass loss following 125 days of exposure is limited to just 10.5% and 7.3% of the initial nanocomposite mass, respectively. The ATR-FTIR spectra in Figure 2-13A show that after 125 days of photolysis, where photodegradation has ceased for all of the samples, the concentration of PCL in the near surface region (< 2 μm), as observed by PCLs' characteristic ester stretch at 1720 $cm^{-1}$, increases systematically as the CNT loading increases. This suggests that the reason for the reduction in mass loss observed as CNT loading increases is because CNTs reduce the effective depth of UV penetration and consequently the extent of polymer degradation. This is supported by the C(1s) data (Figure 5-12D), which shows

that for the highest loading nanocomposite, 5.0% CNT, there is evidence of ester groups still being present in the uppermost surface layers (< 5 nm depth) after 20 days of irradiation. In contrast, XPS analysis shows no evidence of ester groups being present for any of the other lower CNT loadings or the pure PCL after similar periods of irradiation.

Experimental data also supports the idea that the metal nanoparticles associated with the CNTs do not alter the photodegradation mechanism (Norrish Type II reaction). Thus, the diminishment of spectral features in both XPS and ATR-FTIR indicate that the introduction of CNTs (and associated metal catalysts) reduce the depth of photolysis. However, there is no spectroscopic evidence of new features emerging as a result of a secondary degradation process driven by the presence of the metal catalysts. Additionally, TEM imaging reveals that the metal nanoparticles are encapsulated by carbonaceous material (Figure 2-2A and Figure 2-14A), preventing direct contact of the metal nanoparticles to either the polymer matrix or water/dissolved oxygen molecules that could generate reactive oxygen species. Thus, any impact the metal nanoparticles may have on photodegradation would seem to be limited to light attenuation and as such this would be spectroscopically indistinguishable from the impact of the CNTs.

A more detailed analysis of the relationship between mass loss and polymer degradation (Figure 2-13B) reveals that after 125 days of UVC exposure, the measured mass loss and the fractional decrease in carbonyl peak area both exhibit a very similar decrease as a function of the CNT loading. Moreover, Figure 2-13C reveals that a linear correlation exists between mass loss and the fractional decrease of carbonyl area, both measured after 125 days. The discovery of such a correlation between these two independently determined quantities provides strong support for the idea that the

attenuation of mass loss observed upon CNT addition is a consequence of a "shading effect" caused by the CNTs absorbing UVC, reducing the effective penetration depth of the photolyzing radiation, and thus the extent of polymer mass loss. The idea that the CNTs are acting as photon absorbers/scatters is also supported by the observation that mass loss decreases exponentially with increased CNT loading/concentration, consistent with the Beer-Lambert law for light attenuation in the presence of a chromophore.

CNT Release vs. Retention

The detection and quantification of SWCNTs released during photolysis is accomplished with sp-ICP-MS, using embedded Y nanoparticles (Figure 5- 14A and 5-14B), residual from their use as a catalyst during SWCNT production, as a proxy for CNTs [29-30]. The integrated $^{89}Y$ signal from well dispersed SWCNTs suspensions is proportional to the SWCNT mass concentration (Figure 2-5). This linear relationship between $^{89}Y$ signal and SWCNT concentration allows us to determine mass of SWCNTs released from the nanocomposites at different stages of photolysis. In addition, analysis of the distribution of $^{89}Y$ pulse intensities allows us to determine the form of released SWCNTs (individual SWCNTs vs. aggregates).

Figure 2-15A shows the total mass of CNT released from a CNT-PNC generally increases with the initial CNT loading, with the 5.0% CNT samples releasing over eight times the mass of CNTs as compared to the 0.25% CNT samples following 125 days of irradiation. However, although CNTs are released as the polymer nanocomposites photodegrade, a comparison of Figures 2-15A and 2-15B indicates that for the 5.0% CNT and 0.25% CNT samples, CNTs are lost at a significantly lower rate than the polymer. This observation is also summarized in Table 2-1, where it is quantitatively clear that

compared to mass of polymer lost the CNTs are releasing to lesser extent than predicted, based on their initial loading. For the 5.0% CNT this preferential CNT retention is clearly evinced by SEM images (Figure 2-7), which reveal that a dense CNT mat has formed at the surface after 20 days of photolysis while no CNTs were observed at the surface prior to irradiation. This observation is similar to CNT surface aggregation observed in previous studies. [10, 21, 37-39] The absence of visible CNTs on the surface of the 0.25% CNT and 1.5% CNT samples following photolysis is attributed to both their lower initial CNT concentration and the accumulation of hydrophobic capped polymer fragments, which occurs as a consequence of PCL photodegradation.

The preferential retention of SWCNTs during photodegradation is attributed to the SWCNTs' high aspect ratio (1.4 – 1.6 nm in diameter as determined by Raman spectra shown in Figure 2-3 and up to 3 μm long, as reported by the manufacturer). This facilitates an anchoring effect because many SWCNTs in the near surface region that experiences photolysis will still have some fraction embedded within the bulk of the nanocomposites. Additionally, CNT entanglement of anchored CNTs to surface confined CNTs will further restrain CNTs to the surface of the nanocomposite. The net result is a preferential retention of SWCNTs in the interfacial regions, as shown in Figure 2-19.

The kinetics of CNT mass loss from the CNT-PNCs qualitatively mirrors the mass loss kinetics for the polymer (comparing Figure 2-15A and Figure 2-6, respectively). Thus, following the first 20 days of exposure, as polymer mass loss begins to plateau (Figure 2-6), the rate of CNT release is abated as well. This similarity in behavior supports the idea that degradation of the surrounding polymer matrix is the principal means of CNT release from the PNCs as seen for other CNT-polymer

nanocomposites. [9] For the 5.0% CNT sample, Figure 2-6A shows that once the CNT mat has formed there is almost no further measureable CNT mass loss, highlighting the photostability of this structure and also that the metal nanoparticles remain attached to the CNTs.

Form of released CNTs

The integrated $^{89}Y$ signal in sp-ICP-MS reflects the mass loss of CNTs that occurs during polymer photodegradation. As a complement to this information, analysis of $^{89}Y$ pulse distribution can provide insight into the form of released CNT (individual CNTs vs. aggregates of CNT contained in polymer fragments): thus, pulse binning of sp-ICP-MS data obtained from reference samples of 1ppb SWCNT suspensions (Figure 2-14C) shows that 48% of the measured mass is from CNTs yielding 4-10 $^{89}Y$ counts. The contribution to total measured mass quickly drops off with increasing pulse bin intensity, with no other pulse bin contributing more than 20% of total measured mass. Furthermore, only 20 CNTs (of 4572 total particles detected) were found to yield $^{89}Y$ pulses with intensities greater than 100 $^{89}Y$ counts. This analysis of well dispersed SWCNTs provides a "baseline" for the $^{89}Y$ pulse intensity distribution and establishes that individual SWCNTs are most likely to yield a signal of 4-10 $^{89}Y$ counts when detected with sp-ICP-MS. In contrast, large aggregates of CNTs will produce much larger pulse heights as they will contain many more Y nanoparticles.

Examination of the measured $^{89}Y$ pulses (Figure 2-16A) and $^{89}Y$ pulse distribution (Figure 2-16D) from the 5.0% CNT during the initial 10 day period of photolysis and SWCNT release is in stark contrast to the pulse distribution found from individually suspended SWCNTs (Figure 2-14C). Of 7668 total particles detected, 474

particles were detected with a $^{89}Y$ pulse intensity greater than 100 $^{89}Y$ counts; of those particles, 206 particles yielded a pulse intensity greater than 200 $^{89}Y$ counts and 32 particles were detected with greater than 500 $^{89}Y$ counts (data not explicitly depicted within figure). Additionally, the 474 particles with pulse intensities greater than 100 $^{89}Y$ counts account for 66% of the total measured CNT mass released during the first 10 day period of exposure, the latter measured by the integrated $^{89}Y$ signal. From the contrasting pulse intensity distributions, it is suggested that the 5.0% CNT sample released large CNT-containing fragments during the initial stage of photolysis, when mass loss (Figure 2-6) and photolysis (Figure 2-10, 2-12) are most rapid. Comparing the dominant pulse intensity of well dispersed SWCNTs (4-10 $^{89}Y$ counts) to the dominant pulse intensity of released material (100-500 $^{89}Y$ counts) suggests these released fragments contained anywhere from about 10-125 CNTs. These CNTs are most likely being released embedded in polymer fragments rather than as CNT bundles because, prior to sp-ICP-MS analysis, all samples are spiked with dilute surfactant and sonicated for 30 minutes, in the same way that the suspensions of CNT powder are prepared. Such a treatment would therefore be expected to debundle CNT aggregates but would not loosen CNTs embedded in polymer fragments.

During the next 10 days of polymer mass loss and degradation, CNT release from the 5.0% CNT nanocomposite continues. However as seen in Figure 2-15A the overall mass of CNTs released during this period of exposure (7.30 +/-1.79μg) is significantly smaller than released initially (24.48 +/-7.42μg). Additionally, it was observed that the form of released SWCNTs change during this intermediate period of irradiation. The overall pulse data in Figure 2-16B shows particles with fewer CNTs/particle being

released as compared to the first 10 days of irradiation (Figure 2-16A). Quantitatively (Figure 2-16E), this is reflected by the pulse intensity now being centered on particles of 11 – 20 $^{89}$Y counts (contributing to 40% of the total measured mass), with very similar contributions to the total mass measured from particles of 4 – 10 $^{89}$Y counts and 21 – 50 $^{89}$Y counts. From this, it was deduced that fewer CNTs are embedded in polymer fragments releasing from the surface than before. This may simply be a reflection of smaller polymer fragments being released. Alternatively, it is noted that the relative rate of CNT to polymer release decreases in this time interval (compare Figure 2-15A and 2-15B) and this change in pulse intensity distribution may reflect a greater degree of CNT retention due to increased CNT concentration and connectivity in the near surface region. During the final period of exposure, from 21 – 125 days, where the CNT mat has formed, Figure 2-15A reveals that there is very little CNT loss (3.7 μg), despite the continued loss of a small but measureable amount of polymer (Figure 2-6). Additionally, it was observed that the pulse distribution is largely made up of particles of 4-10 $^{89}$Y counts, accounting for 92% of the total mass measured (Figure 2-16F). This suggests that any released CNTs are in the form of individual CNT particles, although it is now not possible to determine if they are still embedded in polymeric fragments. The progression of CNT released-form as described above for PNCs with high initial CNT concentrations, as a function of duration of photolysis, is shown in Figure 2-19.

For the 0.25% CNT sample, the $^{89}$Y pulse distribution during the first 10 days of photolysis (Figure 2-17D) yields pulses with predominantly 4-10 $^{89}$Y counts, in contrast to the 5.0% CNT sample. In fact, it was observed that 4-10 $^{89}$Y counts is the dominant pulse distribution of released material for all three periods of photolysis and release

(Figures 2-17D, 2-17E, and 2-17F). Since the experimental evidence indicates that the nanocomposites degrade through the same mechanism, irrespective of CNT loading, it is asserted that the fragments of polymer released will likely be of comparable physical dimensions. From this, it follows that since the 0.25% CNT sample possesses $1/20^{th}$ the initial CNT concentration as the 5.0% CNT sample, there would be on average $1/20^{th}$ the number of CNTs released in each polymer fragment. As a result, during the first 10 days of photolysis, when SWCNT mass release is greatest, this would shift the pulse distribution to one where $^{89}Y$ pulses in the 4-10 range dominate, as observed experimentally in Figure 2-17D. Thus, the $^{89}Y$ pulse distribution and its invariance to irradiation time is simply a reflection of the fewer SWCNTs present in the 0.25% CNT sample when compared to the 5.0% CNT sample. The contrast in the behavior of the 0.25% CNT and 5.0% CNT sample does, however, demonstrate that nanocomposites with higher CNT loadings will likely exhibit greater variance in the form and number of released CNTs as they photodegrade, as shown in Figure 2-19.

Although the detailed nature of polymer photodegradation processes are often complex and system specific, they are typically initiated by photon absorption.[47] Consequently, these findings suggest that the presence of both SWCNTs and MWCNTs will decrease the extent of polymer photodegradation in other polymer CNT nanocomposites by virtue of their ability to absorb incoming light over a wide range of wavelengths.[31] In addition to the decrease in polymer mass loss, another important consequence of this "shielding effect" is that the total number of CNTs released during PNC photodegradation will not vary in direct proportion to the CNT loading. Thus, although the absolute CNT mass loss will increase with CNT loading, the fraction of

CNTs released from a CNT-PNC will decrease as the CNT loading increases as is seen Table 2-1. It is postulated that similar "shading" effects will be operative for other nanoparticles/polymer additives such as fullerenes, graphene and carbon fibers.[48] It is expected that the mechanism by which CNTs mitigate polymer photodegradation (through their shading effect), including the functional dependence on CNT loading, to be conserved amongst different polymer/CNT systems. The absolute magnitude of the retardation effect exerted by CNTs, however will be system specific due to differences in both the wavelength of light responsible for polymer photodegradation and a given polymer matrix's overall susceptibility to both photodegradation and indirect effects such

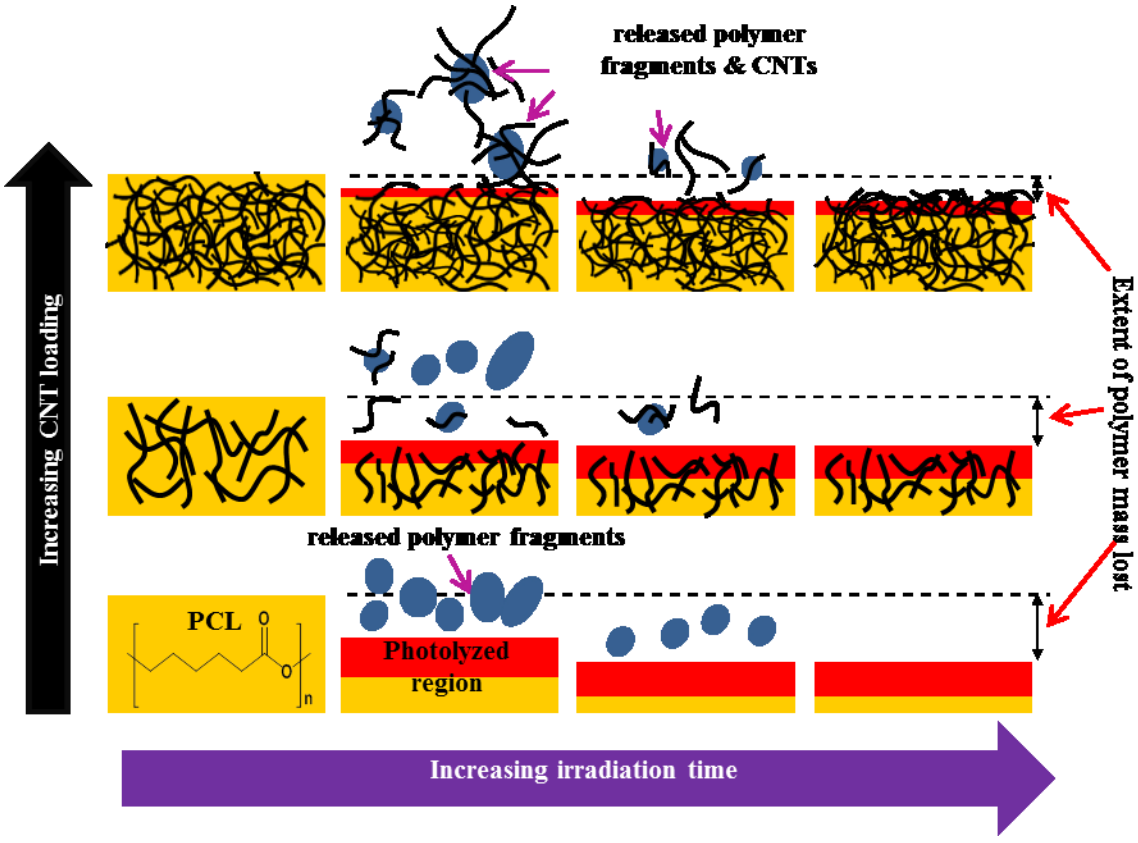


**Figure 2-19**: Depiction of how both the interface of polymer-CNT nanocomposites and the nature of release fragments evolve as photodegradation proceeds, shown as a function of CNT loading.

as increased temperature of black composites under irradiation lamps. It is also expected that polymer fragments containing multiple CNTs will be prevalent during the initial stages of photodegradation, particularly for PNCs with higher CNT loadings. Additionally, photodegradation and release will also be regulated by exposed surface area. Consequently, when small PNC fragments, such as those released during an abrasion process are weathered, they will release more CNTs as compared to the original material of the same volume, by virtue of their increased surface area. However, CNTs contained within such fragments will still inhibit the extent of photodegradation by the same mechanism.

**Conclusions**

To better understand the effect that CNT inclusion has on polymer photodegradation, an experimental approach was taken that photodegraded CNT-PCL polymer nanocomposites that contained a range of initial CNT loadings (0%-5% w/w) under accelerated photodegradation conditions, monitoring changes to the polymer and correlating these changes to the extent, rate, and form of released CNTs. Through spectroscopic characterization (ATR-FTIR and XPS) and mass loss measurements of the CNT-PNCs, it was determined that PCL's principle route of photolysis, cleavage of ester groups in the polymer backbone, occurs regardless of the presence or absence of CNTs. However, while the mechanism of photodegradation is invariant to the presence of CNTs, the extent of polymer photodegradation systematically decreases with increasing initial CNT loading. This inhibition of polymer degradation is attributed to be a consequence of the CNTs' light absorbing/scatting properties. The kinetics of CNT release during polymer photodegradation mirrors polymer mass loss, although CNTs are preferentially

retained in the CNT-PNC matrix. For CNT-PNCs of sufficiently high initial CNT loading (5%), sp-ICP-MS revealed that multiple CNTs are principally released embedded in photodegraded polymer fragments. As the rate of CNT-PNC mass loss decreases, the rate and magnitude of CNT release decreases as well, due to both increased attenuation of light by CNTs accumulating in the near surface region and the simultaneous accumulation of a hydrocarbon layer resulting from PCL photolysis. These results indicate that the fractional release of CNTs as well as the extent of polymer photodegradation will decrease as the CNT loading increases.

**Acknowledgments**

Work described above was a collaborative effort between the labs of Prof. Howard Fairbrother and Prof. James Ranville. Irradiation experiments and all PNC characterization was carried out by the author of this text, Ronald S. Lankone. spICP-MS measurements were carried out by Jingjing Wang, under the supervision of her advisor, Prof. James Ranville.

## References


1. De Volder, M. F. L.; Tawfick, S. H.; Baughman, R. H.; Hart, A. J., Carbon Nanotubes: Present and Future Commercial Applications. *Science* **2013,** *339* (6119), 535.
2. Kausar, A.; Rafique, I.; Muhammad, B., Review of Applications of Polymer/Carbon Nanotubes and Epoxy/CNT Composites. *Polymer-Plastics Technology and Engineering* **2016,** *55* (11), 1167-1191.
3. Kuhlbusch, T. A. J.; Asbach, C.; Fissan, H.; Göhler, D.; Stintz, M., Nanoparticle exposure at nanotechnology workplaces: A review. *Particle and Fibre Toxicology* **2011,** *8*, 22-22.
4. Muller, J.; Huaux, F.; Moreau, N.; Misson, P.; Heilier, J.-F.; Delos, M.; Arras, M.; Fonseca, A.; Nagy, J. B.; Lison, D., Respiratory toxicity of multi-wall carbon nanotubes. *Toxicology and Applied Pharmacology* **2005,** *207* (3), 221-231.
5. Fent, K., Ecotoxicology of Engineered Nanoparticles. In *Nanoparticles in the Water Cycle: Properties, Analysis and Environmental Relevance*, Frimmel, H. F.; Niessner, R., Eds. Springer Berlin Heidelberg: Berlin, Heidelberg, 2010; pp 183-205.
6. Kostarelos, K., The long and short of carbon nanotube toxicity. *Nat Biotech* **2008,** *26* (7), 774-776.
7. Peralta-Videa, J. R.; Zhao, L.; Lopez-Moreno, M. L.; de la Rosa, G.; Hong, J.; Gardea-Torresdey, J. L., Nanomaterials and the environment: A review for the biennium 2008–2010. *Journal of Hazardous Materials* **2011,** *186* (1), 1-15.
8. Tinh, N.; Wendel, W.; Lipiin, S., Mechanisms of Aging and Release from Weathered Nanocomposites. In *Safety of Nanomaterials along Their Lifecycle*, CRC Press: 2014; pp 315-334.
9. Duncan, T. V., Release of Engineered Nanomaterials from Polymer Nanocomposites: the Effect of Matrix Degradation. *ACS Applied Materials & Interfaces* **2015,** *7* (1), 20-39.
10. Nguyen, T.; Pellegrin, B.; Bernard, C.; Gu, X.; Gorham, J. M.; Stutzman, P.; Stanley, D.; Shapiro, A.; Byrd, E.; Hettenhouser, R.; Chin, J., Fate of nanoparticles during life cycle of polymer nanocomposites. *J Phys: Conf Ser* **2011,** *304*.
11. Kingston, C.; Zepp, R.; Andrady, A.; Boverhof, D.; Fehir, R.; Hawkins, D.; Roberts, J.; Sayre, P.; Shelton, B.; Sultan, Y.; Vejins, V.; Wohlleben, W., Release characteristics of selected carbon nanotube polymer composites. *Carbon* **2014,** *68*, 33-57.
12. Chin, J. E., Ned ; Garver, J.; Dickens, B.; Finn, T.; Martin, J. W., Accelerated UV weathering device based on integrating sphere technology. *Review of scientific instruments* **2004,** *75* (11), 8.
13. Petersen, E. J.; Lam, T.; Gorham, J. M.; Scott, K. C.; Long, C. J.; Stanley, D.; Sharma, R.; Alexander Liddle, J.; Pellegrin, B.; Nguyen, T., Methods to assess the impact of UV irradiation on the surface chemistry and structure of multiwall carbon nanotube epoxy nanocomposites. *Carbon* **2014,** *69*, 194-205.
14. Hirth, S.; Cena, L.; Cox, G.; Tomović, Ž.; Peters, T.; Wohlleben, W., Scenarios and methods that induce protruding or released CNTs after degradation of nanocomposite materials. *Journal of Nanoparticle Research* **2013,** *15* (4), 1-15.
15. Vilar, G.; Fernández-Rosas, E.; Puntes, V.; Jamier, V.; Aubouy, L.; Vázquez-Campos, S., Monitoring migration and transformation of nanomaterials in polymeric composites during accelerated aging. *Journal of Physics: Conference Series* **2013,** *429* (1), 012044.
16. V. Pillai, K.; Gray, P. J.; Tien, C.-C.; Bleher, R.; Sung, L.-P.; V. Duncan, T., Environmental release of core-shell semiconductor nanocrystals from free-standing polymer nanocomposite films. *Environmental Science: Nano* **2016,** *3* (3), 657-669.
17. Wohlleben, W.; Meier, M. W.; Vogel, S.; Landsiedel, R.; Cox, G.; Hirth, S.; Tomovic, Z., Elastic CNT-polyurethane nanocomposite: synthesis, performance and assessment of fragments released during use. *Nanoscale* **2013,** *5* (1), 369-380.
18. Rhiem, S.; Barthel, A.-K.; Meyer-Plath, A.; Hennig, M. P.; Wachtendorf, V.; Sturm, H.; Schäffer, A.; Maes, H. M., Release of 14C-labelled carbon nanotubes from polycarbonate composites. *Environmental Pollution* **2016,** *215*, 356-365.
19. Schlagenhauf, L.; Nüesch, F.; Wang, J., Release of Carbon Nanotubes from Polymer Nanocomposites. *Fibers* **2014,** *2* (2), 108-127.

20. Vilar, G.; Fernández-Rosas, E.; Puntes, V.; Jamier, V.; Aubouy, L.; Vázquez-Campos, S., Monitoring migration and transformation of nanomaterials in polymeric composites during accelerated aging. *J Phys: Conf Ser* **2013,** *429*, 012044.
21. Wohlleben, W.; Brill, S.; Meier, M. W.; Mertler, M.; Cox, G.; Hirth, S.; von Vacano, B.; Strauss, V.; Treumann, S.; Wiench, K.; Ma-Hock, L.; Landsiedel, R., On the lifecycle of nanocomposites: comparing released fragments and their in-vivo hazards from three release mechanisms and four nanocomposites. *Small* **2011,** *7* (16), 2384-95.
22. Wohlleben, W.; Neubauer, N., Quantitative rates of release from weathered nanocomposites are determined across 5 orders of magnitude by the matrix, modulated by the embedded nanomaterial. *NanoImpact* **2016,** *1*, 39-45.
23. Petersen, E. J.; Flores-Cervantes, D. X.; Bucheli, T. D.; Elliott, L. C. C.; Fagan, J. A.; Gogos, A.; Hanna, S.; Kägi, R.; Mansfield, E.; Bustos, A. R. M.; Plata, D. L.; Reipa, V.; Westerhoff, P.; Winchester, M. R., Quantification of Carbon Nanotubes in Environmental Matrices: Current Capabilities, Case Studies, and Future Prospects. *Environmental Science & Technology* **2016,** *50* (9), 4587-4605.
24. Attal, S.; Thiruvengadathan, R.; Regev, O., Determination of the Concentration of Single-Walled Carbon Nanotubes in Aqueous Dispersions Using UV−Visible Absorption Spectroscopy. *Analytical Chemistry* **2006,** *78* (23), 8098-8104.
25. Porter, A. E.; Gass, M.; Muller, K.; Skepper, J. N.; Midgley, P. A.; Welland, M., Direct imaging of single-walled carbon nanotubes in cells. *Nat Nano* **2007,** *2* (11), 713-717.
26. Schierz, A.; Parks, A. N.; Washburn, K. M.; Chandler, G. T.; Ferguson, P. L., Characterization and Quantitative Analysis of Single-Walled Carbon Nanotubes in the Aquatic Environment Using Near-Infrared Fluorescence Spectroscopy. *Environmental Science & Technology* **2012,** *46* (22), 12262-12271.
27. Schierz, A.; Espinasse, B.; Wiesner, M. R.; Bisesi, J. H.; Sabo-Attwood, T.; Ferguson, P. L., Fate of single walled carbon nanotubes in wetland ecosystems. *Environmental Science: Nano* **2014,** *1* (6), 574-583.
28. Schlagenhauf, L.; Buerki-Thurnherr, T.; Kuo, Y.-Y.; Wichser, A.; Nüesch, F.; Wick, P.; Wang, J., Carbon Nanotubes Released from an Epoxy-Based Nanocomposite: Quantification and Particle Toxicity. *Environmental Science & Technology* **2015,** *49* (17), 10616-10623.
29. Reed, R. B.; Goodwin, D. G.; Marsh, K. L.; Capracotta, S. S.; Higgins, C. P.; Fairbrother, D. H.; Ranville, J. F., Detection of single walled carbon nanotubes by monitoring embedded metals. *Environmental science. Processes & impacts* **2013,** *15* (1), 204-13.
30. Wang, J.; Lankone, R. S.; Reed, R. B.; Fairbrother, D. H.; Ranville, J. F., Analysis of single-walled carbon nanotubes using spICP-MS with microsecond dwell time. *NanoImpact* **2016,** *1*, 65-72.
31. Rance, G. A.; Marsh, D. H.; Nicholas, R. J.; Khlobystov, A. N., UV–vis absorption spectroscopy of carbon nanotubes: Relationship between the π-electron plasmon and nanotube diameter. *Chemical Physics Letters* **2010,** *493* (1–3), 19-23.
32. Bandow, S.; Asaka, S.; Saito, Y.; Rao, A. M.; Grigorian, L.; Richter, E.; Eklund, P. C., Effect of the Growth Temperature on the Diameter Distribution and Chirality of Single-Wall Carbon Nanotubes. *Physical Review Letters* **1998,** *80* (17), 3779-3782.
33. Sahoo, N. G.; Rana, S.; Cho, J. W.; Li, L.; Chan, S. H., Polymer nanocomposites based on functionalized carbon nanotubes. *Progress in Polymer Science* **2010,** *35* (7), 837-867.
34. Hatchard, C. G.; Parker, C. A., A New Sensitive Chemical Actinometer. II. Potassium Ferrioxalate as a Standard Chemical Actinometer. *Proceedings of the Royal Society of London. Series A. Mathematical and Physical Sciences* **1956,** *235* (1203), 518.
35. Pace, H. E.; Rogers, N. J.; Jarolimek, C.; Coleman, V. A.; Higgins, C. P.; Ranville, J. F., Determining transport efficiency for the purpose of counting and sizing nanoparticles via single particle inductively coupled plasma mass spectrometry. *Anal Chem* **2011,** *83* (24), 9361-9.
36. Bernard, C.; Nguyen, T.; Pellegrin, B.; Holbrook, R. D.; Zhao, M.; Chin, J., Fate of graphene in polymer nanocomposite exposed to UV radiation. *Journal of Physics: Conference Series* **2011,** *304* (1), 012063.
37. Nguyen, T.; Pellegrin, B.; Mermet, L.; Shapiro, A.; Gu, X.; Chin, J., Network aggregation of CNTs at the surface of epoxy/MWCNT composite exposed to UV radiation. *Nanotechnology* **2009,** *1*, 90-93.

38. Ging, J.; Tejerina-Anton, R.; Ramakrishnan, G.; Nielsen, M.; Murphy, K.; Gorham, J. M.; Nguyen, T.; Orlov, A., Development of a conceptual framework for evaluation of nanomaterials release from nanocomposites: Environmental and toxicological implications. *Science of The Total Environment* **2014,** *473–474*, 9-19.
39. Hirth, S.; Cena, L.; Cox, G.; Tomovic, Z.; Peters, T.; Wohlleben, W., Scenarios and methods that induce protruding or released CNTs after degradation of nanocomposite materials. *J Nanopart Res* **2013,** *15*.
40. Schlagenhauf, L.; Kianfar, B.; Buerki-Thurnherr, T.; Kuo, Y.-Y.; Wichser, A.; Nuesch, F.; Wick, P.; Wang, J., Weathering of a carbon nanotube/epoxy nanocomposite under UV light and in water bath: impact on abraded particles. *Nanoscale* **2015,** *7* (44), 18524-18536
41. Elzein, T.; Nasser-Eddine, M.; Delaite, C.; Bistac, S.; Dumas, P., FTIR study of polycaprolactone chain organization at interfaces. *Journal of Colloid and Interface Science* **2004,** *273* (2), 381-387.
42. Fractional decrease in ester band area of a given sample is determined by the quotient of the ester band area of unexposed PCL/EC over the ester band area of the sample (COOi/COOf ). Following this convention, an unphotolyzed sample will yield a value of 1 and with increasing loss of ester band area, the value will increase.
43. Taylor, J. R., *An Introduction to Error Analysis, The Study of Uncertainties in Physical Measurements* 2nd ed.; University Science Books Sausalito, CA, 1997.
44. Iqbal, M., Chapter 3 - THE SOLAR CONSTANT AND ITS SPECTRAL DISTRIBUTION. In *An Introduction to Solar Radiation*, Academic Press: 1983; pp 43-58.
45. UV-B Monitoring and Research Program. http://uvb.nrel.colostate.edu/UVB/index.jsf (accessed Feb. 10th).
46. Ikada, E., Photo decomposition of Aliphatic Polyesters. V. *Journal of Photopolymer Science and Technology* **1998,** *11* (1), 23-27.
47. Rabek, J. F., *Photodegradation of Polymers: Physical Characteristics and Applications*. Springer: Germany, 1996; p 212.
48. Wohlleben, W.; Meyer, J.; Muller, J.; Muller, P.; Vilsmeier, K.; Stahlmecke, B.; Kuhlbusch, T. A. J., Release from nanomaterials during their use phase: combined mechanical and chemical stresses applied to simple and multi-filler nanocomposites mimicking wear of nano-reinforced tires. *Environmental Science: Nano* **2016,** *3* (5), 1036-1051.

**Chapter 3.** Development and Application of a Methodology for Quantifying Engineered Nanomaterial Release from Diverse Product Matrices Under Outdoor Weathering Conditions and Implications for Life Cycle Assessment

Reproduced from

Lankone, R. S.; Challis, K. E.; Bi, Y.; Hanigan, D.; Reed, R. B.; Zaikova, T.; Hutchison, J. E.; Westerhoff, P.; Ranville, J.; Fairbrother, H.; Gilbertson, L. M., Methodology for quantifying engineered nanomaterial release from diverse product matrices under outdoor weathering conditions and implications for life cycle assessment. Environmental Science: Nano 2017, 4 (9), 1784-1797.

**Abstract**

Accurate measurement of engineered nanomaterial (ENM) release from diverse product lines and matrices during use is critical to evaluating environmental impacts across the life cycle of a nano-enabled product. While indoor, accelerated weathering and a handful of outdoor weathering case studies exist, there has not been a standard methodology applied to characterize ENM release during outdoor weathering suitable for simultaneous use in multiple geographic locations. Such an approach has been established and is presented herein, to quantify ENM release and product transformations with the additional goal of improving life cycle impact assessments (LCIA) of nano-enabled products. A team of experimentalists and life cycle practitioners engaged in the development of the methodology to ensure the data collected is useful to inform improved LCIA and environmental impact characterization. While the method was developed to be broadly applicable, the examples included here are representative polymer nanocomposite (PNC) platforms, including multiple ENMs (i.e., nano-silver and carbon nanotubes) within different polymer matrices (i.e., polystyrene, poly (methyl methacrylate), and polycaprolactone). This unique methodology enables the study of ENM release under real climate conditions (i.e., composites are weathered outside) that coordinates: (i) multiple locations with distinct climates, (ii) the application of appropriate techniques to quantify ENM release at low (μg) released masses, (iii) tracking changes in efficacy as a function of weathering, and (iv) acquiring data to inform life cycle impact assessment. Initial findings (following one year of weathering polymer matrices) are included to demonstrate the type of data acquired and utility of the analysis enabled by this method.

## Introduction

Significant research has been dedicated to characterizing the potential environmental and human health impacts associated with the incorporation of engineered nanomaterials (ENMs) into products. Impact characterization is predicated on having well-characterized material flows, including the release of ENMs from products across all life cycle stages. Knowing how much ENM is released, the time scale of release, and in what form (e.g., as an ion, surface modified or complex composite material) is the first step towards impact characterization that includes the nano-enabled product use phase. Release is additionally a critical component of regulatory evaluation since the demonstrated (or possibility of) release of a known or potentially hazardous substance makes exposure to humans and the environment a possibility.[1-2]

Life cycle impact assessment (LCIA) is a systems-level tool that is increasingly used as an approach to identify potential adverse impacts associated with the use of ENMs in consumer products and to inform their responsible development.[3-4] While release of ENMs can occur across the life cycle of a product, there are very few LCIA studies to date that include quantitative release data across *all* stages. This is in part due to lack of inventory data and characterization factors for ENMs as well as uncertainty surrounding release during the use and end-of-life stages.[5-7] The current approach to incorporating ENM release into impact assessment is based on informed assumptions, often a compilation of empirical and model estimations.[8-9] In a hypothetical scenario approach, best (e.g., 0% release) and worst (e.g., 100%) cases are evaluated to provide an upper and lower bound to the magnitude of a given impact.[8-10] While such approaches provide valuable insight into the contribution of ENM release to the magnitude of impact across

the product life cycle, there is increasing realization that empirically-derived release data, including quantity, physicochemical form, and rates, are needed to provide added realism to impact characterization. Since LCIA and experimental studies are often performed in isolation of each other, yet simultaneously rely heavily on one another, there is an urgent need for enhanced coordination of modeling and experimental research. Such a bridge between two distinct yet interdependent fields will further catalyze research aimed at safer nanotechnology development.[11]

When considering ENM release pathways, natural weathering of nano-enabled products such as building materials (e.g., concrete, wood, composites)[12], outdoor sporting equipment (e.g., water sports, skis, baseball bats)[13-14], and vehicles (e.g., cars, airplanes, buses) [15] should be considered, as it represents a principle route towards degradation and subsequent release during a product's lifetime. There are several approaches to examining the weathering of materials.[16] Indoor simulated or accelerated weathering[17] is the most common approach and is conducted in a controlled laboratory setting.[18-19] Outdoor weathering studies are less common, requiring more time, yet offer a more accurate representation of degradation and release caused by exposure to variable climate conditions.[20-26] Another approach is to combine laboratory and outdoor weathering to compare and contrast a materials' degradation in both settings.[27-31] However, to date, these combined studies have focused primarily on tracking changes in product/matrix properties and largely do not track and quantify ENM release. To specifically monitor ENM release, accelerated degradation protocols have been developed and applied to polymer nanocomposites (PNCs).[32] However, a recent review that examines the accelerated weathering of 27 ENM-containing polymers aptly points out that reported

release (in units of mg/MJ of light exposure) spans five orders of magnitude.[33] This wide range in ENM release values under accelerated conditions further complicates the prediction of release behavior under real world exposure conditions. There are only a handful of studies that examine ENM release from a substrate or composite under outdoor weathering conditions, including Cloisite 30B from polylactide[34], silver nanoparticles (AgNP) from paint[35], and titanium dioxide ($TiO_2$) from paint. [36] While these studies offer insight into the release characteristics of the studied ENM in the given matrix, they are carried out using different approaches that were tailored to their specific material of interest, thus limiting the global applicability and comparison of results across studies.

In addition to accounting for ENM release from products during weathering, characterization of product efficacy (i.e., how well the product provides the intended function) during weathering is also a key component to an LCIA (e.g., as it defines the useful product lifetime). One example is the incorporation of AgNPs in a matrix (e.g., polymer, textile) with the intended function of reducing microbial growth. The functional lifetime of this AgNP-enabled product will be defined by how long the microbial growth inhibition (i.e., efficacy) is sustained. A study by Reed, et al. demonstrated that nano-silver enabled textiles (specifically t-shirts) retain antimicrobial efficacy following successive washing cycles and down to only a few ppm silver content. [37] While the results indicate there is significant ENM release (a potential environmental impact), the product indeed maintains its efficacy (useful product lifetime).

The goal of the work described below is two-fold, (i) to establish a methodology for measuring ENM release from representative polymer composites that can be

implemented in any climate scenario, and (ii) to demonstrate the utility of the collected data (ENM release and product efficacy) to inform enhanced LCIA. The methodology is presented through implementation in three unique climate locations: Baltimore, MD, Golden, CO, and Tempe, AZ, with ongoing expansion to additional locations. Two different ENMs, AgNPs and carbon nanotubes (CNTs), embedded in three different polymer composites (polystyrene, poly (methyl methacrylate) and polycaprolactone) at multiple loadings 0.04%, 1.5%, and 2% (w/w) were weathered at all three locations. AgNP-textile samples were also weathered for two weeks to demonstrate the incorporation of measuring climate impacts on efficacy (i.e., antimicrobial activity). Quantities of released ENMs were expected to be small, on the order of several micrograms of release material per month, so appropriate analytical techniques, specifically inductively coupled plasma mass spectrometry (ICP-MS), were employed to accurately and reliably measure monthly release quantities. Results from the first year of data collection are included to demonstrate the variety of natural weathering and release data collected as well as the utility of unique analyses enabled by this method.

## Experimental Methods

### Nanomaterial and matrix selection

Silver nanoparticles (AgNPs) and carbon nanotubes (CNTs) were selected for this study because they constitute two of the top five most commonly used ENMs in consumer products[38-40] and AgNPs and CNTs have been found to have contrasting release behavior. AgNPs readily oxidize and thus, release silver ions[37, 41], while CNTs are relatively inert and are largely retained within their embedded polymer matrix.[42-43] The polymer matrices were chosen to represent commercial polymers (polystyrene (PS) and

poly methyl (methacrylate) (PMMA)), which degrade through photooxidative pathways (i.e. radical formation)[44-45] , as well as one with a greater propensity for photodegradation (poly caprolactone (PCL)), which photodegrades though a Norrish Type II pathway.[46] Sample matrices prepared in the lab were selected as initial test samples, as opposed to using commercial products, because only with lab prepared materials could the composition and physical characteristics (e.g., size, ENM mass loading) be well-controlled and varied. Details on PNC preparation can be found in the Appendix (Chapter 5). The prepared PNCs (circular 'coupons', approximately 1.5" in diameter) used in this study contain concentrations of embedded ENMs that are representative of those found in commercial products.

Characterization of polymer nanocomposites

The surface chemistry, morphology, and initial ENM concentration (loading) of the prepared composites were characterized using X-ray photoelectron spectroscopy (XPS), scanning electron microscopy (SEM), attenuated total internal reflectance Fourier transform infrared spectroscopy (ATR-FTIR), and inductively coupled plasma mass spectrometry (ICP-MS). XPS characterization was carried out prior to weathering in order to assess the initial chemical composition of the PNC surfaces (within the top ~5 nm of the sample surface). To complement the surface sensitivity provided by XPS, bulk sample acid digestion followed by ICP-MS quantification was carried out to measure the total initial Ag content of the 2% Ag-PS and 2% Ag-PMMA samples. A summary of the silver concentration measured by XPS and ICP-MS is provided in Table 3-1, along with a summary of macroscopic sample measurements such as PNC mass and surface area. While there is some variability in the silver initially present at the surface (3% - 6%, final

column, Table 3-1), the total amount of silver available for release (contained within the bulk) is consistent from batch to batch and across both Ag-PS and Ag-PMMA sample types, as measured by ICP-MS following sample digestion. Representative electron microscopy images, XPS, and ATR-FTIR spectra of Ag-PNC sample surfaces prior to weathering are shown in Figures 3-7, 3-8, 3-9, and 3-10, respectively. Spectra and imaging following the weathering of Ag-PNCs is shown in Figures 3-9 and 3-10, respectively. SWCNT-PNCs were also characterized before and after weathering and their ATR-FTIR spectra and SEM images are shown in Figures 3-9 and 3-11, respectively. Details of XPS, SEM, ATR-FTIR, and ICP-MS characterization procedures can also be found in the Appendix (Chapter 5).

Outdoor Weathering

*Site Selection*

Baltimore, MD (Johns Hopkins University), Golden, CO (Colorado School of Mines), and Tempe, AZ (Arizona State University) were selected as distinct climate locations for this study. The *Main Koppen-Gieger Climate Classes for US Counties* (Figure 3-1)[47] map confirms that each location has a unique climate with distinct precipitation and temperature patterns. Baltimore County (Baltimore, MD site) is class designated as "Cfa", which represents warm temperate/fully humid/hot summer.

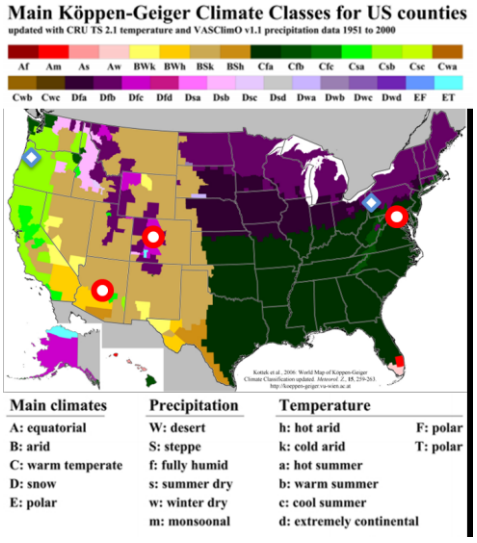


**Figure 3-1**: Climate class map showing the experimental locations (phase 1 = red circles and phase 2 = blue diamonds) representing unique climate regions. Phase 2 are expansion locations to be included for future weathering studies.

Jefferson County (Golden, CO site) is designated as “Dfb”, which represents snow/fully humid/warm summer. Maricopa County (Tempe, AZ site) has four designations: “BSk” - arid/steppe/cold arid, “Csa”- warm temperate/steppe/hot summer, “BWh”-arid/desert/hot arid, and “BSh”- arid/steppe/hot arid.

*Rooftop Weathering Installation*

As shown in Figure 3-2a, cement blocks are placed on the roof of a building at each site; cement blocks were chosen because they are low-cost and sturdy, providing a secure mechanism to stabilize the collection jars. A single collection jar (Ball Mason jar, Muncie, Indiana) is placed within each cement block hole, wrapped in a cotton towel to

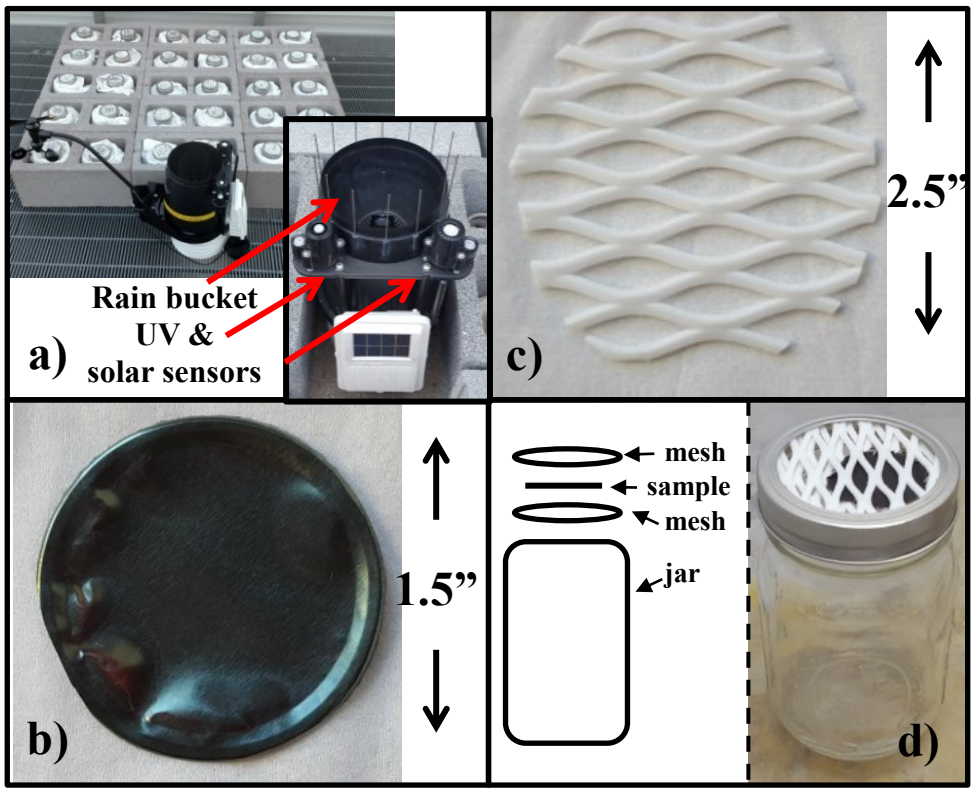


**Figure 3-2**: Key components of the outdoor weathering set up. (a) Cement block sample holders and location specific weather monitoring station (with components labeled with red arrows). (b) Nanocomposite sample for weathering. (c) Teflon mesh with 48% open surface area. (d) Sample is held in between two mesh layers above the glass jar (Left: schematic, Right: photograph).

prevent the glass from directly contacting the concrete while also filling the space. PNC samples (Figure 3-2b) are held in place between two pieces of Teflon netting (Industrial Netting, ET9000), as shown in Figure 3-2c, that is then screwed in placed above the collection jar (Figure3-2d). With this setup, the samples are held securely in place and the rainwater runoff (including released ENMs) is collected passively within the jars.

Weather stations (Wireless Vantage Pro2™ Plus including UV & Solar Radiation Sensors, Figure 3-2a) at each site collect and record data (in half hour increments) on climate variables, including temperature (° F), precipitation (inches), solar fluence ($w/m^2$), UV index, wind speed (mph), and barometric pressure (mm Hg). Data is transmitted from the weather station to a data logger, at 30 minute intervals, and retrieved on a monthly basis. Due to the physical proximity (< 5 meters) of the weather monitoring station and the PNC samples (Figure 3-2a), the recorded data is a more accurate representation of the sample conditions than is local weather station data collected by a third party at regional climate monitoring station. For example, any protection (e.g., shading, rain shadow) that may occur at a particular location is captured in the current experimental design. The total cost of supplies required for the outdoor weathering setup will depend on the total number of samples. For reference, the set up described herein (for 20 samples including replicates and controls), is approximately $1,300.00 (USD). Since the most significant expense is the weather station (≈ $1,100 USD), additional cost to accommodate more samples is marginal.

*Sample Collection*

Release was sampled every month. A schematic of the monthly sampling procedure is shown in Figure 3-3 and is carried out at each location. The procedure requires an initial gentle rinse of the nanocomposite and mesh using 20 mL of deionized

(DI)-water (Figure 3-3, step 1). This is followed by removal of the nanocomposite sample (remaining secured between the mesh layers) from the current jar (referred to here as the "A"), securing it to a clean jar ("B"), and placing this new jar B into the cement block holder (Figure 3-3, step 2). Jar A, containing accumulated precipitation and the rinse water, is carefully swirled to displace any ENMs deposited on the interior jar surface (e.g., sides) and then poured into a clean graduated cylinder (Figure 3-3, step 3). The jar is then further rinsed with 15 mL of 2% nitric acid to collect any remaining released ENM, which is then added to the graduated cylinder (Figure 3-3, steps 4 and 5). The total combined volume of precipitation, mesh rinse, and acid jar rinse are recorded for later data processing. At this stage a 15 mL aliquot of the combined volume is added to a clean pre-labeled (following standard labeling procedure) polypropylene Falcon tube and promptly shipped to a single analytical center (Golden, CO) for ICP-MS analysis (Figure 3-3, step 6). The role of a single analytical location reduces analytical variability that would arise from analysis performed at different times or locations. Hereafter, "release samples" is used to refer to the accumulated precipitation, mesh rinse, and acid rinse collected each month (as described in Figure 3-3). Following sample collection, the removed A jars are cleaned and dried so that they may replace the B jars the following month. This process is repeated each month. In an extreme weather event (e.g., heavy rainfall), sampling occurs more frequently than once per month to ensure no overflow and follows the same procedure described above (Figure 3-3). In these instances, the multiple samples are combined at the end of the month to produce one monthly sample for analysis. However, the allowable collection volume in the rooftop set up is ~450 mL,

so the frequency of such an intervention is low (this has occurred twice at a single location during sustained rain events).

The total mass release for a given monthly collected sample is calculated from the total concentration (mg/L) of released material (Ag for Ag-PNCs and Yttrium (Y) for SWCNT-PNCs) multiplied by the sample's total collection volume. Each ENM composite sample is weathered in triplicate at each site. To ensure Ag and Y measurements represent released ENMs from the PNCs only (i.e., not inclusive of environmental deposition), control jars (with Teflon mesh, no sample) were deployed at each location and their precipitation accumulation was collected in the same manner as all other samples. Baseline subtraction of this control blank is applied when significant amounts of the analyte are detected.

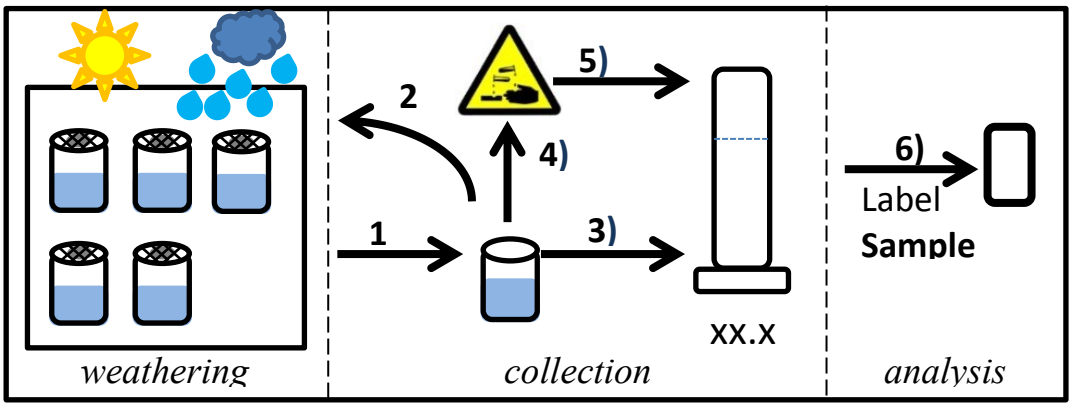


**Figure 3-3**: Schematic of monthly sampling procedure, with numbers corresponding to steps detailed in *Monthly Sample Collection* subsection.

Efficacy Testing

AgNP-enabled textile, containing approximately 35 μg Ag/ g fabric, produced by Dune Science[37] was used for antimicrobial efficacy testing. Sample efficacy testing was carried out to demonstrate the ability to incorporate this analysis simultaneous with the collection of release profiles. The AgNP impregnated textile, cut into 14 $cm^2$ swatches, was tested in quadruplicate for antimicrobial efficacy following a two-week weathering period during July, 2016 at all three locations. At the end of the weathering period, antimicrobial evaluation (following the AATCC test method 100-2004 [37], depicted schematically in Figure 3-4) was conducted in triplicate (i.e., efficacy testing completed on three of the samples from each location) and the fourth sample was acid digested to determine the remaining silver concentration by ICP-MS. As a control, prior to weathering, 14 $cm^2$ sections of AgNP-enabled and AgNP-free textile were examined for initial antimicrobial efficacy as well as acid digested and analyzed with ICP-MS to determine initial silver concentration.

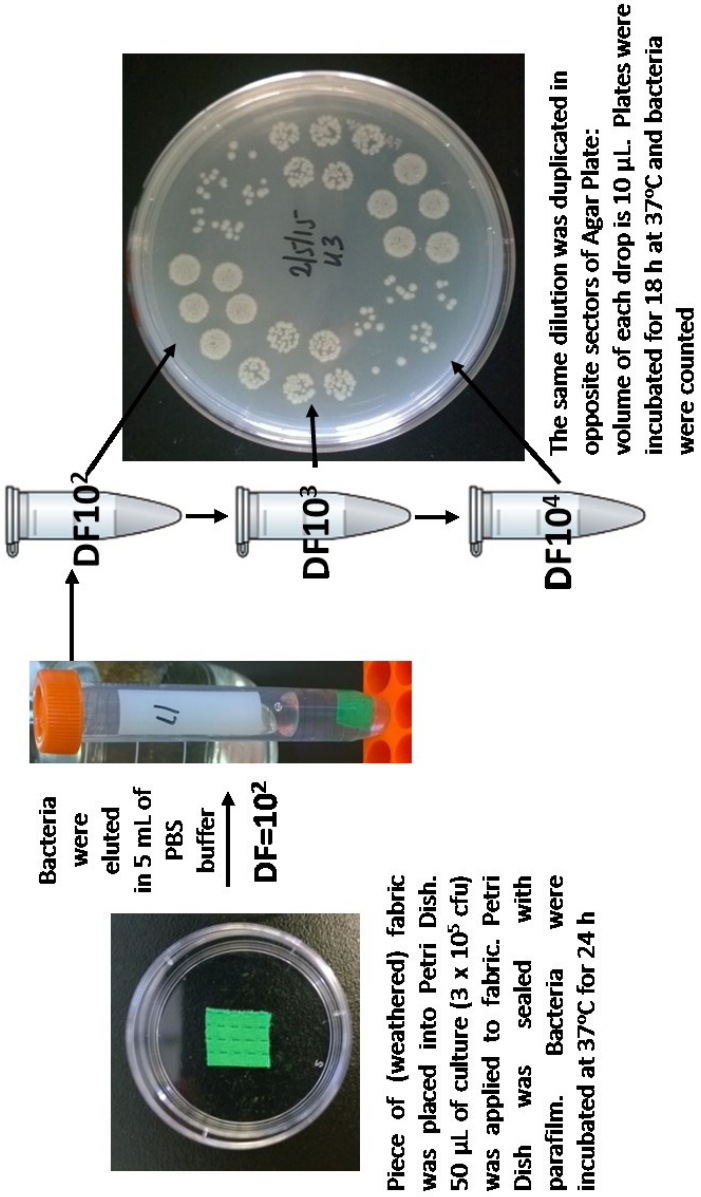


**Figure 3-4**: Outline of experimental procedures used to determine efficacy of Ag textile.

Capturing ENM flows

Since material flows serve as the foundation of LCIA, the ability to capture the movement of the ENM throughout the product life time is a critical underpinning of improved impact characterization (Figure 3-5). Here, a set of AgNP-enabled textiles were used to demonstrate the approach to capturing ENM flows within the weathered system. Upon completion of a weathering experiment, samples can be digested and analyzed for the amount of Ag that remains in the samples. The known initial silver concentration (pre-weathered sample), the released silver (collected), and the amount remaining in weathered sample capture key components of the ENM mass balance (Figure 3-6). While the current set up does not capture volatilization (release of ENM to atmosphere, $C_{r,atm}$), it is identified in Figure 3-6 as a known potential release pathway. Potential scenarios in which this could be a significant release pathways include locations with high solar irradiation (e.g., causing degradation of a UV sensitive matrix materials) that are also arid and windy (e.g., the Tempe, AZ site studied here). Combined, $C_{r,atm}$ and experimental error, provide two explanations for potential unaccounted ENM mass.

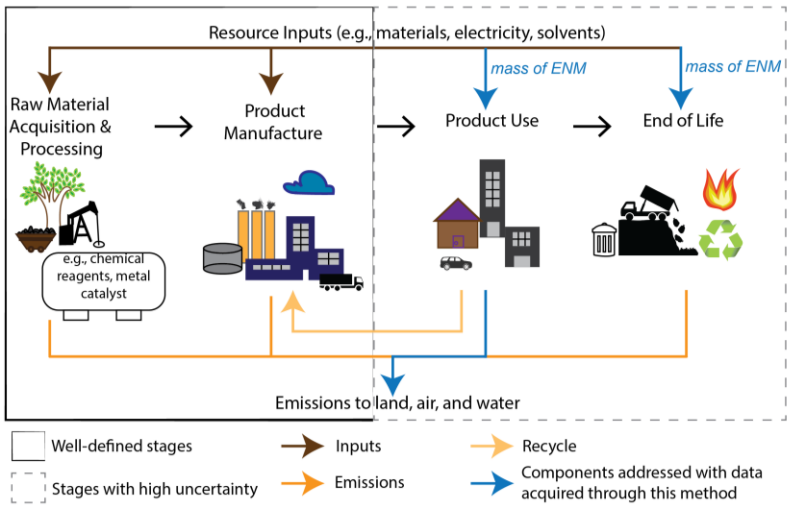


**Figure 3-5**: Life cycle schematic identifying i) the primary life cycle stages, ii) components that are well-defined, namely inputs, emissions and processes within the raw material acquisition and processing, and manufacturing stages, iii) components that are not currently well-defined for nano-enabled products (i.e., suffer from high uncertainty, namely ENM inputs and emissions during use and end of life stages), and iv) components that the method described herein address, including ENM input in the use stage (i.e., known initial concentration incorporated into the product), ENM release during use (measured in the described methodology), and ENM input in the end of life stage (attained through establishment of ENM 'use-phase' mass balance).

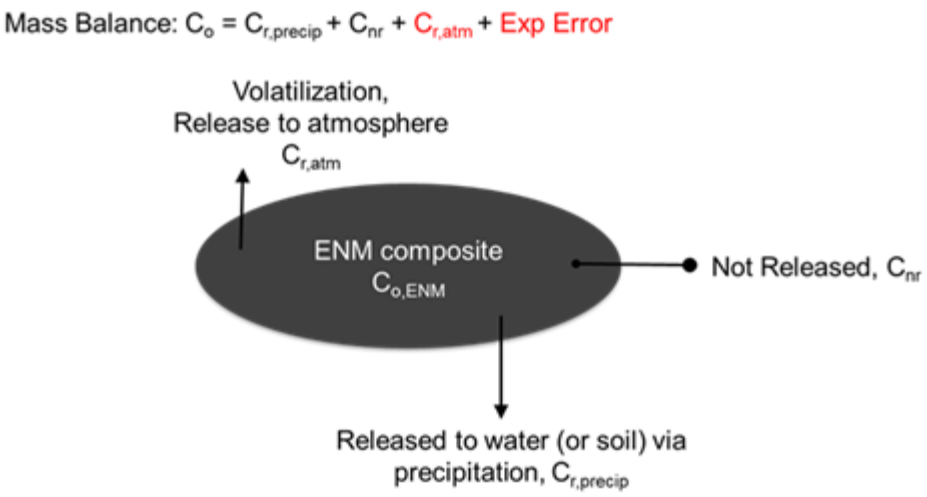


**Figure 3-6**: Schematic of the engineered nanomaterial (ENM) mass balance for the composites tested. The initial ENM concentration is determined for all samples ($C_{o,ENM}$) prior to commencing the weathering experiments, ENM release during weathering is captured monthly via precipitation collection and/or rinse of collection jar ($C_{r,precip}$), and ENM retained in the composite is determined from sacrificing samples and pre-determined time intervals ($C_{nr}$). One potential release pathway that is not captured in this method is volatilization or release to the atmosphere ($C_{r,atm}$). Finally, a certain level of experimental error is expected.

## Results and Discussion

Sample characterization before and after natural weathering

The following table and five figures (3-7, 3-8, 3-9, 3-10, and 3-11) summarize sample characterization prior to and following natural weathering – interpretation of this data is discussed in subsequent sections.

| | mass (mg) | SA of PNC ($cm^2$) | [Ag] by ICP-MS | [Ag] by XPS |
|---|---|---|---|---|
| 2% Ag-PS | 54.0 (± 5.2) | 8.1 (± 0.6) | 1.32 (± 0.12)% | 5.1 (± 0.6)% |
| 0.04% Ag-PS | 46.5 (± 3.6) | 7.0 (± 0.7) | - | 0.06 (± 0.01)% |
| 2% Ag - PMMA | 73.1 (± 4.4) | 8.9 (± 0.6) | 1.62 (± 0.19)% | 3.7 (± 3.9)% |
| 1.5% SWCNT-PCL | 41.2 (± 1.2) | 11.1 (± 0.4) | - | - |
| 1.5% SWCNT-PS | 69.3 (± 2.7) | 10.1 (± 0.4) | - | - |

**Table 3-1**: Sample characteristics, surface and bulk composition of the PNC sample including its mass, surface area (SA), percent silver of the total sample mass ([Ag]/sample mass *100, [Ag%]) quantified using ICP-MS and surface silver concentration ([Ag]) quantified by XPS. PNC SA is a measurement of the macroscopic SA determined by geometric measurements. Mass and SA values reflect measurements of the nine independent PNC samples (for each PNC type), prior to weathering. ICP-MS and XPS values represent nine independent samples, comprised of triplicate samples from three different PNC batches used to produce samples for each site (with one sample from each batch going to each location).

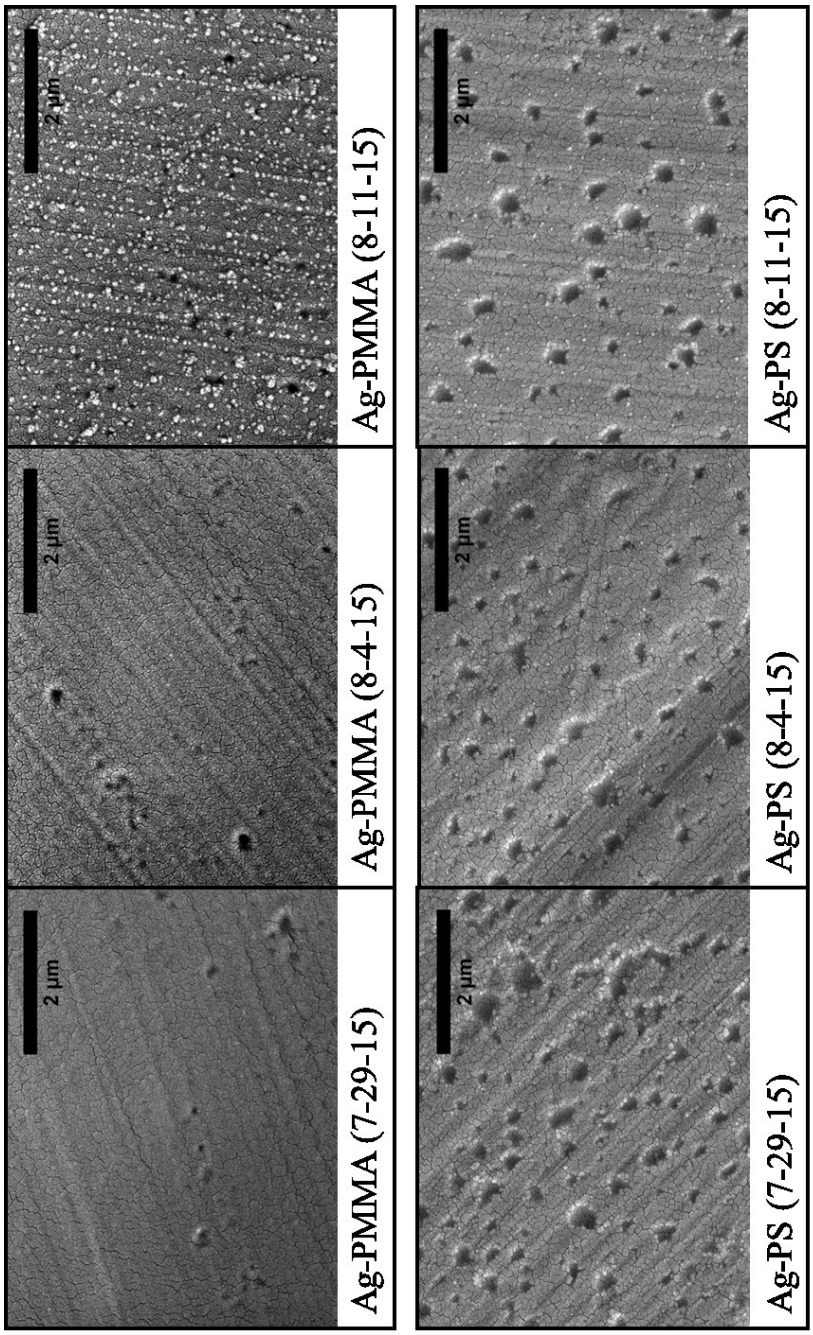


**Figure 3-7**: Representative SEM image of silver nanocomposites from each batch used in the study (Polystyrene – PS, Poly (methyl methacrylate) – PMMA). Silver nanoparticles appear as white dots in images collected and are approximately 20nm in diameter, when monodispersed.

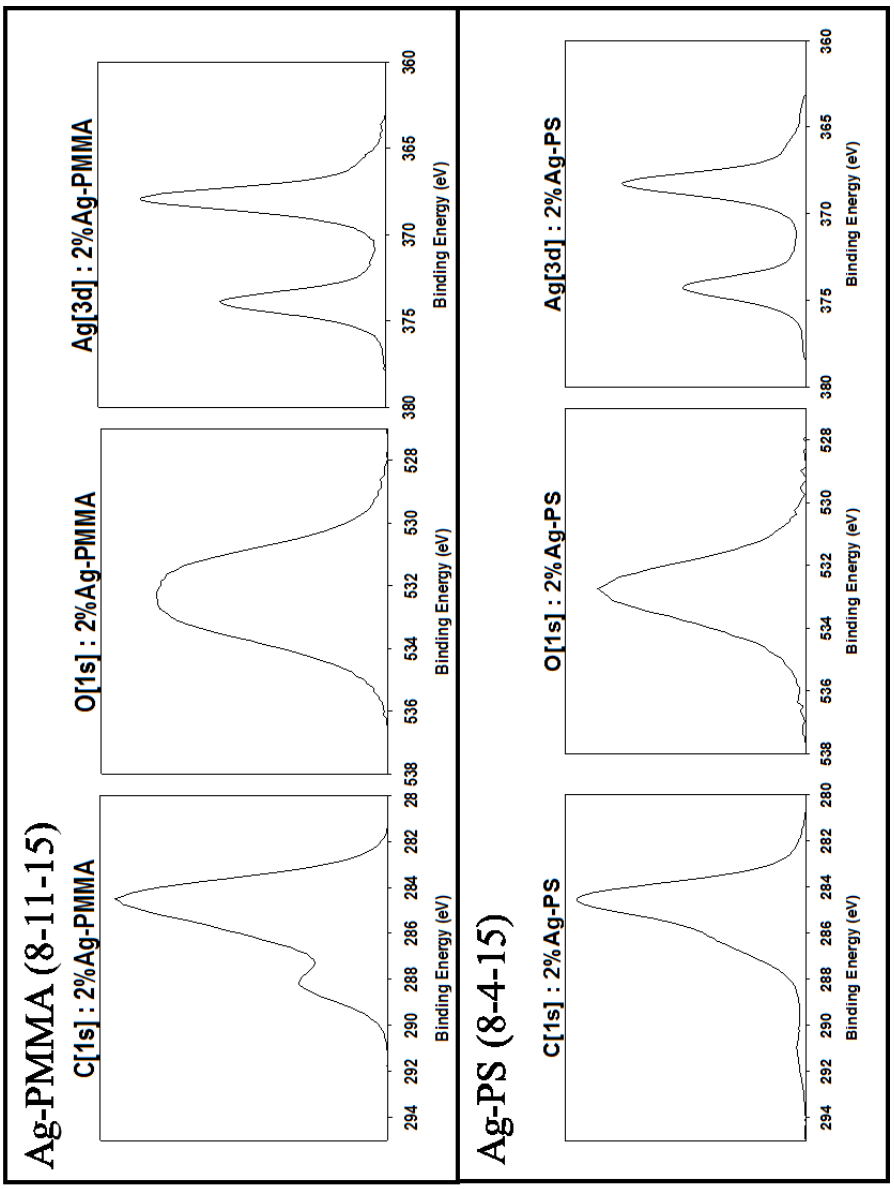


**Figure 3-8**: Representative XPS spectra collected of Ag-PNCs, used for determining surface composition , with batch denoted in parenthesis (note, XPS intensity are shown in arbitrary units).

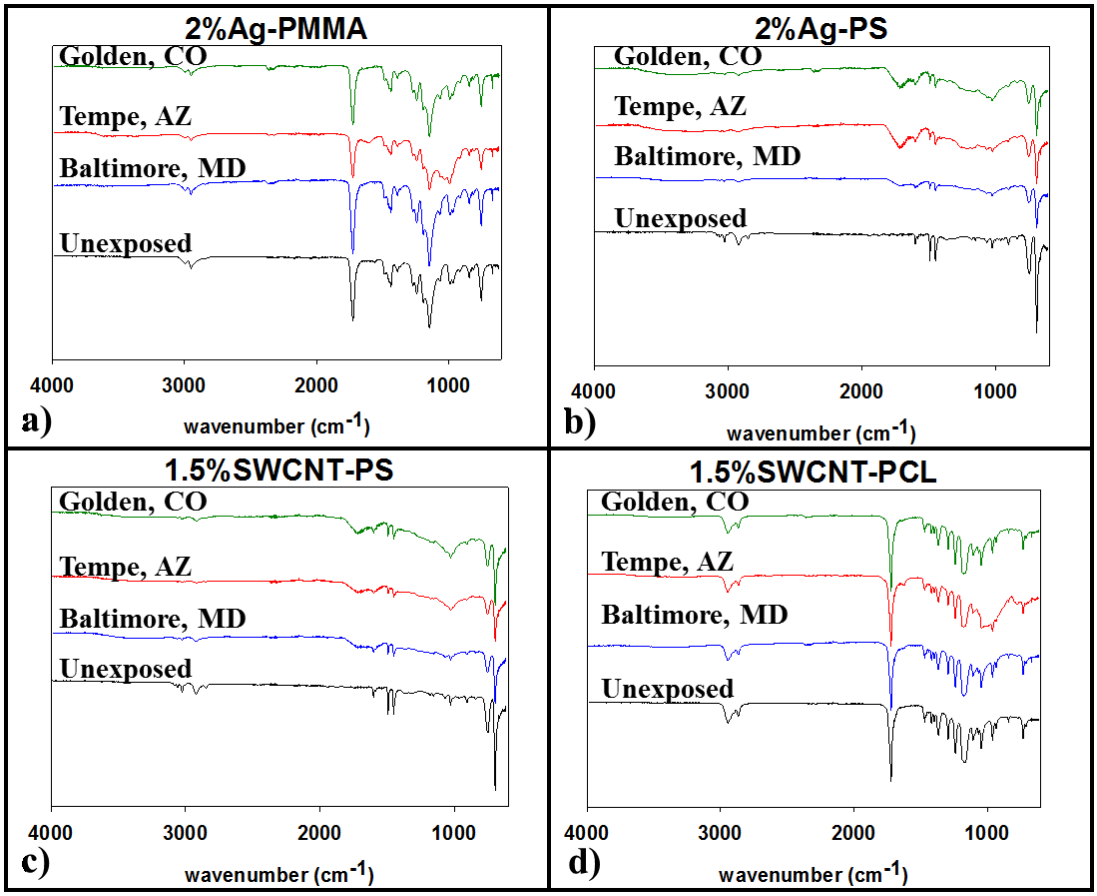


**Figure 3-9**: ATR-FTIR spectra of PNCs following weathering finds that the spectra collected of samples weathered at each location are consistent with each other, suggesting that samples weathered at each location experienced similar, shallow, depths of photodegradation.

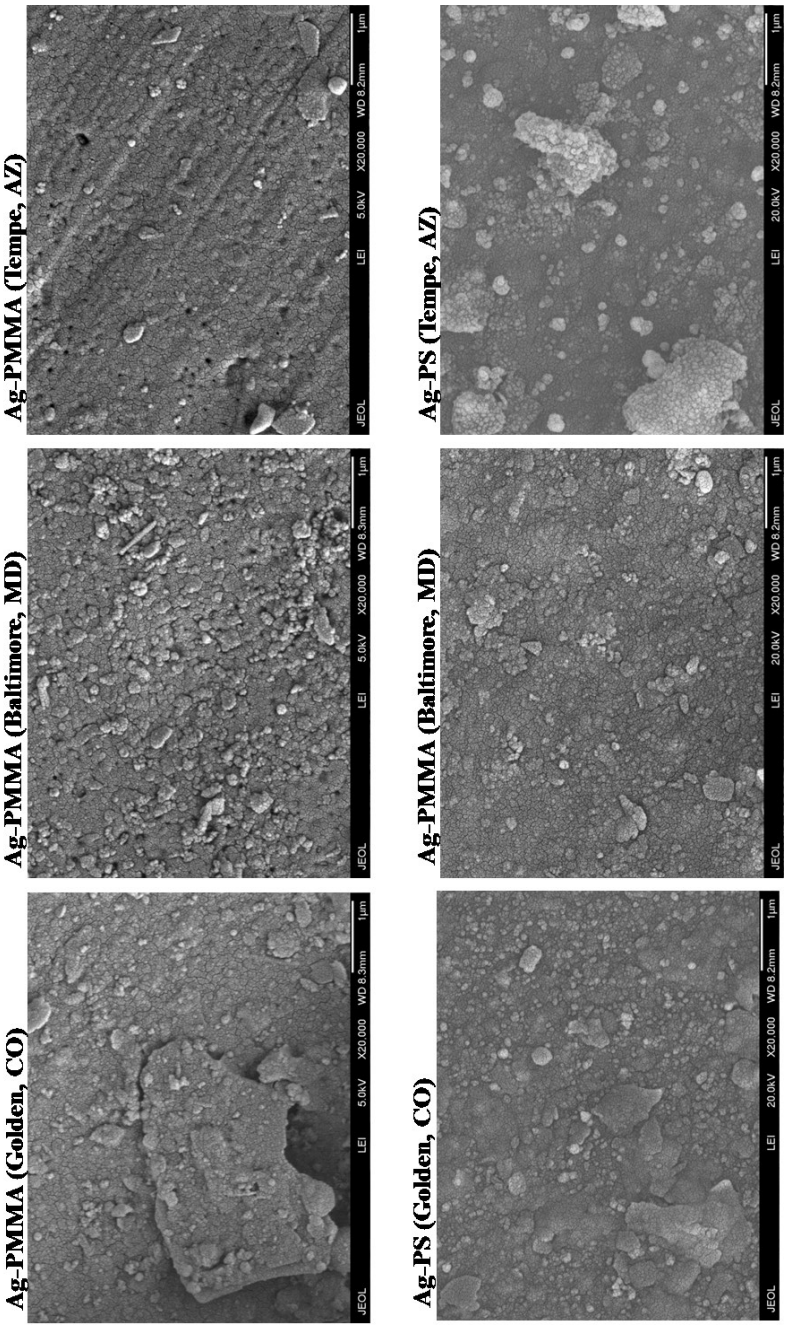


**Figure 3-10**: SEM images of Ag-PNC samples following weathering reveals no Ag nanoparticles remain visible at the surface for either PNC type, at all three locations.

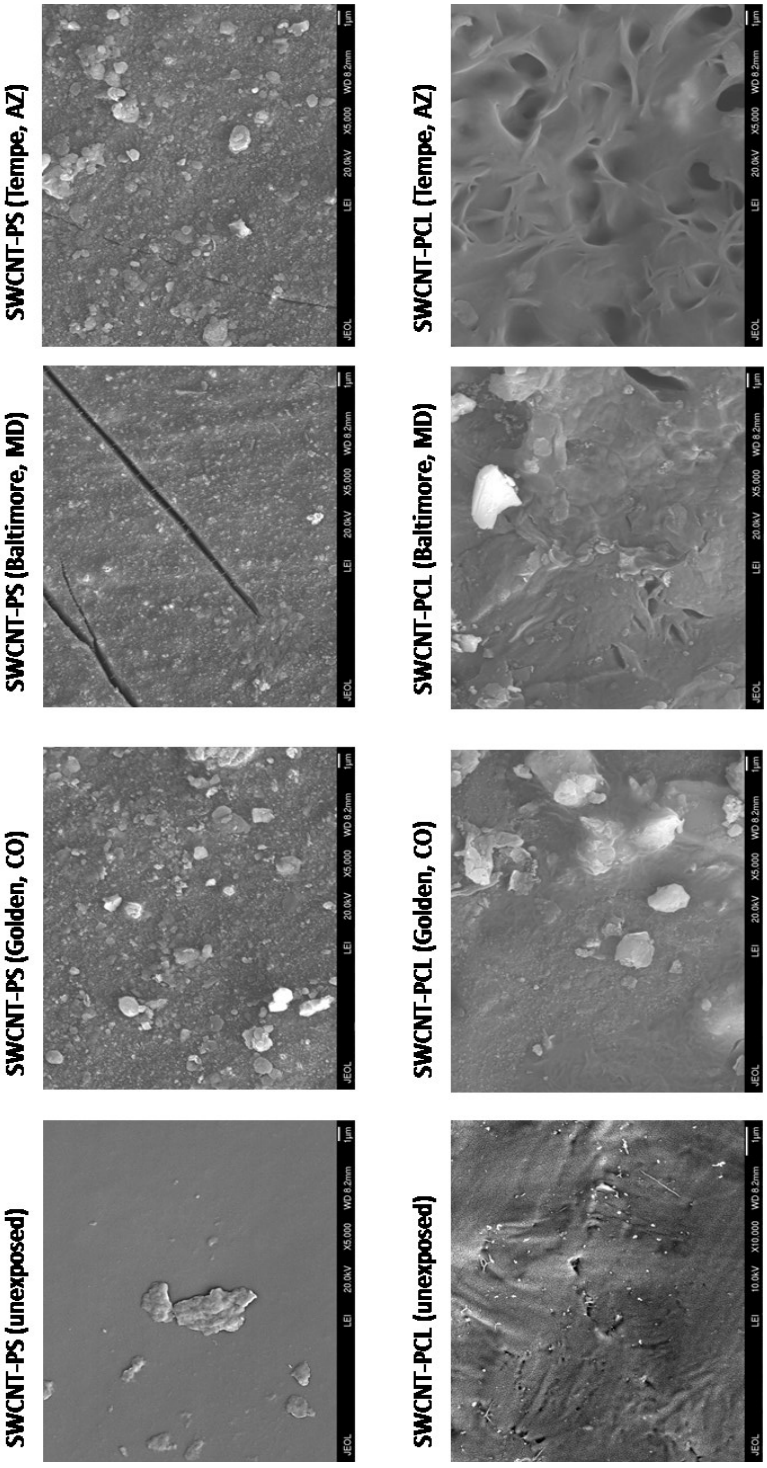


**Figure 3-11**: SEM imaging of SWCNT-PNC samples before and after weathering reveals no CNT accumulation at the surface of any PNC type or at any of the location

Sample setup and design

In the design of the current outdoor weathering setup and sample assembly, several factors were considered, with sample security and efficient collection of precipitation runoff being most important. To this end, securing the sample (Figure 3-2b) between two Teflon mesh layers (Figure 3-2c) and then screwing the sample into place atop the jar (Figure 3-2d) provides access of precipitation and sunlight exposure while simultaneously securing the sample, preventing it from either falling into the jar or blowing away. The size of the mesh openings was optimized to sufficiently secure the sample while providing maximum sample exposure. In this configuration, rainwater is passively collected, flowing through the sample and collected in the jar below. The passive approach to capturing precipitation runoff from samples during weathering allows for assessment of ENM release and provides a level of realism that is not attainable through accelerated weathering studies. Still, the combined release under natural conditions, as described in this methodology, provides a benchmark for comparison to release measurements made during lab based accelerated and simulated weathering studies.

The monthly sample collection schedule was determined as a timeframe that allowed for a measurable ENM concentration resulting from the accumulation of released material, while preventing overflow of the jars. This physical setup and procedures, which differ from previous studies that follow standard protocols (ASTM D1435 [34]), enable (a) the collection of precipitation runoff containing released nano-material and (b) the retention of weathered samples for subsequent characterization and efficacy testing. In some cases, significant sample degradation and fragmentation occurred. Larger

product fragments that fell into the collection jar were recovered and placed back in the mesh to continue weathering during monthly sample collection. A finer Teflon mesh size was considered to prevent this occurrence, however due to the hydrophobic nature of Teflon, smaller mesh "pore" sizes would have prevented rainwater flow from the sample into the collection jar and instead resulted in rainwater pooling on the mesh surface, without being collected. Appropriate documentation of observed sample fragmentation ensures that any spikes in release occurring during months in which fragmentation was observed are accounted for during final data analysis. If the sample becomes too small, it is collected and inventoried for further characterization.

Method Versatility

While representative PNC samples are used in this study, the established experimental design and methodology are versatile and can be applied to a wide range of commercial products with little to no alteration to the methods. Adaptations to accommodate larger products include cutting samples from larger materials to a size that fits over or can be securely suspended in a larger collection jar. For example, separate studies are examining the release of copper (Cu) from pressure treated lumber which has been added to the established weathering installations. As shown in Figure 3-12a, Teflon straps are affixed to the wood sample and it is secured in place above the collection jar. The adaptability of the sample holder is not limited to pressure treated lumber samples. As shown in Figure 3-12b, TX Active cement samples (provided by Lehigh Heidelberg Cement Group, study also on going) are used as received and held in place above the collection jar with thin nylon netting. For commercial products such as pressure treated lumber, $TiO_2$ enabled concrete, automotive paints on metal substrates, or any material

with intrinsic structural integrity (i.e., they are rigid and will not fracture as a result of weathering), a Teflon strap or thin nylon netting can be used to affix samples above the jars, thus eliminating the need for the mesh configuration used for the PNC samples. While the PNC samples used in this study were weathered for just over a year, the overall durability of the weathering setup described herein permits future samples and commercial products to be weathered in perpetuity (i.e., multiple years). For studies of longer durations, or of materials that release low amounts of nanomaterial on monthly basis, the sampling schedule can be easily modified to allow for sample collection bimonthly, quarterly, or semiannually, as appropriate. The ability to accommodate nano-enabled products of different sizes, compositions, and shape, for extended periods of time, enhances the overall utility of the methodology for assessing ENM release from commercial products in the natural environment.

Finally, two aspects of the sample collection method described herein required focusing on quantifying total mass of nanomaterial release and not identifying the form (e.g., particle vs. ion). These were use of an acid rinse and the monthly sampling

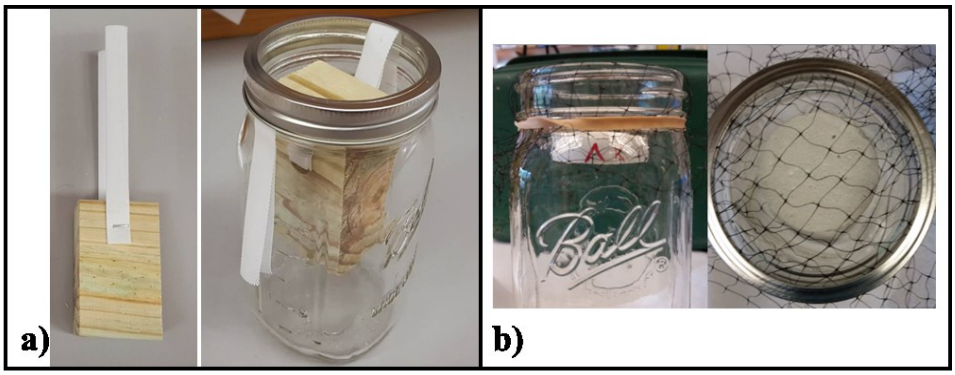


**Figure 3-12**: (a) Pressure treated lumber is used, as purchased, with the only alteration being cut down in size to fit within the collection jar and affixed to Teflon straps so it may hang freely and weather passively. (b) TX Active Cement puck provided by Lehigh Heidelberg Cement Group is held in place with thin nylon netting.

frequency that could permit released NP to be exposed to solution for sufficient time (up to 30 days) to allow dissolution. However, use of deionized water and collection of sample immediately after a precipitation event would allow further characterization of the form of the released element of interest with single-particle ICP-MS. However, availability and access to a single-particle ICP-MS limits the range in available climates for immediate characterization of released form for readily soluble NPs, requiring further research on sample preservation and stability.

Characterizing climate across all test sites

Climate and ENM release data are presented below to demonstrate the utility of data collected following the experimental method described above. Figures 3-13a-c include the average monthly temperature, total monthly precipitation, and total monthly solar irradiation recorded at each location. The climate data provide a straightforward approach to confirming and quantifying the similarities and differences among the weather patterns, and thus sample weathering conditions, at the different sites – both within a given month and annual weather patterns. On average, Tempe, AZ experiences the highest temperatures from month to month (10 – 20 °F greater than the other two locations, depending on the season), while Baltimore, MD and Golden, CO experience more moderate temperatures (Figure 3-13a). Annual temperatures trend as expected with seasonal weather changes. Cumulative climate variables are attained by summing the monthly values, and make the differences in climate at each site more apparent (Figures 3-13d-f). For example, the marginal rainfall in Tempe, AZ, relative to the other two locations, is clearly indicated in Figure 3-13e compared to Figure 3-13b. The cumulative plot of precipitation also indicates that Baltimore, MD receives the most precipitation of

the three locations, more than double that of the next city, Golden, CO (Figure 3-13e). The solar fluence data indicates that on a monthly basis, the samples in Baltimore received the lowest amount of visible sunlight of the three locations (Figure 3-13c). This distinction in sunlight received by samples in Baltimore, compared to both Tempe, AZ and Golden, CO is highlighted by examining the cumulative solar irradiance (Figure 3-13f). With this approach, it is clearly seen that from November 2015 through October 2016, Baltimore received just half the visible sunlight (2,402 $MJ/m^2$ total, Figure 3-13f), of Tempe, AZ and Golden, CO (5,869 and 5,704 $MJ/m^2$, respectively). To make use of recorded UV-index data, the measured values are summed over the monthly collection period to assess the extent of UV irradiation at each location. This approach makes clear that Tempe, AZ received over double the amount of UV light compared to both Golden, CO and Baltimore, MD (Figure 3-13d).

It is also noted the weather monitoring station located at each location only recorded weather conditions – that is, it did not monitor local air quality or the pH of precipitation. Acidification of rainfall and/or the presence of tropospheric pollution such as ozone, $NO_x$ could also contribute to nanocomposite degradation. While such factors were not quantified in this methodology, future studies that seek to examine the role of pollution in leading to nanocomposite degradation and nanomaterial release could add recording of pollution conditions into the weathering protocol.

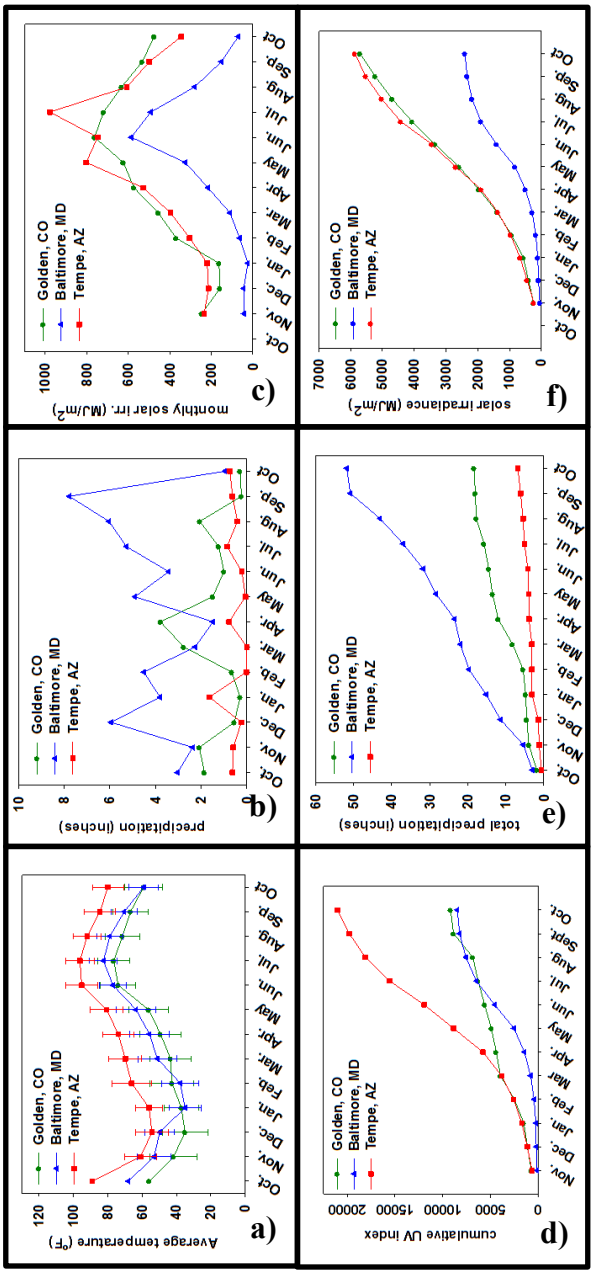


**Figure 3-13**: Monthly weather data collected, including (a) temperature, (b) precipitation, and (c) solar irradiance. Weather data is continuously monitored and recorded in 30 minute intervals, at each site. Also shown are the cumulative values for (d) UV-index and both (e) precipitation, (f) solar irradiance at each location. Since the dta is recorded in 30-minute intervals, the monthly temperature values reflect the average and standard deviation of each of those measurements while monthly precipitation and solar irradiance are the sum of those values over the duration of a month.

Distinguishing released ENM from environmental background

The sensitivity of ICP-MS provides for the quantification of low amounts of ENM release. Comparisons of low release masses of Ag and Y (as a surrogate for the presence of CNTs[48-49]) to controls are necessary to prevent false attribution of atmospheric particle deposition of these elements in the collection jar as ENM release. To test this method's ability to distinguish release from environmental background, the 0.04% Ag-PS (lowest Ag loading) and 1.5% CNT-PS monthly release values were closely examined. These samples were selected due to the low ENM loading and resiliency of polystyrene to photodegradation, as these factors are expected to limit release from the respective nanocomposites. Results from all three locations are compiled in Figure 3-14 and indicate that both Ag and Y release measurements are generally above measured background values obtained from the blank sample collection jars. The termination of release plots prior to October was due to sample fragmentation and removal from the weathering station. During instances in which elevated background concentrations are observed (July - September in Tempe, AZ, Figure 3-14f), the background trends with that of the ENM release. The identification and quantification of such elevations in the background levels informs subsequent background subtraction ($release_{corrected} = release_{measured} - deposition_{BG}$), ensuring that all release values evaluated are attributed solely to the measurement of ENM released.

Importantly, these measurements confirm the capability of the established analytical method to quantify extremely low ENM release masses (μg) and distinguish those values from environmental contributions (here, Ag or Y from dust, particulates, aerosols) to the control jars. This distinction will be particularly useful in future studies that examine

ENM release from commercial products specifically engineered to resist the release of their embedded nanoparticles (automotive paints, for example), resulting in ENM release masses that are comparable to environmental deposition masses.

In the present study, the distinction of released material from environmental deposition of material was simplified due to the fact that Ag and Y are elements not present in the environment in large quantities. In future studies, for nano-enabled products containing nanoparticles composed of elements that are more ubiquitous and at higher concentrations in the natural environment, such Cu, Si, and Ti (in $TiO_2$), the limit of detection of such elements may be impacted due to their elevated natural concentrations. One potential solution to this challenge is to examine the elemental composition of the background and released ENPs on a particle by particle basis. Conventional sp-ICP-MS overcomes some of the limitations of conventional approaches such as SEM-EDX. However the sp-ICP-MS method is currently limited to detecting only 1 to 2 elements in each particle.[50] Recent developments in the application of single particle multi-element fingerprinting, using time of flight ICP-MS, may lead to improvements in discriminating engineered nanoparticles released from nano-enabled materials from the environmental concentrations of those elements of interest. [51] However, at the current stage of analytical method development, elevated background concentrations of elements of interest present a unique challenge in distinguishing release measurements from natural deposition that is most readily resolved via simple subtraction of control jar values from the samples.

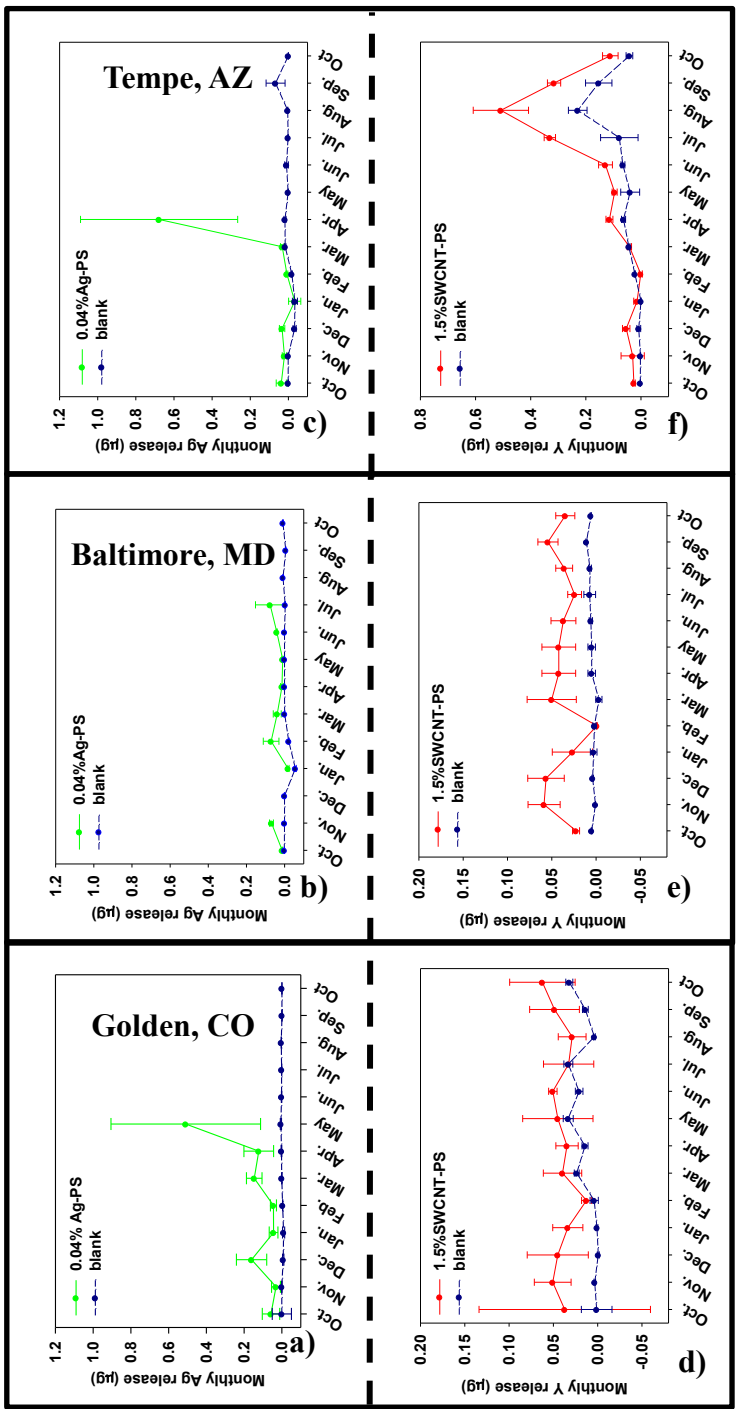


**Figure 3-14**: Monthly release values for 0.04% Ag-PS and 1.5% CNT-PS compared to the elemental concentration of blank (no composite) sample jars at each of the three weathering locations. (Note: in panel b), data is missing in December due to spilled sample.) Error bars are calculated from the release mass measured from each of the triplicate samples. Incomplete data (panels a, b, & c) for the 0.04% Ag-PS sample results from sample fragmentation and removal from the weathering installation.

Analyzing ENM release

With robust methods to quantify ENM release in hand, the collected monthly release data can be processed and interpreted considering the climate variables of interest. The data included here results from 13 months of outdoor weathering. The resulting cumulative release plots are compiled in Figure 3-16, which are generated from the monthly release plots presented in Figure 3-15. Examination of the cumulative release plots in tandem with monthly reporting of macroscopic sample fragmentation, location specific weather data, and spectroscopic characterization following weathering suggests that an interplay of climate, polymer matrix, and embedded ENM are what influence release characteristics.

*Climate Effects*

From October through May, the magnitude and rate of Ag release from two different polymer matrices track similarly at each location (e.g., 2% Ag-PS and 2% Ag-PMMA share similar Ag release profiles in Golden, CO, Figure 3-16a and 3-16b). Furthermore, the data during this time period suggest that for Ag-PNCs, a climate such as the one in Golden, CO (a combination of moderate amounts of both weathering agents, sunlight and rain, "Dfb") leads to the greatest release of Ag (green circles in Figures 3-16a and 3-16b). During this period of weathering, PNC samples at each location were reported to have remained intact and did not experience macroscopic sample fragmentation. Therefore, it is surmised that Ag release at each location from October through May was largely released from the surface or near surface region that was readily accessible to precipitation and sunlight. This is supported by SEM imagining of the pre- and post-weathered Ag-PNCs in which the AgNPs that were visible at the surface prior to

weathering (Figure 3-7) are no longer visible on the surface of Ag-PS or Ag-PMMA at each location (Figure 3-10) post-weathering. The absence of previously visible AgNPs suggests that it was these surface bound AgNPs that were either released or dissolved during weathering.

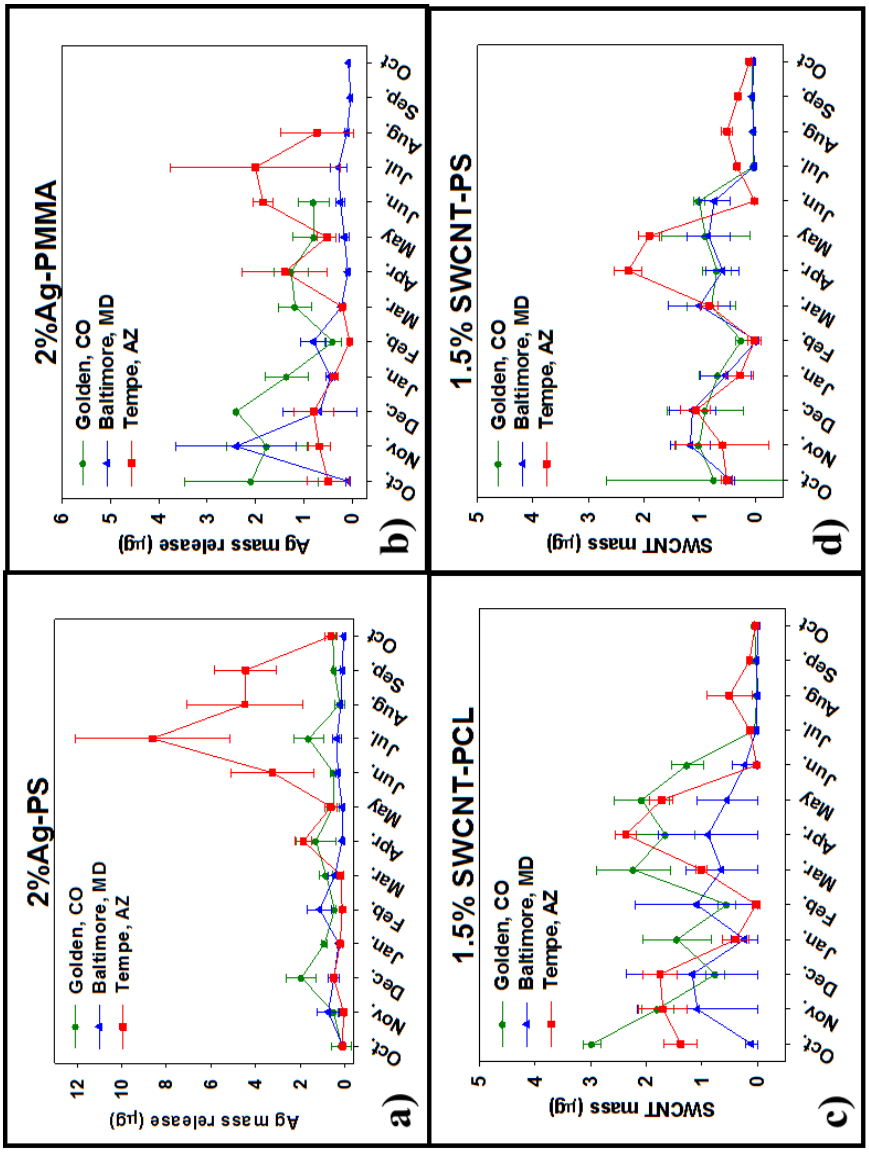


**Figure 3-15**: (a,b) Monthly Ag release mass measurements comparing Ag-PNCs located at all three sites. (c,d) Monthly SWCNT mass release measurements from SWCNT-PNCs located at all three sites. Error bars represent standard deviation of release mass measured from triplicate samples at each location. Release data demonstrates SWCNT and Ag release, however as it is shown in monthly increments, overall release trends are difficult to discern.

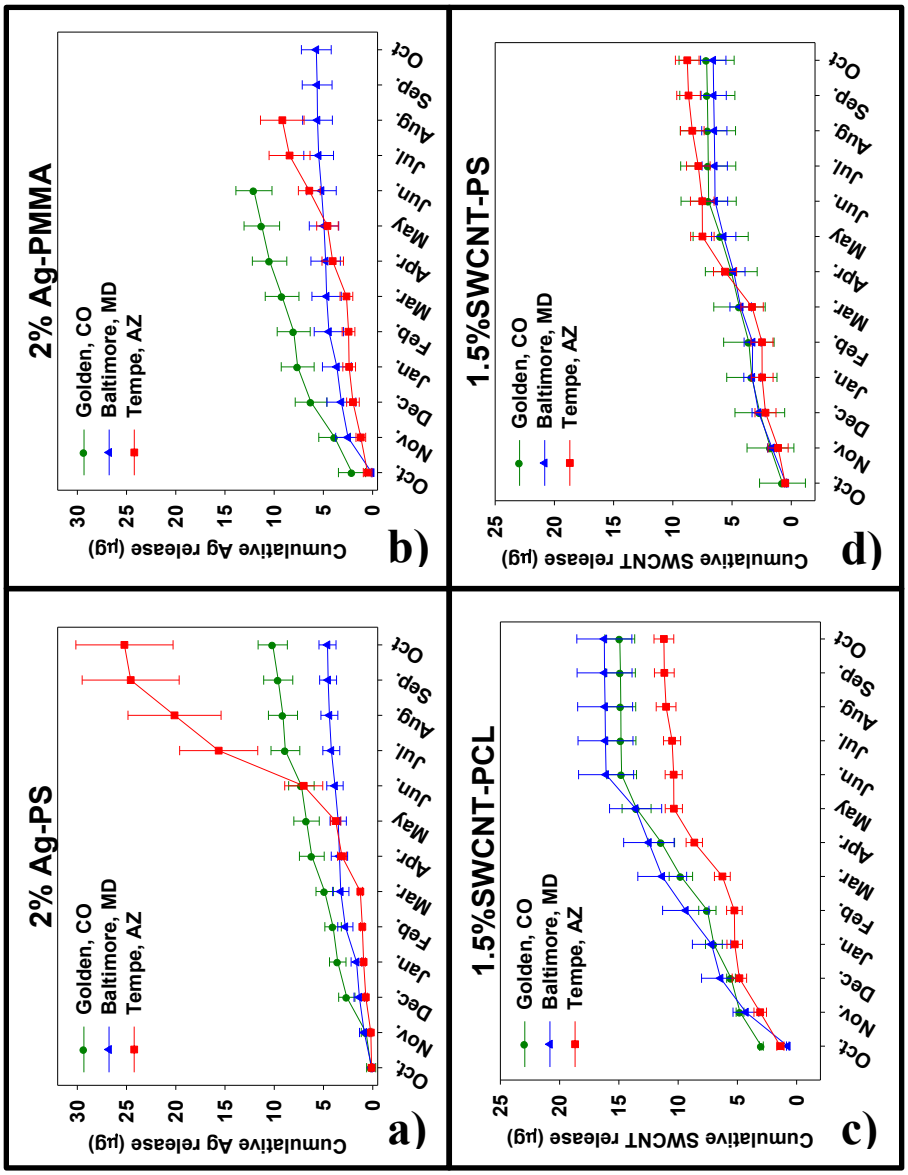


**Figure 3-16**: a) and b) Cumulative Ag release mass measurements from 2% Ag-PNCs located at the three sites. c) and d) Cumulative CNT mass release measurements from 1.5% SWCNT-PNCs located at the three sites. The error bars represent the sum of independent uncertainties for measurements each month of a triplicate sample set. Incomplete data for the 2%Ag-PMMA samples (i.e., Golden, CO and Tempe, AZ) due to sample fracturing resulting in removal of nanocomposite samples from weathering installations.

*Macroscopic Polymer Matrix Degradation*

Beginning in June (month 9), the 2%Ag-PS samples in Tempe, AZ experience a rapid increase of silver release (Figure 3-16a). In addition to a concomitant rise in cumulative UV index (Figure 3-13d), participants in Tempe reported macroscopic fragmentation of the 2% Ag-PS samples. As macroscopic fragmentation occurs, previously unexposed embedded AgNPs would then be exposed and were likely to be more readily released than when they were fully embedded within the PNC. This behavior of sample fragmentation and subsequent nanoparticle exposure is believed to have led to the observed increase in magnitude and rate of nano-material release. Interestingly, other sites reported similar sample fragmentation without a simultaneous surge in measured release (e.g., 2% Ag-PMMA sample during June in Golden, CO, Figure 3-16b), suggesting that fragmentation does not uniformly contribute to increases in ENM release across all climates and PNC types. This contrasting release behavior highlights the importance of surrounding matrix in regulating nanomaterial release to a comparable extent as weathering/exposure conditions.

*Molecular Polymer Matrix Degradation*

The rapid increase in release for 2% Ag-PS that occurred in Tempe, AZ motivated a thorough examination of the climate data during that period as well as spectroscopic characterization of the weathered samples to determine if the climate conditions led to measurable deterioration of polymer structure that could be related to the release of the embedded Ag. From November through May, the cumulative visible solar irradiance experienced in Tempe, AZ is approximately 2,700 $MJ/m^2$. This is near equivalent to the solar irradiance experienced in the three months, June through August, (~2,330 $MJ/m^2$)

(Figure 3-13f) when the surge in release occurred. In addition, the average temperatures within those two timeframes were 69 °F (+/- 12 °F) and 94 °F (+/- 9 °F), respectively (Figure 3-13a). The near doubling of total solar irradiation, including both visible light and UV, experienced in a short time period, combined with the significant increase in average temperature suggests that polymer matrix degradation for samples weathered in Tempe, AZ is significantly more extensive than the other locations. However, the lack of significant change in the ATR-FTIR spectra following 13 months of weathering in Tempe, AZ (Figure 3-9), indicates there is no significant change in the molecular structure of the PNC in the near surface region (< 2μm, which is the sampling depth of ATR-FTIR). This absence of significant changes in spectra is reflected in samples across all study locations as well and similarly indicates that weathering in each location did not result in extensive photodegradation beyond the ATR-FTIR sampling depth (< 2μm).

*Total fraction of ENM released*

The overall fraction of nanomaterial release from each sample at each location is largely similar (Figure 3-17). From this plot, it is found that the 2% Ag-PS and 2% Ag-PMMA samples released only 0.5% - 1.5% of their initially embedded silver (Figure 3-17a and b), with the 2% Ag-PS samples in Tempe, AZ experiencing greater release following PNC fragmentation. Hence, even the sample fragmentation which caused a spike in release only resulted in the release of less than 4% of the total initial silver. Regardless of climate, the 1.5% SWCNT-PS samples released less than 1% of the SWCNTs embedded in the polymer after a year of outdoor weathering (Figure 3-17d). In addition to considering the released fraction of material, release mass normalized to surface area is an important unit to consider, since for a given nano-enabled product

utilized in the environment, the mass of ENM released will scale with the surface area exposed to weathering. It is found that with this approach, similar ENM release profiles are also realized when the data is normalized to macroscopic exposed surface area (Table 3-2).

*Polymer matrix*

The overall greater release of SWCNTs from PCL (Figure 3-17c) than from PS (Figure 3-17d) suggests that the polymer matrix itself will play a role in regulating ENM release, as PS is more resilient to photodegradation than PCL, due to its lack of a photolabile chromophore. Additionally, the greater mass of SWCNTs released from SWCNT-PCL than from SWCNT-PS samples (comparing Figures 3-16c and 3-16d) in all locations indicates that a photolabile polymer matrix, like PCL, will release its embedded nanomaterial regardless of climate. It is also noted that SWCNT-PS and SWCNT-PCL samples at all three locations do appear to enter a plateau in release during the final months of weathering. However, SEM imaging was unable to reveal accumulated CNTs at the surface of any weathered samples (Figure 3-11), as has been seen in other accelerated weathering studies.[52-55] The measured low CNT mass detected suggests that release is restricted to ENMs present in the near surface region.

Moreover, ENM release from certain matrices and products is not always expected to be linear with exposure time. For example, release of ENMs from a product may only be significant during the early stages of outdoor exposure. This could occur if the ENM forms a protective surface layer as the polymer matrix degrades, a scenario that been observed in several lab based weathering studies involving CNT/polymer nanocomposites[54-57], although there are reported examples of accelerated studies that do

not show this surface accumulation.[42] These contrasting observations suggest that accelerated weathering experimental variables (e.g., intensity or length of UV exposure, PNC composition, and/or initial CNT concentration) can significantly influence the resulting CNT release. Regarding the weathered PNC samples studied here, SEM images indicate there is no accumulation at the surface (Figure 3-11). Considering the morphological changes observed following accelerated weathering are not always in agreement, the observations of this study highlight the need for natural weathering experiments to provide realistic benchmarks for accelerated studies to compare observed changes in PNC morphology.

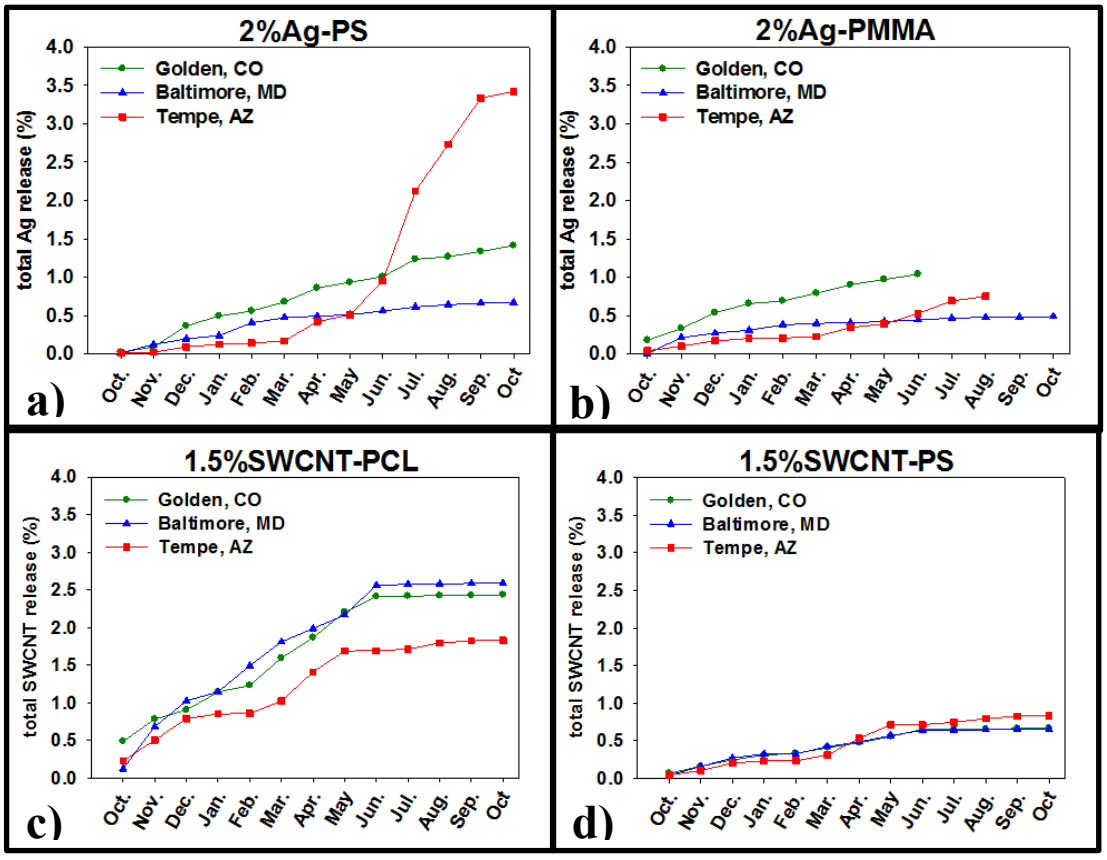


**Figure 3-17**: Cumulative fraction of Ag and SWCNT release, scaled to initial ENM mass present in PNC samples. Incomplete data for the 2% Ag-PMMA samples (i.e., Golden, CO and Tempe, AZ) due to sample fracturing resulting in removal of nanocomposite samples from weathering installations.

Examining efficacy following weathering

In addition to capturing ENM release and analyzing the contribution of system variables to cumulative release, the methodology presented is designed to incorporate efficacy testing (a method that quantifies the intended function of a product). Here, a Dune Science AgNP-enabled textile, used in previous release studies[37], is used to demonstrate the efficacy testing. AgNPs are incorporated into textiles to introduce the function of microbial growth inhibition, with a range of intended outcomes from odor reduction to infection prevention. Therefore, the efficacy is measured here as the reduction of bacteria viability using XL1-Blue strain of *E. coli* (Figure 3-4).[37] Representative results for the weathered and unweathered AgNP-treated textile at each location are shown in Figure 3-19 (a complete set of images is included in Figure 3-18). The results indicate that the unweathered AgNP-treated textile samples elicit complete reduction in *E. coli* viability (no colony growth, Figure 3-18 top row and Figure 3-19a top row). This inhibition of microbial growth is maintained following two weeks of weathering during the summer at all three locations (Figure 3-18 bottom three rows). Two weeks was chosen as a reasonable timeframe that someone would wear this shirt between washes (as the addition of silver is intended to increase the number of wears per wash). Untreated textile controls (no AgNPs) were included and indicate that without the silver, there is no significant impact on bacterial growth (Figure 3-19a, bottom row). These findings demonstrate that, for this specific product, the efficacy is retained following two weeks of weathering in three distinct climates.

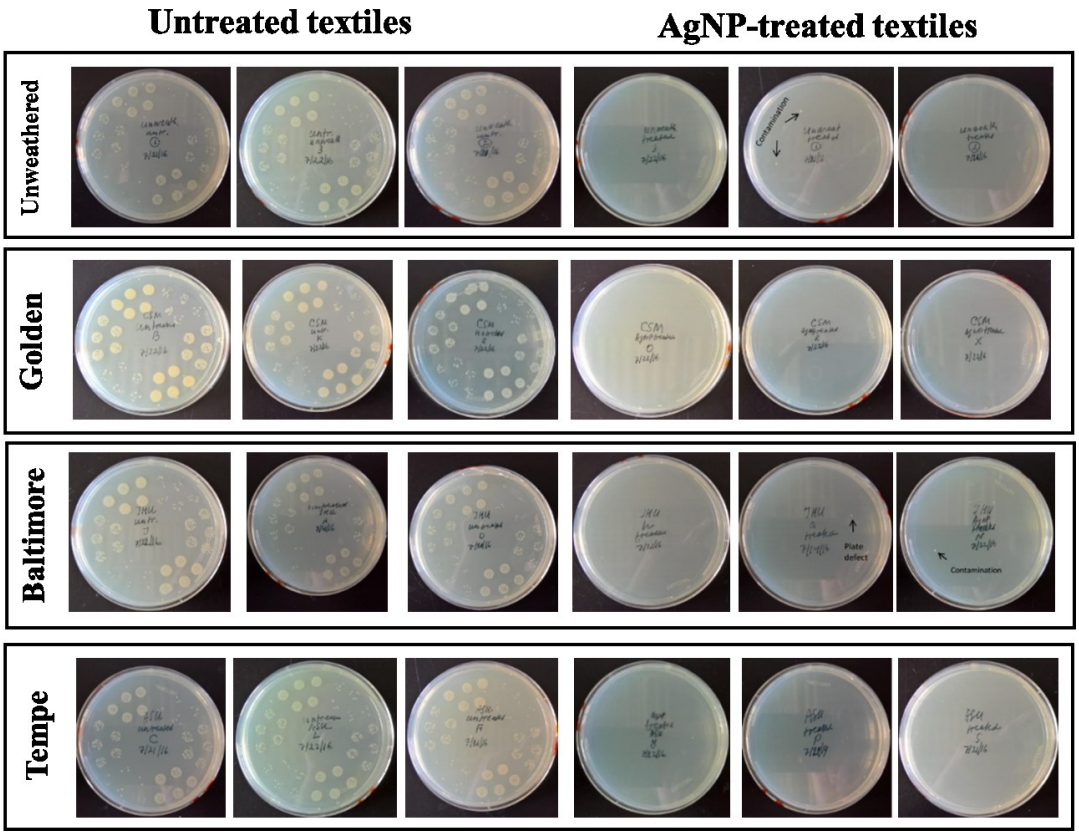


**Figure 3-18**: Pictures captured of triplicate antimicrobial efficacy test results, for each location. Images show that anti-microbial efficacy is maintained for all Ag treated textile samples in each location and that weathering has no impact on the antimicrobial efficacy of the untreated textile samples weathered in each location.

Construction of the ENM mass balance

Characterizing ENM materials flows across the life cycle of the product or process of interest is a critical underpinning of LCIA. A silver enabled textile (same as used above for efficacy testing) is used here to demonstrate how such accounting and analysis of a commercial product can and should be included in the outdoor weathering methodology. ENM releases were collected and measured using identical procedures as was used for the PNCs. The initial AgNP-treated textile contains approximately 35 μg of Ag/g of fabric (Figure 3-19b). Following two weeks of weathering, sacrificed fabric samples from each site were digested and analyzed by ICP-MS and found to retain 25 – 29 μg of Ag/g of fabric. Measurements of the collected precipitation runoff samples at all three sites determined a total Ag ~1.7 μg of Ag/g of fabric was released. Silver concentration values shown in Figure 3-19b were normalized to the initial silver content of the control AgNP-treated sample to determine the recovered fraction (Figure 3-19c) of Ag. For samples weathered in each location, ENM recovery ranges from 80-85%. This reasonably high recovery suggests that losses due to incomplete removal of metals from the glass jar, or loss due to windblown removal of fragments of test material are relatively small. The recovery of analyte from the jar, which may have been subjected to partial or complete drying, could be quantified by additional controls in which a known amount of NPs are added to a collection jar and sampled following a month of exposure. Additionally, loss by wind erosion of fragments can be accounted for by tracking the mass of exposed material each month.

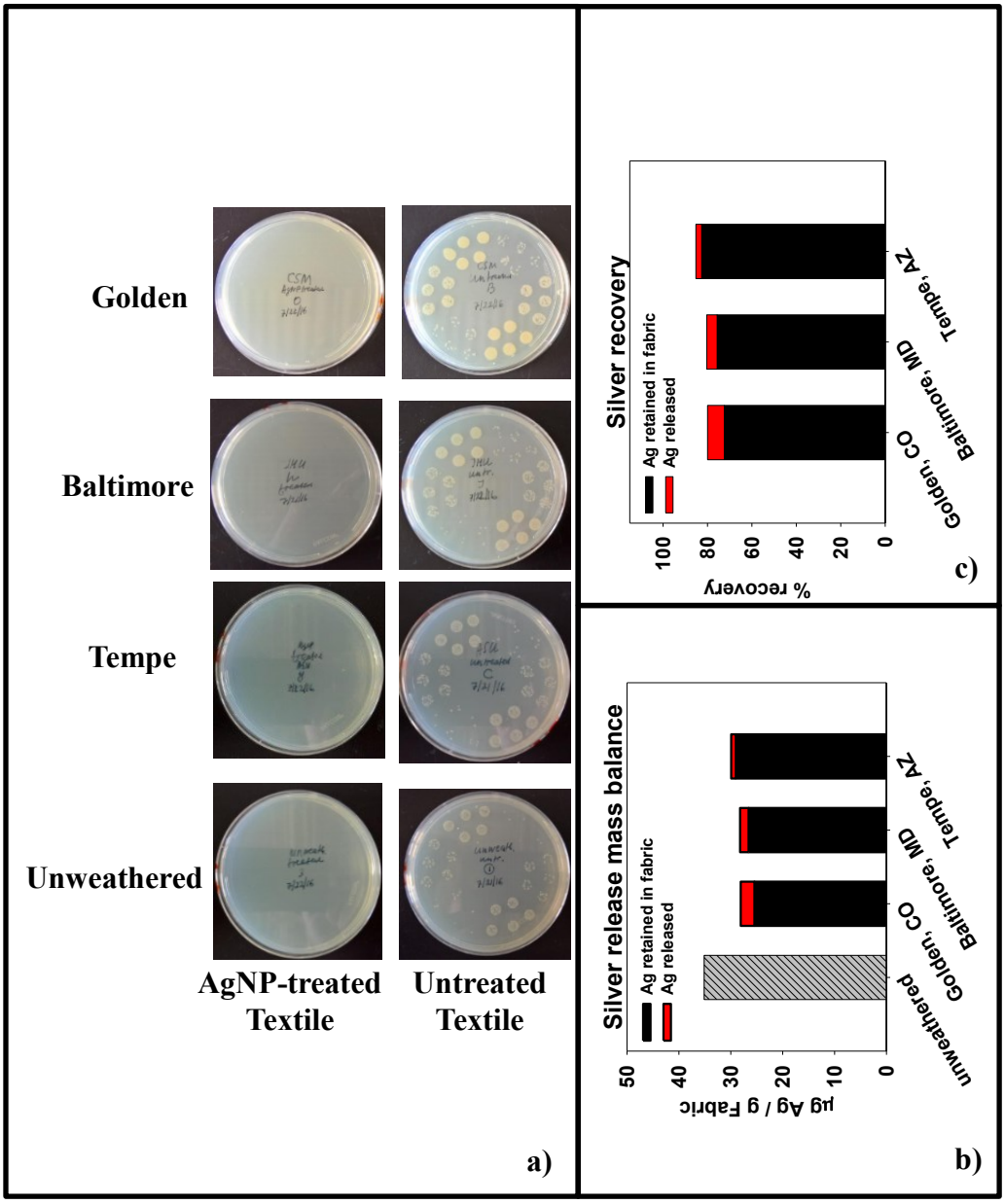


**Figure 3-19**: a) Representative images of antimicrobial efficacy testing results of the Ag-textile after two weeks of weathering. Accounting and tracking Ag release as, b) a mass released (mass of Ag per gram of fabric), and c) total silver recovery (based on known initial concentrations quantified prior to commencing textile weathering).

Integrating release data into life cycle impact assessment

At the foundation of a LCIA is a comprehensive inventory that includes process and material flows in which all resource inputs (e.g., materials, energy, water, solvents) and emissions (e.g., waste, byproducts, solvents, etc. released to soil, water, or air) are accounted across all life cycle stages included in a given system boundary (e.g., raw material acquisition, material and product processing, use, and end of life, Figure 3-5). The inventory analysis compiles all the fundamental elements (e.g., $NO_x$, $SO_x$, $CH_4$, $CO_2$), which are then translated into environmental and human health impact categories to quantify the burden imposed by the product or process of interest. In this way, impact characterization is directly related to the emissions across the life cycle, highlighting the criticality of accurate release data in the attainment of robust and meaningful impact assessment results. While this established LCIA approach can be applied to any system of interest, there remains significant uncertainty surrounding release of ENMs from products they enable. This has limited the scope and certainty of results from existing LCIA studies. The method established and described herein, intends to better characterize ENM release to the environment from products that are regularly exposed to outdoor climate conditions (offering a direct environmental release pathway) and thus, reduce uncertainty of impact characterization in the use and end of life (EoL) stages.

A brief overview of the current nano-LCA literature highlights the important advancements enabled by their findings and the need for enhanced certainty surrounding ENM release across the life cycle. ENM release, when included in a LCIA, is typically based on assumptions and/or includes a best and worst case scenario approach.[8-10] For example, Eckelman, et al.[10] provide an order of magnitude

comparison of the ecotoxicity impacts from downstream CNT release and upstream CNT production. The conclusions from that study were informative and the first to establish the relative impacts of CNT synthesis and ecotoxicity potential, shifting the focus upstream (e.g., redesign of CNT production processes) to reduce life cycle impacts of CNT-enabled products. Similar studies have elucidated the relative ecotoxicity potential of nano-silver[58]. The influence of release kinetics of silver ion from a silver nanoparticle-enabled textile were investigated and shown to have an influence on the magnitude of ecotoxicity potential, particularly under low initial silver loading.[9] Release kinetics are also important from an efficacy perspective and thus, lifetime (product replacement) perspective. Many products that incorporate ion-releasing nanoparticles utilize this phenomenon to prevent microbial growth on surfaces.[59-60] The lifetime of such products will be directly related to efficacy that requires the ENM to be present. If 90% of the active ingredient (i.e., ENM) is released within the first month of product use and product efficacy is reduced significantly, the lifetime of this product will be very short. This has implications on upstream processing impacts, and will for example, motivate product reuse or recycle to offset virgin materials use. Conversely, if 90% of the embedded nanoparticle is released, but efficacy remains unchanged, two important outcomes are informed, (i) upstream product design and manufacturing processes should aim to lower initial nanoparticle loadings, and (ii) the focus of ENM release impacts is shifted to the end of life (EoL) stage.

Several key attributes of the method design described herein, have been identified in order to promote coordination between the attained release results and LCIA. In particular, quantifying the initial ENM loading, released ENM, and retained ENM,

enables the establishment of the ENM flow into and out of the product (here, the PNC). Coordination with experimentalists in developing this outdoor weathering methodology ensures the data is defined with greater certainty and in turn, (i) decrease uncertainty in release quantities and rates, (ii) decrease uncertainty in the ultimate impact characterization (which is based on the quantity and rate of release), and (iii) better inform handling during the use and end of life (EoL) stages (Figure 3). In addition to better quantifying release and accounting for ENM flows, the described efficacy characterization as weathering proceeds allows for a more accurate assessment of changes in product function, which is critical to defining its useful lifetime.

In the case of minimal ENM release during the use phase, as shown here for some ENM-PNC substrate combinations, associated use-phase impacts of the ENM will concomitantly be insignificant. This informs LCA in two important ways, (i) it suggests likely maintenance of product efficacy, and (ii) directs impact characterization associated with release to EoL. Assuming the ENM is incorporated to impart an added or unique functionality, retaining the ENM is critical to a long useful product lifetime. When ENM release during use is minimal, the burden of concern shifts to the EoL stage where potential environmental and human exposure can occur through each of the primary

| | 0.4% Ag-PS | 2 % Ag-PS | 2 % Ag-PMMA | 1.5% SW-PCL | 1.5% SW-PS |
|---|---|---|---|---|---|
| **Baltimore, MD** | **0.1 – 0.2** | **1.3 – 2.6** | **0.7 – 1.4** | **1.5 – 3.0** | **0.7 – 1.4** |
| **Golden, CO** | **0.2 – 0.4** | **0.6 – 1.2** | **1.4 – 2.8** | **1.4 – 2.8** | **0.7 – 1.4** |
| **Tempe, AZ** | **0.1 – 0.2** | **3.2 – 6.4** | **1.0 – 2.0** | **1.0 – 2.0** | **0.9 – 1.8** |

**Table 3-2**: Final cumulative nanomaterial release mass, normalized to the total geometric surface area and the surface assuming consistent 48% shading of the PNC due to the mesh sample holder, of individual weathered samples (units of $\mu g/cm^2$). % refers to the %wt of the nanomaterial embedded in the composite. PS = polystyrene, PMMA = poly (methyl methacrylate), SW = single-walled carbon nanotubes.

handling scenarios when appropriate control measures are not in place, including leaching to the environment when landfilled, human and environmental exposure during recycling (e.g., grinding, crushing) and aerosolization during incineration.

**Conclusions**

A unique and reproducible physical setup, experimental design, and sampling procedure were developed in order to characterize ENM release from polymer nanocomposites and nano-enabled commercial products under real climate conditions (outdoor weathering). In addition to measuring release, the methodological design allows for the preservation of the weathered sample for characterization and efficacy testing throughout the weathering period. Location specific weather data was continuously collected and recorded, in 30-minute intervals, at each site. It was identified that one month sampling intervals permits a measurable accumulation of released nano-material and found that cumulative metrics present the most straightforward approach to presenting both release and climate data.

The 13 months of weathering data collected in three distinct climates were included here to demonstrate the utility and value of the methodological design to capture information useful to inform what governs ENM release as well as improved environmental impact characterization. Low ENM release was determined for all PNC samples studied during this time period, with 3.5% being the greatest observed release (as percent of the original concentration). Furthermore, the initial results indicate that the polymer matrix is a more important characteristic in determining release than the ENM type and climate. Extending this method beyond the immediate findings related to the samples weathered in this initial study, the suite of data that is generated pertaining to

both climate (e.g. precipitation, solar fluence, temperature) and ENM release (magnitude and rate) provides valuable benchmarks for comparison to laboratory accelerated weathering studies. These two approaches to characterizing release of ENMs from enabled products are complimentary, in that the data collected following natural weathering can be used to inform improved accelerated weathering design by identifying variables (e.g., temperature, solar fluence, or type of polymer) that regulate ENM release.

Additionally, the outdoor weathering of a specific Ag enabled textile was found to not result in a significant release of Ag and that the efficacy of this product is unchanged following weathering in three distinct climates. While this work focuses on disseminating the methodology and identifying the necessary components to coordinate research between experimentalists and LCIA practitioners, ongoing research on these PNC samples and commercial nano-enabled products will offer further analysis and resolve the contribution of each system component on ENM release.

**Acknowledgments**

The methodology developed above involved the contribution of many researchers (under supervision of their advisors) with unique skillsets: sample preparation, characterization, methodology development, and coordination was carried out by the author of this work, Ronald S. Lankone. Monthly sample analysis was conducted by Katie Challis and Robert Reed. Monthly sample collection was carried out by Katie Challis, Robert Reed, David Hanigan, and Yuqiang Bi. Antimicrobial efficacy testing was carried out by Tatiana Zaikova. LCA implication considerations were developed by Leanne Gilbertson.

## References


1. Nanomaterials https://echa.europa.eu/regulations/nanomaterials (accessed August 22).
2. Reviewing New Chemicals under the Toxic Substances Control Act (TSCA). https://www.epa.gov/reviewing-new-chemicals-under-toxic-substances-control-act-tsca/control-nanoscale-materials-under#regs.
3. *A research strategy for environmental, health and safety aspects of engineered nanomaterials*. National Academies Press: Washington, D.C., 2012.
4. National Science and Technology Council Committee on Technology; Subcommittee on Nanoscale Science, E., and Technology *National Nanotechnology Initiative - Environmental, Health, and Safety Research Strategy* Washington D.C., 2011.
5. Miseljic, M.; Olsen, S. I., Life-cycle assessment of engineered nanomaterials: a literature review of assessment status. *Journal of Nanoparticle Research* **2014,** *16* (6), 1-33.
6. Hischier, R.; Walser, T., Life cycle assessment of engineered nanomaterials: State of the art and strategies to overcome existing gaps. *Science of The Total Environment* **2012,** *425*, 271-282.
7. Gavankar, S.; Suh, S.; Keller, A. F., Life cycle assessment at nanoscale: review and recommendations. *The International Journal of Life Cycle Assessment* **2012,** *17* (3), 295-303.
8. Walser, T.; Demou, E.; Lang, D. J.; Hellweg, S., Prospective Environmental Life Cycle Assessment of Nanosilver T-Shirts. *Environmental Science & Technology* **2011,** *45* (10), 4570-4578.
9. Hicks, A. L.; Gilbertson, L. M.; Yamani, J. S.; Theis, T. L.; Zimmerman, J. B., Life Cycle Payback Estimates of Nanosilver Enabled Textiles under Different Silver Loading, Release, And Laundering Scenarios Informed by Literature Review. *Environmental Science & Technology* **2015,** *49* (13), 7529-7542.
10. Eckelman, M. J.; Mauter, M. S.; Isaacs, J. A.; Elimelech, M., New Perspectives on Nanomaterial Aquatic Ecotoxicity: Production Impacts Exceed Direct Exposure Impacts for Carbon Nanotoubes. *Environmental Science & Technology* **2012,** *46* (5), 2902-2910.
11. Gilbertson, L. M.; Wender, B. A.; Zimmerman, J. B.; Eckelman, M. J., Coordinating modeling and experimental research of engineered nanomaterials to improve life cycle assessment studies. *Environmental Science: Nano* **2015,** *2* (6), 669-682.
12. Lee, J.; Mahendra, S.; Alvarez, P. J. J., Nanomaterials in the Construction Industry: A Review of Their Applications and Environmental Health and Safety Considerations. *ACS Nano* **2010,** *4* (7), 3580-3590.
13. Vapor Nano. http://www.sportiva.com/products/ski/skis/vapor-nano (accessed 2016-03-14).
14. Zyvex technologies. http://www.zyvextech.com/sports/ (accessed 2016-03-16).
15. Khanna, V.; Bakshi, B. R., Carbon Nanofiber Polymer Composites: Evaluation of Life Cycle Energy Use. *Environmental Science & Technology* **2009,** *43* (6), 2078-2084.
16. Froggett, S. J.; Clancy, S. F.; Boverhof, D. R.; Canady, R. A., A review and perspective of existing research on the release of nanomaterials from solid nanocomposites. *Particle and Fibre Toxicology* **2014,** *11* (1), 1-28.
17. Al-Kattan, A.; Wichser, A.; Vonbank, R.; Brunner, S.; Ulrich, A.; Zuin, S.; Nowack, B., Release of TiO2 from paints containing pigment-TiO2 or nano-TiO2 by weathering. *Environmental Science: Processes & Impacts* **2013,** *15* (12), 2186-2193.
18. Nguyen, T. V.; Nguyen Tri, P.; Nguyen, T. D.; El Aidani, R.; Trinh, V. T.; Decker, C., Accelerated degradation of water borne acrylic nanocomposites used in outdoor protective coatings. *Polymer Degradation and Stability* **2016,** *128*, 65-76.
19. Kaynak, C.; Sarı, B., Accelerated weathering performance of polylactide and its montmorillonite nanocomposite. *Applied Clay Science* **2016,** *121–122*, 86-94.
20. Butylina, S.; Martikka, O.; Kärki, T., Weathering properties of coextruded polypropylene-based composites containing inorganic pigments. *Polymer Degradation and Stability* **2015,** *120*, 10-16.
21. Braun, U.; Wachtendorf, V.; Geburtig, A.; Bahr, H.; Schartel, B., Weathering resistance of halogen-free flame retardance in thermoplastics. *Polymer Degradation and Stability* **2010,** *95* (12), 2421-2429.

22. Fufa, S. M.; Jelle, B. P.; Hovde, P. J., Effects of TiO2 and clay nanoparticles loading on weathering performance of coated wood. *Progress in Organic Coatings* **2013,** *76* (10), 1425-1429.
23. Rabea, A. M.; Mohseni, M.; Mirabedini, S. M.; Tabatabaei, M. H., Surface analysis and anti-graffiti behavior of a weathered polyurethane-based coating embedded with hydrophobic nano silica. *Applied Surface Science* **2012,** *258* (10), 4391-4396.
24. Pandey, J. K.; Raghunatha Reddy, K.; Pratheep Kumar, A.; Singh, R. P., An overview on the degradability of polymer nanocomposites. *Polymer Degradation and Stability* **2005,** *88* (2), 234-250.
25. Li, J.; Yang, R.; Yu, J.; Liu, Y., Natural photo-aging degradation of polypropylene nanocomposites. *Polymer Degradation and Stability* **2008,** *93* (1), 84-89.
26. Maury-Ramirez, A.; Demeestere, K.; De Belie, N., Photocatalytic activity of titanium dioxide nanoparticle coatings applied on autoclaved aerated concrete: Effect of weathering on coating physical characteristics and gaseous toluene removal. *Journal of Hazardous Materials* **2012,** *211–212*, 218-225.
27. Lv, Y.; Huang, Y.; Yang, J.; Kong, M.; Yang, H.; Zhao, J.; Li, G., Outdoor and accelerated laboratory weathering of polypropylene: A comparison and correlation study. *Polymer Degradation and Stability* **2015,** *112*, 145-159.
28. Gu, X.; Stanley, D.; Byrd, W. E.; Dickens, B.; Vaca-Trigo, I.; Meeker, W. Q.; Nguyen, T.; Chin, J. W.; Martin, J. W., Linking Accelerated Laboratory Test with Outdoor Performance Results for a Model Epoxy Coating System. In *Service Life Prediction of Polymeric Materials: Global Perspectives*, Martin, J. W.; Ryntz, R. A.; Chin, J.; Dickie, R. A., Eds. Springer US: Boston, MA, 2009; pp 3-28.
29. Diepens, M.; Gijsman, P., Outdoor and accelerated weathering studies of bisphenol A polycarbonate. *Polymer Degradation and Stability* **2011,** *96* (4), 649-652.
30. Santos, R. M.; Botelho, G. L.; Cramez, C.; Machado, A. V., Outdoor and accelerated weathering of acrylonitrile-butadiene-styrene: A correlation study. *Polymer Degradation and Stability* **2013,** *98* (10), 2111-2115.
31. Miklečić, J.; Blagojević, S. L.; Petrič, M.; Jirouš-Rajković, V., Influence of TiO2 and ZnO nanoparticles on properties of waterborne polyacrylate coating exposed to outdoor conditions. *Progress in Organic Coatings* **2015,** *89*, 67-74.
32. Wohlleben, W.; Vilar, G.; Fernández-Rosas, E.; González-Gálvez, D.; Gabriel, C.; Hirth, S.; Frechen, T.; Stanley, D.; Gorham, J.; Sung, L.-P.; Hsueh, H.-C.; Chuang, Y.-F.; Nguyen, T.; Vazquez-Campos, S., A pilot interlaboratory comparison of protocols that simulate aging of nanocomposites and detect released fragments. *Environmental Chemistry* **2014,** *11* (4), 402-418.
33. Wohlleben, W.; Neubauer, N., Quantitative rates of release from weathered nanocomposites are determined across 5 orders of magnitude by the matrix, modulated by the embedded nanomaterial. *NanoImpact* **2016,** *1*, 39-45.
34. Zaidi, L.; Kaci, M.; Bruzaud, S.; Bourmaud, A.; Grohens, Y., Effect of natural weather on the structure and properties of polylactide/Cloisite 30B nanocomposites. *Polymer Degradation and Stability* **2010,** *95* (9), 1751-1758.
35. Kaegi, R.; Sinnet, B.; Zuleeg, S.; Hagendorfer, H.; Mueller, E.; Vonbank, R.; Boller, M.; Burkhardt, M., Release of silver nanoparticles from outdoor facades. *Environmental Pollution* **2010,** *158* (9), 2900-2905.
36. Kaegi, R.; Ulrich, A.; Sinnet, B.; Vonbank, R.; Wichser, A.; Zuleeg, S.; Simmler, H.; Brunner, S.; Vonmont, H.; Burkhardt, M.; Boller, M., Synthetic TiO2 nanoparticle emission from exterior facades into the aquatic environment. *Environmental Pollution* **2008,** *156* (2), 233-239.
37. Reed, R. B.; Zaikova, T.; Barber, A.; Simonich, M.; Lankone, R.; Marco, M.; Hristovski, K.; Herckes, P.; Passantino, L.; Fairbrother, D. H.; Tanguay, R.; Ranville, J. F.; Hutchison, J. E.; Westerhoff, P. K., Potential Environmental Impacts and Antimicrobial Efficacy of Silver- and Nanosilver-Containing Textiles. *Environmental Science & Technology* **2016,** *50* (7), 4018-4026.
38. Keller, A. A.; McFerran, S.; Lazareva, A.; Suh, S., Global life cycle releases of engineered nanomaterials. *Journal of Nanoparticle Research* **2013,** *15* (6), 1-17.
39. Piccinno, F.; Gottschalk, F.; Seeger, S.; Nowack, B., Industrial production quantities and uses of ten engineered nanomaterials in Europe and the world. *Journal of Nanoparticle Research* **2012,** *14* (9), 1-11.

40. Gottschalk, F.; Sun, T.; Nowack, B., Environmental concentrations of engineered nanomaterials: review of modeling and analytical studies. *Environ Pollut* **2013,** *181*, 287-300.
41. Alissawi, N.; Zaporojtchenko, V.; Strunskus, T.; Hrkac, T.; Kocabas, I.; Erkartal, B.; Chakravadhanula, V. S. K.; Kienle, L.; Grundmeier, G.; Garbe-Schönberg, D.; Faupel, F., Tuning of the ion release properties of silver nanoparticles buried under a hydrophobic polymer barrier. *Journal of Nanoparticle Research* **2012,** *14* (7), 1-12.
42. Schlagenhauf, L.; Kianfar, B.; Buerki-Thurnherr, T.; Kuo, Y.-Y.; Wichser, A.; Nuesch, F.; Wick, P.; Wang, J., Weathering of a carbon nanotube/epoxy nanocomposite under UV light and in water bath: impact on abraded particles. *Nanoscale* **2015,** *7* (44), 18524-18536
43. Schlagenhauf, L.; Nüesch, F.; Wang, J., Release of Carbon Nanotubes from Polymer Nanocomposites. *Fibers* **2014,** *2* (2), 108-127.
44. Yousif, E.; Haddad, R., Photodegradation and photostabilization of polymers, especially polystyrene: review. *SpringerPlus* **2013,** *2*, 398.
45. Torikai, A.; Ohno, M.; Fueki, K., Photodegradation of poly(methyl methacrylate) by monochromatic light: Quantum yield, effect of wavelengths, and light intensity. *Journal of Applied Polymer Science* **1990,** *41* (5-6), 1023-1032.
46. Ikada, E., Photo decomposition of Aliphatic Polyesters. V. *Journal of Photopolymer Science and Technology* **1998,** *11* (1), 23-27.
47. Health, I. f. V. P. World Maps of Koppen-Geiger Climate Classification. http://koeppen-geiger.vu-wien.ac.at/usa.htm (accessed August 22).
48. Reed, R. B.; Goodwin, D. G.; Marsh, K. L.; Capracotta, S. S.; Higgins, C. P.; Fairbrother, D. H.; Ranville, J. F., Detection of single walled carbon nanotubes by monitoring embedded metals. *Environmental science. Processes & impacts* **2013,** *15* (1), 204-13.
49. Wang, J.; Lankone, R. S.; Reed, R. B.; Fairbrother, D. H.; Ranville, J. F., Analysis of single-walled carbon nanotubes using spICP-MS with microsecond dwell time. *NanoImpact* **2016,** *1*, 65-72.
50. Montano, M. D.; Badiei, H. R.; Bazargan, S.; Ranville, J. F., Improvements in the detection and characterization of engineered nanoparticles using spICP-MS with microsecond dwell times. *Environmental Science: Nano* **2014,** *1* (4), 338-346.
51. Praetorius, A.; Gundlach-Graham, A.; Goldberg, E.; Fabienke, W.; Navratilova, J.; Gondikas, A.; Kaegi, R.; Gunther, D.; Hofmann, T.; von der Kammer, F., Single-particle multi-element fingerprinting (spMEF) using inductively-coupled plasma time-of-flight mass spectrometry (ICP-TOFMS) to identify engineered nanoparticles against the elevated natural background in soils. *Environmental Science: Nano* **2017,** *4* (2), 307-314.
52. Nguyen, T.; Pellegrin, B.; Mermet, L.; Shapiro, A.; Gu, X.; Chin, J., Network aggregation of CNTs at the surface of epoxy/MWCNT composite exposed to UV radiation. *Nanotechnology* **2009,** *1*, 90-93.
53. Nguyen, T.; Pellegrin, B.; Bernard, C.; Gu, X.; Gorham, J. M.; Stutzman, P.; Stanley, D.; Shapiro, A.; Byrd, E.; Hettenhouser, R.; Chin, J., Fate of nanoparticles during life cycle of polymer nanocomposites. *J Phys: Conf Ser* **2011,** *304*.
54. Wohlleben, W.; Brill, S.; Meier, M. W.; Mertler, M.; Cox, G.; Hirth, S.; von Vacano, B.; Strauss, V.; Treumann, S.; Wiench, K.; Ma-Hock, L.; Landsiedel, R., On the lifecycle of nanocomposites: comparing released fragments and their in-vivo hazards from three release mechanisms and four nanocomposites. *Small* **2011,** *7* (16), 2384-95.
55. Hirth, S.; Cena, L.; Cox, G.; Tomović, Ž.; Peters, T.; Wohlleben, W., Scenarios and methods that induce protruding or released CNTs after degradation of nanocomposite materials. *Journal of Nanoparticle Research* **2013,** *15* (4), 1-15.
56. Lankone, R. S.; Wang, J.; Ranville, J. F.; Fairbrother, D. H., Photodegradation of polymer-CNT nanocomposites: effect of CNT loading and CNT release characteristics. *Environmental Science: Nano* **2017,** *4* (4), 967-982.
57. Nguyen, T.; Pellegrin, B.; Bernard, C.; Gu, X.; Gorham, J. M.; Stutzman, P.; Stanley, D.; Shapiro, A.; Byrd, E.; Hettenhouser, R.; Chin, J., Fate of nanoparticles during life cycle of polymer nanocomposites. *Journal of Physics: Conference Series* **2011,** *304* (1), 012060.

58. Pourzahedi, L.; Eckelman, M. J., Environmental Life Cycle Assessment of Nanosilver-Enabled Bandages. *Environmental Science & Technology* **2015,** *49* (1), 361-368.
59. Travan, A.; Marsich, E.; Donati, I.; Benincasa, M.; Giazzon, M.; Felisari, L.; Paoletti, S., Silver–polysaccharide nanocomposite antimicrobial coatings for methacrylic thermosets. *Acta Biomaterialia* **2011,** *7* (1), 337-346.
60. Dallas, P.; Sharma, V. K.; Zboril, R., Silver polymeric nanocomposites as advanced antimicrobial agents: Classification, synthetic paths, applications, and perspectives. *Advances in Colloid and Interface Science* **2011,** *166* (1–2), 119-135.

**Chapter 4.** Characterizing copper release and transformation following natural weathering of nanoenabled products

**Abstract**

Commercially available lumber pressure-treated with micronized copper azole (MCA) was naturally weathered for up to 20 months in five unique climates across the continental United States. On a monthly basis, copper release masses were measured and local weather conditions were recorded at each location to determine the extent to which local climate regulated the release of copper from this engineered nanomaterial. In addition to natural weathering experiments, MCA-wood leachate solutions were prepared in lab and analyzed with single-particle-ICP-MS (spICP-MS) to determine the form of released copper as well as identify any potential transformations following its release. MCA-wood samples were also exposed to simulated landfill conditions to assess copper release during their end-of-life (EoL) phase. MCA-wood was measured to have an initial copper content of 0.23%$_{w/w}$ (± 0.07) and SEM imaging found copper nanoparticles present in discrete micron-sized aggregates on wood particulates. Following 18 months of weathering, two well-defined release trends were observed: (1) in wetter climates, copper release occurred primarily during the first year of weathering and was the result of surface/near-surface copper washing from the sample, and (2) in drier climates, the wood dried and cracked, producing new copper containing wood surface areas, which facilitated increased copper release into the second year of natural weathering. EoL testing found unweathered MCA wood resisted copper leaching (< 10% of initially embedded copper released) in simulated landfill conditions and that copper released during weathering slightly decreased the amount of copper available to leach during toxicity characteristic leachate (TCLP) testing. Single particle inductively coupled plasma mass spectrometry (spICP-MS) was utilized to examine the fate of copper following its

release in more controlled lab-based settings and found that copper was released from MCA- wood predominantly as ions and particles less than 450nm in size. Following up to 6 weeks in solution, spICP-MS found released copper material was largely resistant to dissolution and retained its particulate form. Findings presented are also contextualized for how they may be useful for future Life Cycle Analyses of MCA-wood

## Introduction

Wood possesses many desirable properties (e.g. natural abundance, high strength, low density) that have led to its use as a building material for centuries. However, a persistent challenge in the utilization of wood for construction is its inherent susceptibility to deterioration due to weathering and wear, fungal/microbial degradation, and insect burrowing. To combat degradation, chemical treatment methods have been used, dating back to at least the Middle Ages, in order to increase lumber's useful lifetime in a given application.[1] More recently, pressure treatments using copper (Cu) based antifungal, antimicrobial, and insect resistant formulations have emerged as a leading treatment.[2]

Prior to 2003, the preferred pressure treatment chemical formulation used by the wood industry for residential purposes was copper chromated arsenate (CCA). However, studies conducted by the U.S. Consumer Product Safety Commission (CPSC) found that CCA-treated wood led to elevated human exposure to arsenic, especially for children in contact with CCA-treated wood at playgrounds.[3] Soon after publication of these findings, CCA was voluntarily phased out in favor of alternative pressure treatment formulations. Several Cu-based wood treatment alternatives were employed, including acid copper chromate (ACC), alkaline copper quaternary (ACQ), and ionic copper azoles; unfortunately these alternatives were found to release significant amounts of copper to the environment.[4] So much so that metal fasteners affixed to the treated wood corroded quickly due to increased copper exposure.[5] To overcome the challenge of copper release, ionic copper formulations such as those mentioned above were abandoned and a micronized copper wood treatment formulation was adopted.

Micronized copper (MC) – the industry preferred term for copper particles possessing dimensions on the nanometer to micron scale – is produced from ball-milling and sieving copper (II) carbonate hydroxide ($Cu_2CO_3(OH)_2$). This mechanical process delivers Cu particles ranging in size from 1nm to 250μm which can be impregnated into wood via pressure treatment.[6] Once impregnated into the wood, MC particles deposit along cell walls and in connective regions between cellular elements in the treated lumber.[7] There are several means by which copper nanoparticles are believed to impart anti-fungal properties to the wood. These particles may act as reservoirs, gradually releasing solubilized/ionic copper,[6] and/or express a Trojan Horse mechanism after contact with fungi, inducing toxic effects from within fungi cell walls.[8-9] The complex interactions between copper and fungi and their mechanism of toxicity have been thoroughly explained by Civardi, *et al.*[10]

Approximately 80% of pressure-treated wood produced in the United States and Canada contains MC.[2] MC treatments usually contain an organic azole fungicide along with the copper carbonate. The industry term for this treatment approach is micronized copper azole (MCA).[2] While MCA-treated wood may be commercially ubiquitous and generally effective at preventing wood rot/deterioration, it is not without its own unique set of concerns, as there are uncertainties regarding copper release such as its magnitude, rate, form, and subsequent toxicity to the environment.[11]

An EPA report published in 2014 provides one of the most comprehensive assessments of copper release from MCA pressure-treated wood.[2] This report included experiments which simulated two environmental exposure scenarios: copper transfer following physical contact (i.e. wiping) and copper leaching into aqueous media during

submersion/soaking. Wiping experiments performed before and after a period of natural weathering found that both unweathered and weathered samples (up to 400 days) released similar amounts of copper, ≈1.5mg total Cu/$m^2$, upon wiping. Aqueous leaching experiments found that unweathered MCA-wood blocks released significant copper, nearly 200 mg total Cu/$m^2$, during 72 hours of submersion. Absent from this study however, was the quantification of copper released during natural weathering.

Several other studies have focused more directly on examining the role of weathering in regulating copper release from pressure-treated lumber, albeit with wood treated with non-MCA formulations. Lebow *et al.* examined southern pine treated with either CCA or alkaline borax-copper (BC), which was then subjected to simulated rainfall via spraying with deionized water and found that following approximately 28 days of spraying spread out over six weeks, CCA and BC wood released a total of 0.6% (+/- 0.2) and 4.8% (+/- 0.8) of total copper available, respectively.[12] Lebow *et al.* also examined how the rate of simulated rainfall impacted the extent of copper release from CCA-wood. Interestingly, experiments indicated that slower rates of rainfall lead to an increase in the mass of copper release from CCA treated samples. [13] Outdoor natural weathering of BC wood was also carried out and it was found that following approximately eight months of exposure, in which approximately 34 inches of precipitation occurred, 4" x 1.5" x 3.5"" samples released ~20% of their initially embedded copper.[14] While well-crafted, this study weathered its wood in only one location which prevented analysis of how natural weathering in different climates would have impacted release.

Contrasting efforts to quantify copper released from pressure treated limber, there are relatively few studies that attempted to characterize copper release form. Once such

attempt, however, was detailed in the EPA report described above. Experimentally, the approach required filtering leached copper samples through successively smaller filters (2.5μm, 0.45μm, and 10kDa). Following each filtration, the concentration of total copper remaining in solution/suspension was quantified with ICP-MS. It was determined that that ~95% of copper released from MCA-wood during aqueous leaching was in its ionic form (i.e., passed through the 10kDa filter) after 72 hours in solution.[2] While informative, this approach relied on inferring copper size from filter size rather than directly measuring it. One technique can be used in tandem with filter to directly determine released copper size is single particle inductively couple plasma mass spectrometry (spICP-MS). spICPMS has previously been used to detect metallic nanomaterials in environmental matrices,[15-17] and is a promising method that can evaluate the form of released copper more directly than filtration. The undergirding principal of spICP-MS is that that once a particle is introduced into and ablated by the plasma, the resulting ions will be measured as a discrete pulse above the background signal,[18] whose area is directly proportional to the particle mass.[19] The absence of pulses considered to be the result of a fully dissolved analyte. By directly measuring the mass of particles present in solution, spICP-MS permits sample analysis that successive filtration experiments cannot achieve – specifically, particle masses measured with spICP-MS can then be used to calculate particle size from a known particle density.

Natural weathering remains a principal degradation and release pathway for commercial MCA-wood. The primary focus of the present study is to explore a gap left by previous studies in the area of natural weathering – specifically, how does the climate in which MCA-wood is utilized regulate copper release & how does copper form change

following its release. To address these knowledge gaps, this study explicitly examined the interplay of natural weathering and copper release from commercially acquired MCA wood samples weathered in five unique climates across the continental United States: Baltimore, MD, Golden, CO, Tempe, AZ, Pittsburgh, PA, and Corvallis, OR. In addition to the monthly collection of rainwater runoff from wood samples for copper concentration measurements with ICP-OES, local weather conditions (e.g. temperature, UV-index, solar flux, and precipitation) were also recorded and collected monthly with location specific weather monitoring stations. End-of-life Toxicity Characteristic Leaching Procedure (TCLP) testing was carried out on weathered and unweathered MCA-wood samples to determine the relationship among use-phase weathering, copper release, and copper leaching in landfills. Lab-based dissolution studies were performed with spICP-MS to characterize the form and potential transformation of copper following its release from MCA wood. Lastly, informed by the data collected in this study, implications towards conducting a life cycle impact assessment (LCIA) to examine the benefits and tradeoffs of MCA wood were assessed.

## Experimental Methods

Sample preparation

Pressure treated lumber was purchased from a commercial home improvement depot and was cut to size in Baltimore, MD. The primary wood examined in the weathering portion of this study was MCA- pressure treated lumber intended for above ground (AB) use, produced by *YellaWood*, and specified to contain *micronized copper azole AA-696*. The treatment contained copper and tebuconazole at a 25:1 mass ratio.[20] Ground Contact (GC) lumber of the same brand and treatment type were used in laboratory studies concerning copper form and dissolution studies described later in the experimental. The single difference between AB and GC lumber is that GC was treated with higher concentrations of the MCA solution. Two pieces of AB lumber (originally 8' x 3.5" x 1.5" in size) were acquired and cut into three sizes: venti (2" x 3.5" x 1.5"), tall (2" x 2.3" x 1.5"), and small (2" x 1.2" x 1.5"). For each size, triplicate samples were cut for distribution and natural weathering at each weathering location. All samples were also weighed and their physical dimensions measured.

Two Teflon straps (purchased from Industrial Netting), were affixed to each sample so that the samples may be secured in place over their respective rain-water runoff collection jar (Figure 4-1). Samples were affixed with the straps such that the grain of the wood was perpendicular to incoming rainfall. Samples were then labeled and distributed for weathering.

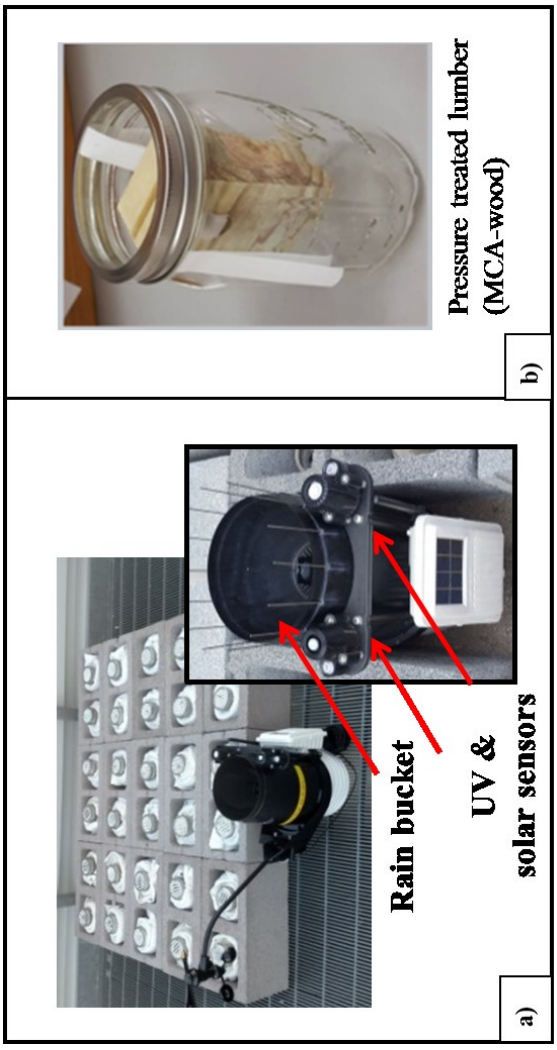


**Figure 4-1**: a) Photo of active outdoor weathering set, with sample jars secured in cinderblocks and location specific weather station. b) Assembled MCA sample suspended in rainwater collection jar

Weathering locations and procedures

Five locations were selected to provide a diverse set of local climates, as described by the Koppen climate classification system, (Figure 4-2): Baltimore, MD – Cfa (warm temperate, fully humid, hot summer), Golden, CO – Dfb (snow, fully humid, warm summer), Tempe, AZ – Bsk (arid, summer dry, cold arid), Csa (warm temperate, summer dry, hot summer) Bwh (arid, winter dry, hot arid), Bsh (arid, summer dry, hot arid), Pittsburgh, PA – Dfb (snow, fully humid, warm summer), Cfa (warm temperate, fully humid, hot summer), and Corvallis, OR – BSk (arid, steppe, cold arid), Csa (warm temperate, summer dry, hot summer).[21]

Once the samples were received at each location and secured in place outdoors on rooftops, monthly sample collection procedures were followed, as described previously by Lankone, *et al* .[22] Each month, the accumulated rainwater in each jar was collected for inductively coupled plasma optical emission spectroscopy (ICP-OES, PerkinElmer Optima 8300 or PerkinElmer Optima 8300) analysis to determine the concentration of released copper from the wood samples. Each jar was rinsed with 20mL of 2% $HNO_3$ to capture any copper residual on the jar after rainwater collection. The final volume of both the rainwater and acid rinse were recorded and used to calculate total copper release for each sample from the measured copper concentration. In addition to the monthly collection of rainwater runoff, climate data including temperature, precipitation, and solar fluence were also recorded. Control experiments to determine copper recovery using this method were also performed (as detailed in Chapter 5, section "Acid rinse control studies").

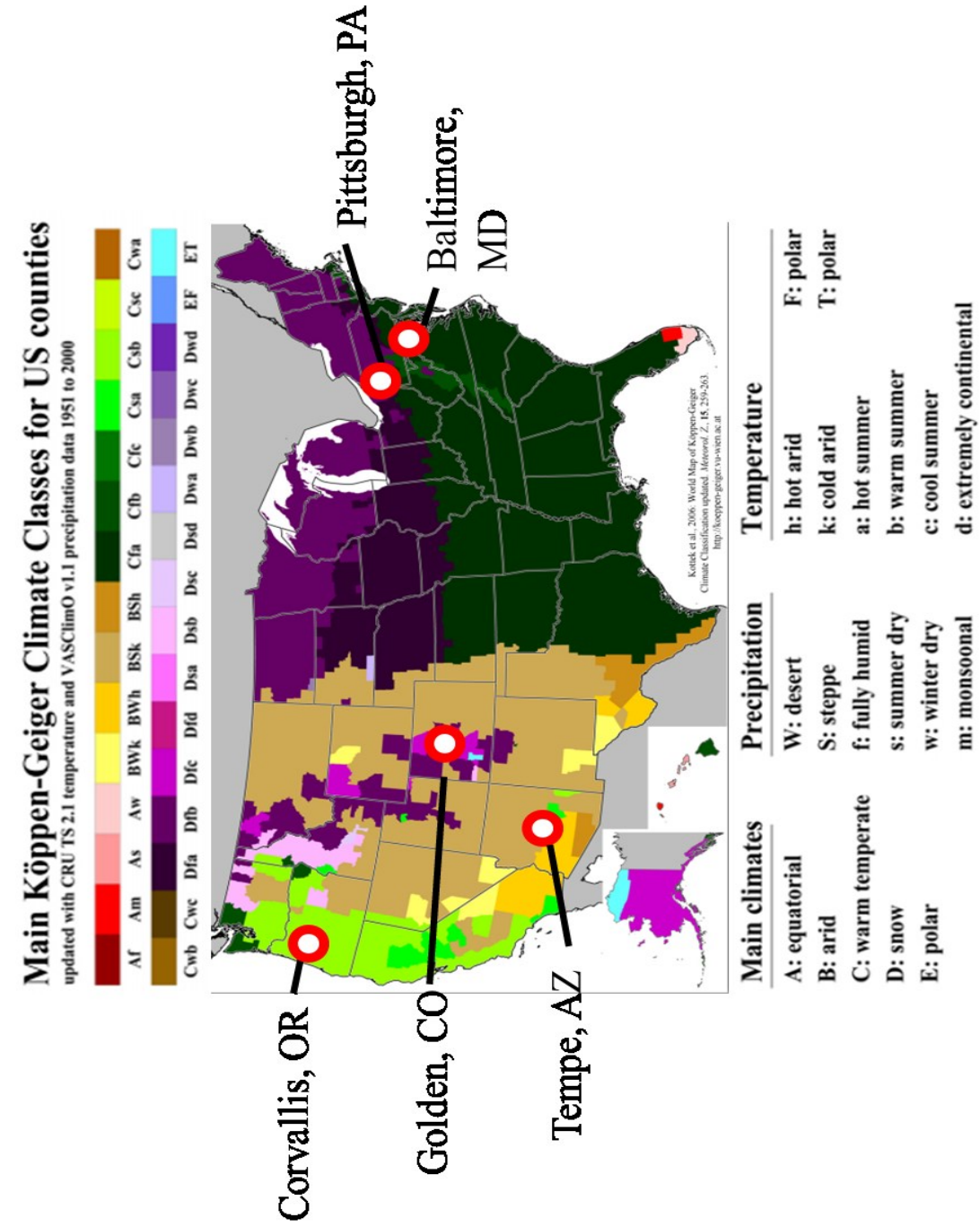


**Figure 4-2**: Climate map shows climate diversity across all weathering locations.

Simulated heat and UV exposure

To determine the extent to which heat and UV exposure impacted copper release, as received venti sized AB wood samples were placed in a photochemical reactor (Rayonet) equipped with 16 low pressure mercury bulbs, that each emitted 300nm light at approximately 15W. Samples were irradiated continuously for five weeks, at approximately $50^0$C. Irradiated samples and control samples (stored in the dark at room temperature) were then submerged in 400mL of water, at ten second intervals, three times in a row. Following each period of submersion, the resulting solution was collected following the acid rinse collection procedure described above. Copper released from each sample during each period of submersion was then measured via ICP-OES. Each test was performed in triplicate.

Embedded Copper concentration analysis

Saw dust samples were collected during the sample cutting process and the initial copper concentration present in the wood was measured with two independent methods. The first method was ICP-OES analysis following EPA method 3051A.[23] Briefly, this first required the addition of 100-200mg of sawdust to a Teflon microwave digestion vial containing concentrated nitric acid. The vials were then sealed according to manufacturer directions, digested, and analyzed with ICP-OES. To assess the uniformity of copper concentration in the wood, these samples were taken at various points along the length of the pressure treated wood to determine the average copper content across the length of the wood. The second method utilized Atomic Absorption Spectroscopy (AAS). In this approach, 100-200mg of copper sawdust was digested in concentrated nitric acid heated to 70 °C for ~5 hours, prior to analysis. Sawdust samples for these analyses were

collected from different depths into the wood to further characterize the uniformity of copper distribution prior to weathering. AAS was also performed on digested MCA-wood collected from weathered samples in order to assess the location from which copper primarily released from the wood (as detailed in Chapter 5 section "Copper concentration distribution").

Copper form and dissolution experiments

The form of copper released from the MCA-wood and the copper's dissolution behavior in solution following release was characterized with spICP-MS (instrumental details provide in Chapter section "Copper single particle ICPMS"). To this end, a pre-weighed block of GC MCA wood was submerged in MilliQ water and shaken for 30 seconds to stimulate copper release. After shaking, the wood was left to sit in the water for another minute and then removed, producing a leachate solution for subsequent characterization. Three separate blocks weighing 3.2-4.2g in 250mL of MilliQ water were used as triplicate samples. The leachate was analyzed at time points 0h, 24h, 48h, 1week, 2wk, 4wk, and 6 wks. At each time point, the unfiltered leachate from each sample was directly analyzed by spICPMS. Leachate collected at each time point was also filtered through 0.02µm and 0.45µm syringe filters and analyzed by spICPMS.

End-of-life testing

End-of-life (EoL) testing was carried on unweathered and weathered samples from each location in accordance with a modified version of USEPA Test Methods for Evaluating Solid Waste: Physical/Chemical Methods (SW-846 method 1311). A full account of experimental details for this method can be found in Chapter 5.

Materials Characterization

Technical details regarding the instrumentation used (AAS, spICP-MS, scanning electron microscopy, energy dispersive X-ray spectroscopy, ICP-OES, and Attenuated Total Internal Reflectance-FTIR) for materials characterization can be found in the Chapter 5.

## Results and Discussion

MCA-wood samples were placed outside to weather in five locations across the continental United States. Each location was selected to provide a unique climate (Figure 4-2)[21] and weather conditions recorded at each location reflect the diversity of weather factors endured by samples weathered in each location (Figure 4-3). The combination of climate-specific copper release measurements utilized in tandem with location-specific weather data permitted examination and determination of which weather factors are most important in regulating both the rate and magnitude of copper release from MCA-wood into the natural environment. Laboratory based experiments were also carried out to explicitly identified the form and potential transformation of engineered copper following its release from MCA pressure treated lumber, through the utilization of spICP-MS.

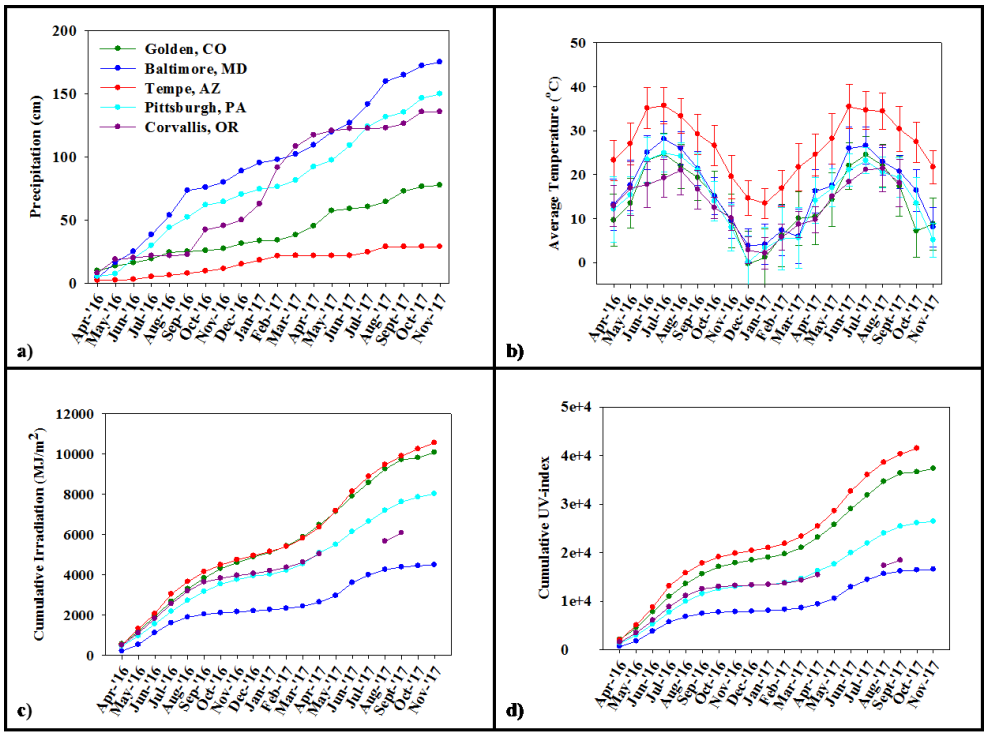


**Figure 4-3**: Summary of weather data collected at each weathering location: a) cumulative precipitation, b) average monthly temperature, c) cumulative visible solar irradiance, d) cumulative UV index.

*Macroscopic wood transformations*

The slight green tint in unweathered MCA wood (top left, Figure 4-4) is due to the MCA impregnated into the wood. In this study, the unweathered wood blocks also appear to be free of any cracks, deformations, or indications of deterioration. Following eighteen months of natural weathering, two clear transformations to the wood samples are observed: The first is a distinct discoloration, with samples weathered in Baltimore, MD, Pittsburgh, PA, and Corvallis, OR appearing more grey in color, and samples weathered in Golden, CO and Tempe, AZ appearing more orange/yellowed. The greying of the samples weathered in Baltimore, MD, Pittsburgh, PA, and Corvallis, OR was driven by extensive precipitation (Figure 4-3) at these three locations rinsing away oleoresin oils (i.e. turpentine and diterpene resin acids) associated with the wood.[24] The color changed observed for samples weathered in Golden, CO and Tempe, AZ, alternatively, is attributed to photobleaching due to the high amount of cumulative sunlight (~10,000 $MJ/m^2$) experienced by samples weathered in these two locations, relative to the other three locations (Figure 4-3c). Interestingly, while the photobleaching of these samples resulted in an obvious change in their color, it did not cause sufficient molecular degradation of the wood to result in a measurable difference in the samples' infrared spectra (Figure 4-5). In a previous study that exposed wood to visible and UV light, this behavior was also reported and attributed to photobleaching being driven primarily by visible light, leaving the infrared spectra unchanged.[25]

The second observed transformation of the MCA wood samples was the formation of small cracks along the sample surfaces, as seen in images of the samples in profile (Figure 4-4, bottom panel). While visible macroscopic cracking occurred to some extent for MCA-wood weathered in all locations, those weathered in Golden, CO and

Tempe, AZ exhibited a greater degree of cracking than samples weathered in the other three locations – with MCA-wood weathered in Tempe, AZ showing the greatest extent of cracking. The increased sample cracking observed in samples weathered in Golden, CO and Tempe, AZ is likely the result of the stress generated from non-uniform wood shrinking caused by wood drying due to each location's limited precipitation.[26] Golden, CO and Tempe, AZ recorded cumulative precipitation values following eighteen months of weathering of 77 and 29 cm, respectively, compared to 175, 150, and 136 cm measured in Baltimore, MD, Pittsburgh, PA, and Corvallis, OR, respectively (Figure 4-3a). For samples weathered in Tempe, AZ, wood drying and cracking was further enhanced due to Tempe, AZ experiencing in any given month temperatures 13º C greater on average than the other four locations (Figure 4-3b). The absence of extensive cracking for samples weathered in the other three locations is attributed to locations' increased precipitation and more moderate temperatures which prevented long periods of wood drying. From these observations, it is clear that extent of macroscopic physical transformations to the wood following weathering will depend directly on its exposure to different climate factors, with precipitation and sun exposure impacting the physical appearance of the wood and dryer climates deleteriously impacting the wood's structural integrity.


**Figure 4-4**: Images of pressure treated venti sized lumber before and after 18 months of outdoor weathering show from the top (top panel) and side profile (bottom panel).

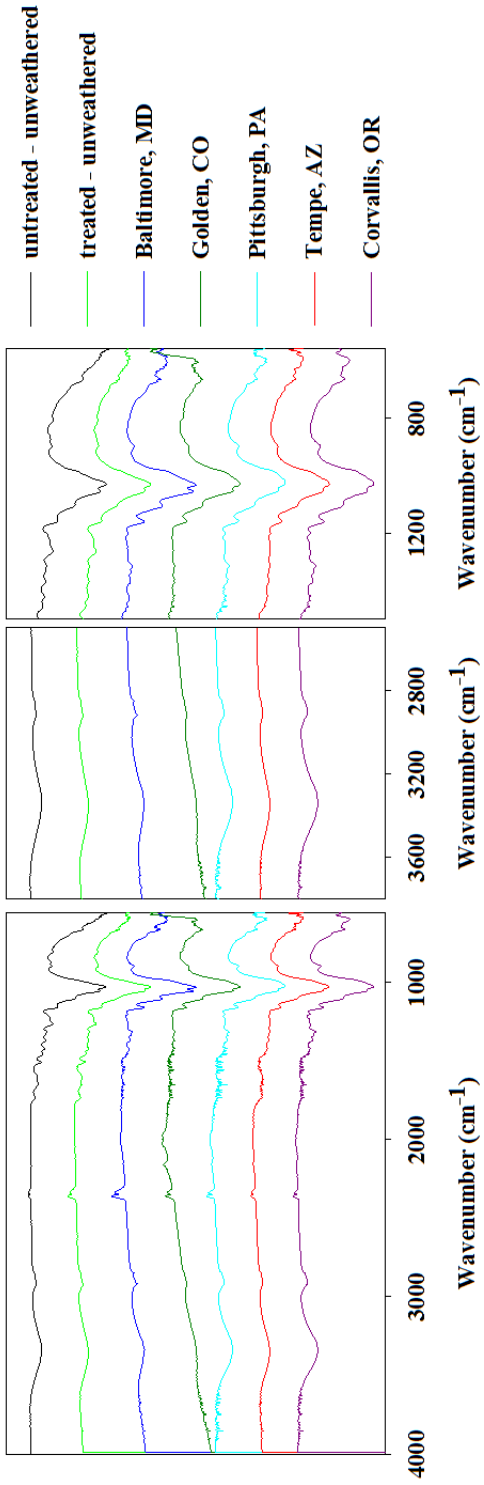


**Figure 4-5**: ATR-FTIR spectra collected from unweathered and weathered samples

*Characterizing the concentration of impregnated copper*

To determine the initial copper concentration present in unweathered MCA-wood, two dozen sawdust samples were collected from various points along the as-purchased 8' x 3.5" x 1.5" planks, including samples collected from both the interior and exterior of the wood at various depths. Following sawdust collection and acid digestion, independent analysis with ICP-OES and AAS found that initial copper content within the MCA wood to be $0.23\%_{w/w}$ (± 0.07), as shown in Figure 4-6. MCA wood samples were also imaged with SEM to visualize the presence of copper prior to weathering. As seen in Figure 4-7a, copper is present in discrete regions along the wood rather than completely dissolved as a result of the pressure treatment process and distributed evenly throughout. EDX spectra (Figure 4-7b) were also collected to confirm the presence of copper observed in during imaging.

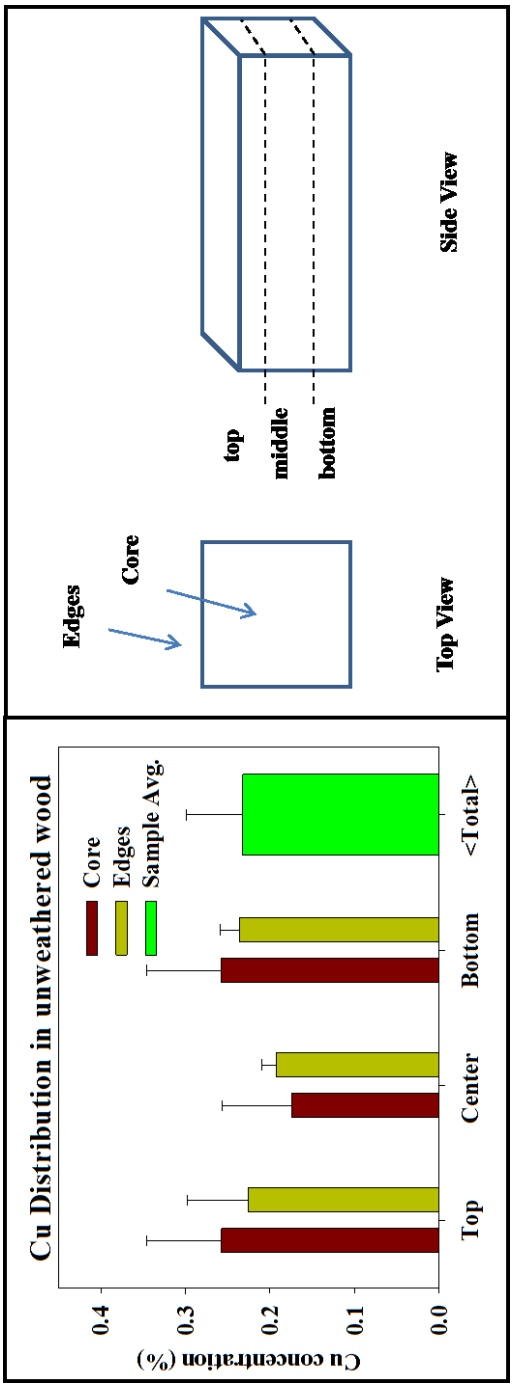


**Figure 4-6**: (Left) Copper concentration as measured by atomic absorption spectroscopy following acid digestion of wood samples collected from different depths and locations throughout an unweathered pressure treated wood sample. (Right) Schematic of orientation labels

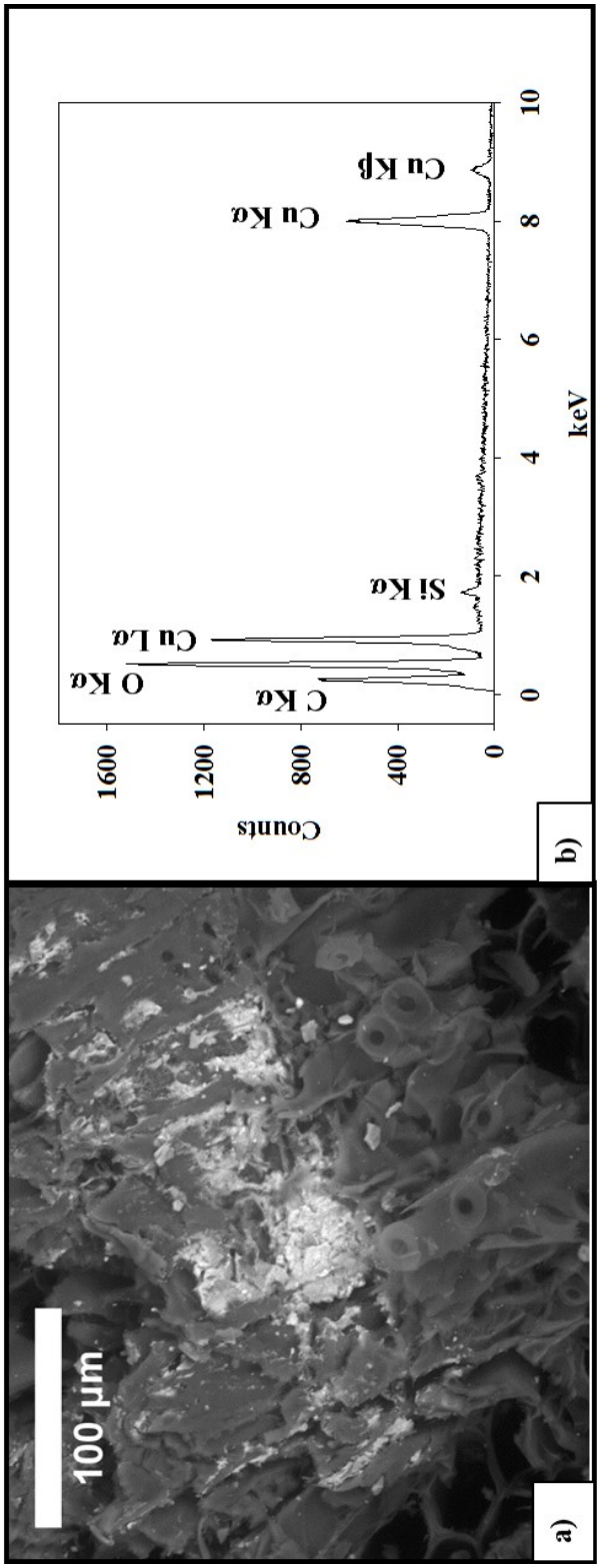


**Figure 4-7**: a) The presence of copper on the surface of pressure treated wood samples was visualized as particulate aggregates with SEM imaging and b) the presence of copper in acquired images was confirmed with EDX spectroscopy.

*Monthly copper release*

Monthly copper release masses (mg) and monthly precipitation values (cm) were measured at each location for 18 continuous months of weathering and are shown in Figure 4-8. The top panel for each location shown displays location specific monthly precipitation and the bottom panel presents the average mass of copper released from each sample size. The error bars are calculated from the standard deviation of copper release mass measured from triplicate samples of each size. Copper recovery control experiments were performed as well, and demonstrated that >95% of copper released into the jars was captured following the acid rinse procedure used in this study (Table 4-1).

The sample holders in this study were designed such that rainfall would hit the samples then flow into collection jars and accumulate below the samples for monthly collection. Samples in Corvallis, OR, however, encountered Typhoon Songda during October 2016, which resulted in sustained rains that submerged the MCA samples within their respective collection jars. For this reason, release data from the Oregon samples is shown separate from the data collected from other locations to highlight that these samples were subjected to an extreme weathering event that resulted in their unintended submersion in water for up to three weeks. As a result, release data from Corvallis, OR is not directly compared to the other four locations because the extent to which this sustained submersion event may have impacted subsequent copper release is unknown. However, copper release data from Corvallis, OR does provide unique insight as to how extreme weather events will impact copper release from MCA wood. During Typhoon Songda 20 cm of precipitation were recorded and resulted in copper release masses upwards of 4 mg. Several months later, Corvallis experienced a month of heavy precipitation receiving 28 cm, but only ~0.5 mg of copper release was measured. This

indicates that following MCA wood submersion, a large portion of readily available copper was leached from the wood and resulted in a sharp reduction in the amount of copper available to release during subsequent precipitation events. Therefore, extreme weathering events that saturate MCA wood in rainwater for an extended period of time have the potential to greatly inhibit future copper release.

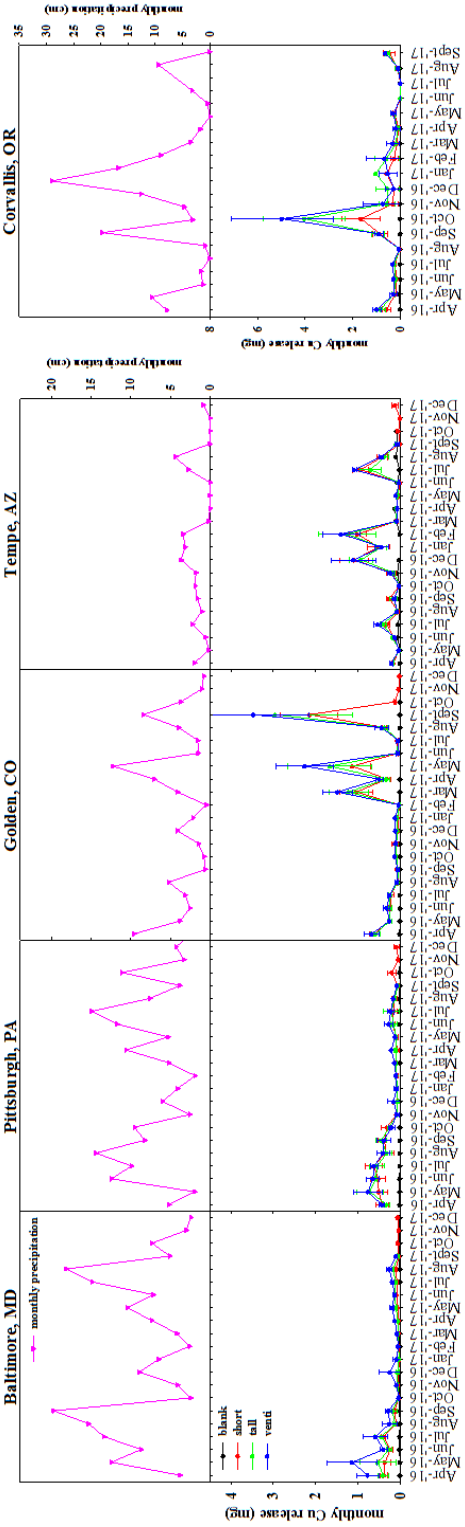


**Figure 4-8**: Monthly precipitation (top) and Cu release values (bottom) measured at each location demonstrate that release occurs only for months in which there is rainfall – but only in drier climates does release continue to occur with rainfall following a year

| | Cu (ppm) | mg/L | mg | | % recovery |
|---|---|---|---|---|---|
| Sample A. Before | 11.9 | 12.0 | 1.078 | capped | 97.0 |
| Sample A. After | 10.5 | 10.5 | 1.046 | | |
| Sample B. Before | 11.7 | 11.7 | 1.054 | capped | 101.1 |
| Sample B. After | 10.6 | 10.7 | 1.065 | | |
| Sample C. Before | 11.8 | 11.8 | 1.065 | capped | 98.1 |
| Sample C. After | 10.4 | 10.4 | 1.044 | | |
| Sample D. Before | 12.1 | 12.1 | 1.089 | uncapped | 97.9 |
| Sample D. After | 3.4 | 3.4 | 1.066 | | |
| Sample E. Before | 11.4 | 11.4 | 1.023 | uncapped | 100.0 |
| Sample E. After | 2.9 | 2.9 | 1.023 | | |
| Sample F. Before | 12.0 | 12.0 | 0.782 | uncapped | 89.1 |
| Sample F. After | 1.9 | 1.9 | 0.697 | | |
| **Sample G: Filt SS** | **12.0** | **12.0** | | | |

| avg | stdev |
|---|---|
| **98.7** | **2.1** |
| **95.7** | **5.8** |

**Table 4-1**: Summary of copper recovery for each sample examined in copper recovery control experiments. Triplicate samples of capped and uncapped released copper solutions were placed outside to weather for one month. The copper recovery for each sample was calculated by comparing the recovered copper mass to the initial copper mass present in solution.

From the plots shown in Figure 4-8, two trends in copper release are observed. The first is that precipitation is absolutely required for copper release, irrespective of location and climate. The second is that for samples weathered in wetter climates (Baltimore, MD and Pittsburgh, PA), copper release is most prominent during the first 10 months of weathering and then subsides, while samples weathered in Golden, CO and Tempe, AZ exhibited sustained copper release (> 1 mg/month) during months with precipitation well into the second year of weathering. This contrasting release behavior between samples weathered in Baltimore, MD and Pittsburgh, PA vs. Golden, CO and Tempe, AZ indicates that in wetter climates, precipitation during the initial months of weathering rinsed off readily available copper on or near the surface of the MCA wood. In dryer climates like those in Golden, CO and Tempe, AZ in which the MCA wood fractured, release was sustained due to physical deterioration of the wood samples: the sample cracking experienced by samples weathered in Golden, CO and even more so in Tempe, AZ increased the overall copper containing surface area of the wood samples and allowed previously not accessible copper impregnated in the interior of the MCA wood to become exposed and rinse off with incident rainwater. These observations make apparent that in dryer climates where sample fracturing occurs, copper release from MCA wood will continue over a longer time (> one year) and is not be restricted to the initial months of exposure.

Copper release was found to be largely independent of the size of MCA wood used in this study, in that all three sizes of wood released similar quantities of copper each month at each location. This suggests release occurs from primarily the top face, which possesses a constant surface area in all sample sizes. To test this hypothesis,

sawdust samples from the top, middle, and bottom of venti MCA samples from Pittsburgh, PA, Golden, CO, and Tempe, AZ were collected, digested, and analyzed with AAS to determine the location (i.e. depth from the top face) from which copper was released from the wood. Results are summarized in Table 4-2 and presented as the fraction of copper, with respect to original copper concentration, lost from the wood following eighteen months of weathering. It was found that for samples weathered in Pittsburgh, PA and Golden, CO, copper release occurs primarily from the top (i.e. the side that faces up) of the MCA wood. This result is unsurprising, as it is the top face which most readily encounters incident rainfall. The decreased copper release from the bottom of samples weathered in Pittsburgh, PA and Golden, CO is attributed to the lack of direct precipitation experienced by that region of the wood reducing the overall copper exposure to water/precipitation. For samples weathered in Tempe, AZ, this trend is not observed but rather the top, middle, and bottom of the wood samples were all found to have released comparable amounts of copper. This is attributed to the extensive sample fracturing that occurred to samples weathered in Tempe (Figure 4-4) allowing rainfall better access to copper embedded throughout the MCA sample. These findings suggest that not only will local climate impact the longevity of copper release from MCA wood, it will also impact the region of wood from which copper is released.

| | Cu Loss (%) | | |
|---|---|---|---|
| | Pittsburgh, PA | Golden, CO | Tempe, AZ |
| Top | 36 (± 8) | 62 (± 12) | 42 (± 17) |
| Center | 39 (± 7) | 69 (± 18) | 39 (± 13) |
| Bottom | 29 (± 1) | 19 (± 11) | 55 (± 33) |

**Table 4-2**: Saw dust samples were collected from weathered wood samples at increasing depths, digested in acid, and analyzed with atomic absorption spectroscopy. Depth profiling of samples reveals copper is not lost uniformly from wood samples, with respect to the top of the sample. Note: the fraction (%) of copper lost is shown in each column, parenthetical values are the calculated standard deviation from sample replicates.

It is also noted that all samples weathered in this study

were oriented such that the wood grain was perpendicular to incident precipitation. To examine the role of orientation in regulating copper release, triplicate cubic inch MCA samples (1" x 1" x 1") were prepared and orientated either parallel or perpendicular to incident precipitation and weathered for eight months in Baltimore, MD. It was found that grain orientation did have an effect on copper release, with parallel oriented samples released approximately 25% more copper than perpendicular samples (Figure 4-9). This indicates that the orientation of MCA wood during its use will have some effect on its propensity to release copper when exposed to precipitation.

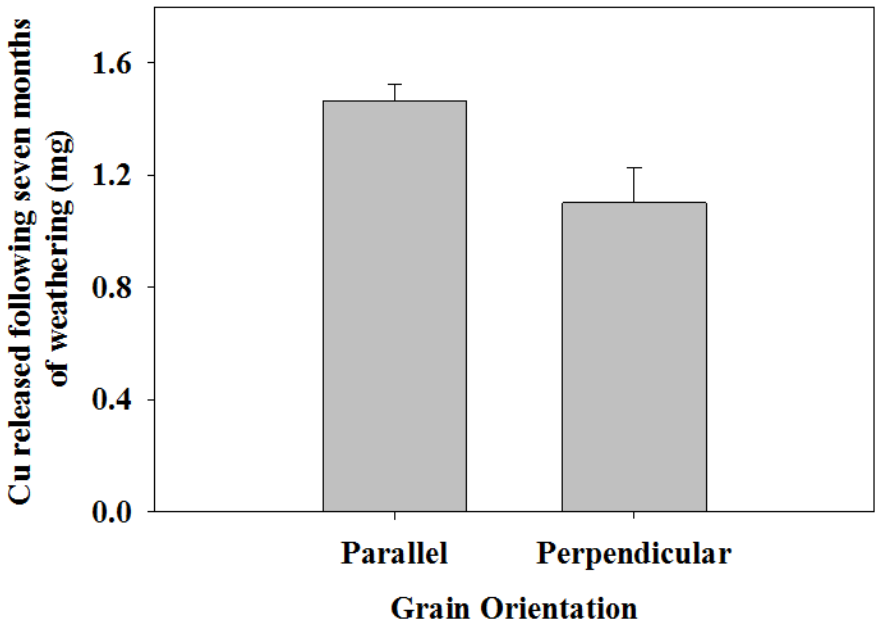


**Figure 4-9**: Copper release (mg) measured from cubic wood samples to assess influence of wood grain orientation with respect to direction of precipitation.

*Climate regulated copper release*

As discussed above, samples in Golden, CO and Tempe, AZ are found to have sustained elevated levels (>1 mg) of copper release many months after samples in wetter climates have abated in their copper release quantities. This is a result of the samples weathering in wetter climates being depleted of readily available copper on their surface, while samples weathered in Golden, CO and especially Tempe, AZ were sufficiently fractured (Figure 4-4) to allow for precipitation to continually encounter newly formed copper bearing surfaces. This contrasting climate dependent copper release behavior is made explicitly clear when monthly copper release values are normalized to monthly precipitation measurements (mg/cm), as seen in Figure 4-10a. From this plot, it is observed that Baltimore's wet and cooler climate (Figure SI. 4-3) led to normalized release values of less than 0.2 mg Cu/cm, for all months weathered. The dry and hot climate in Tempe (Figure 4-3), on the other hand, regularly resulted in monthly normalized copper release values greater than 0.2 mg Cu/cm and as high as 1.2 mg Cu/cm. Meaning, in dryer climates, MCA wood has a greater potential to release larger concentrations of copper during a given precipitation event.

Shown in Table 4-3 are the normalized copper release values for samples weathered in Baltimore, Pittsburgh, Golden, and Tempe for the first month of weathering and for a month of weathering with comparable rainfall at least 16 months later. From this table, is observed that during the first month of weathering, samples in each location released similar amounts of copper, normalized to the precipitation they received. However, following over a year of weathering, both Baltimore, MD and Pittsburgh, PA have very diminished normalized copper release values (0.01 mg Cu/cm), while Golden, CO and Tempe, AZ released and increased amount of copper normalized to precipitation (0.1 and

0.26 mg Cu/cm, respectively). These comparisons further indicated that climates which facilitate wood drying and subsequent wood cracking will lead to greater copper release. This hypothesis was tested and substantiated by additional lab based MCA wood drying control experiments. Triplicate venti sized MCA wood samples that were heated to ~50 $^{o}$C and exposed to UVB for five weeks released six times the amount of copper (0.51 ± 0.06 mg Cu) as triplicate unheated/unexposed samples (0.08 ± 0.02 mg Cu) following 30 seconds of submersion in 400mL of deionized water.

While dryer climates will lead to higher copper release during a given precipitation event, the overall lack of precipitation in dry climates limits the overall quantity of copper released, as seen in Figure 4-10b. Following 18 months of weathering, it is observed that MCA wood samples weathered in Golden, CO released the greatest total mass of copper normalized to initial top face surface area, ~3 mg/m$^2$, following 77cm of total precipitation while samples weathered in Tempe, AZ released a total ~2 mg/m$^2$ of copper following 28cm of total precipitation. Both Baltimore, MD and Pittsburgh, PA experienced similar precipitation totals (175 and 149 cm, respectively) and comparable copper release quantities (~1-1.5 mg/m$^2$). This suggests that while contrasting wet and dry climates will lead to different patterns of copper release from MCA wood, a climate such as the one in Golden, CO (Dfb – snow, fully humid, warm summer) has the greatest propensity for spurring copper release from MCA wood. Likely, due to it having conditions in which the wood will become dry enough to crack and expose embedded copper but also experience sufficient precipitation to rinse away newly exposed copper.

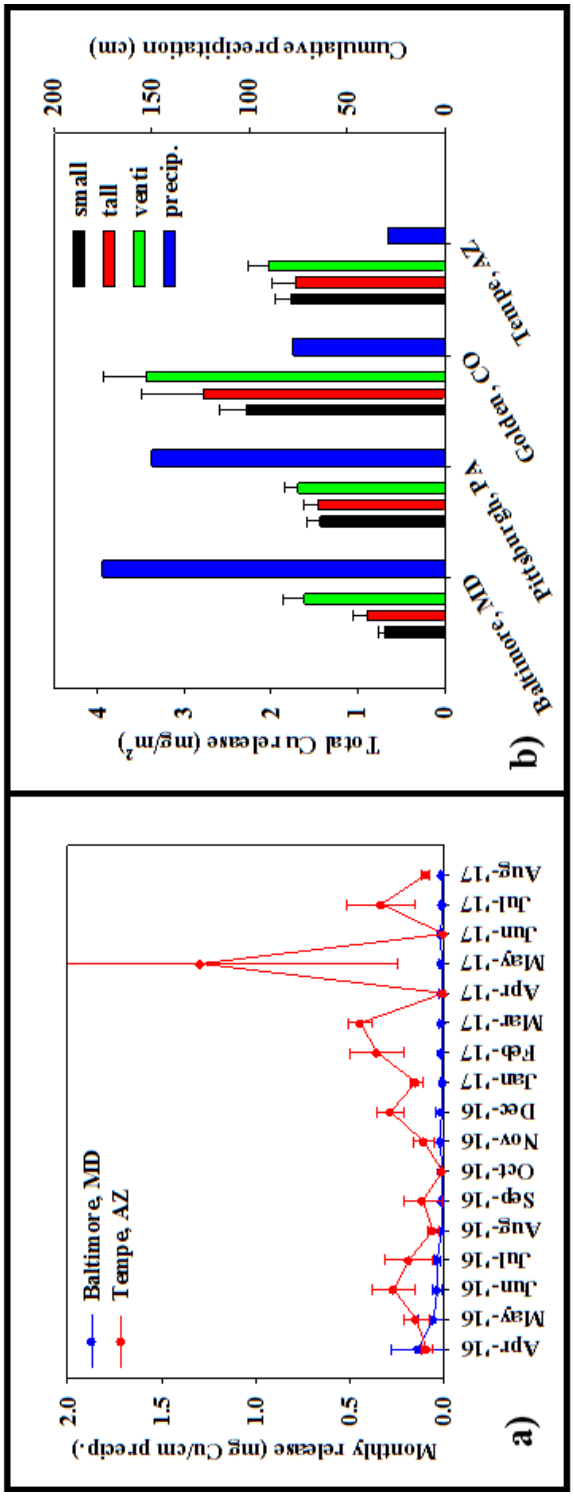


**Figure 4-10**: a) Monthly Cu release (normalized to monthly precipitation) for pressure treated lumber weathered in Baltimore, MD & Tempe, AZ. b) Total copper release masses normalized to top face surface area (mg/m$^2$) and cumulative precipitation values (inches) measured at four weathering locations.

| | Sampled at month one | | Sampled at month 18* | |
|---|---|---|---|---|
| | precipitation (cm) | release (mg/cm) | precipitation (cm.) | release (mg/cm) |
| Baltimore, MD | 3.8 | 0.10 (±0.02) | 5.1 | 0.01 (± 0.01) |
| Pittsburgh, PA | 5.2 | 0.06 (± 0.01) | 3.8 | 0.01 (± 0.01) |
| Golden, CO | 9.6 | 0.06 (± 0.01) | 4.0 | 0.1 (± 0.01) |
| Tempe, AZ | 2.0 | 0.09 (± 0.02) | 2.7 | 0.26 (± 0.08) |
| | | | *Tempe, AZ month 16 & Golden, CO month 17 | |

**Table 4-3**: Comparison of Cu release, normalized to precipitation, during the first month of weathering and a single month of weathering more one year later. Note: in "release" columns, parenthetical values are the calculated standard deviation from sample replicates.

*Characterizing copper release form*

SEM of unweathered sawdust samples visualized the form of copper present. Copper nanoparticles were found to be distributed in micron sized clusters along the surface of sawdust fragments (Figure 4-11a); the presence of copper in these clusters was confirmed with EDX spectroscopy (Figure 4-11b) along with copper elemental mapping (Figure 4-11c). Due to the low concentration of copper present in the wood, however, very few sawdust particles were found to contain any copper at all and in fact, most imaged dust samples appeared smooth, featureless, and copper-free as shown in Figure 4-12.

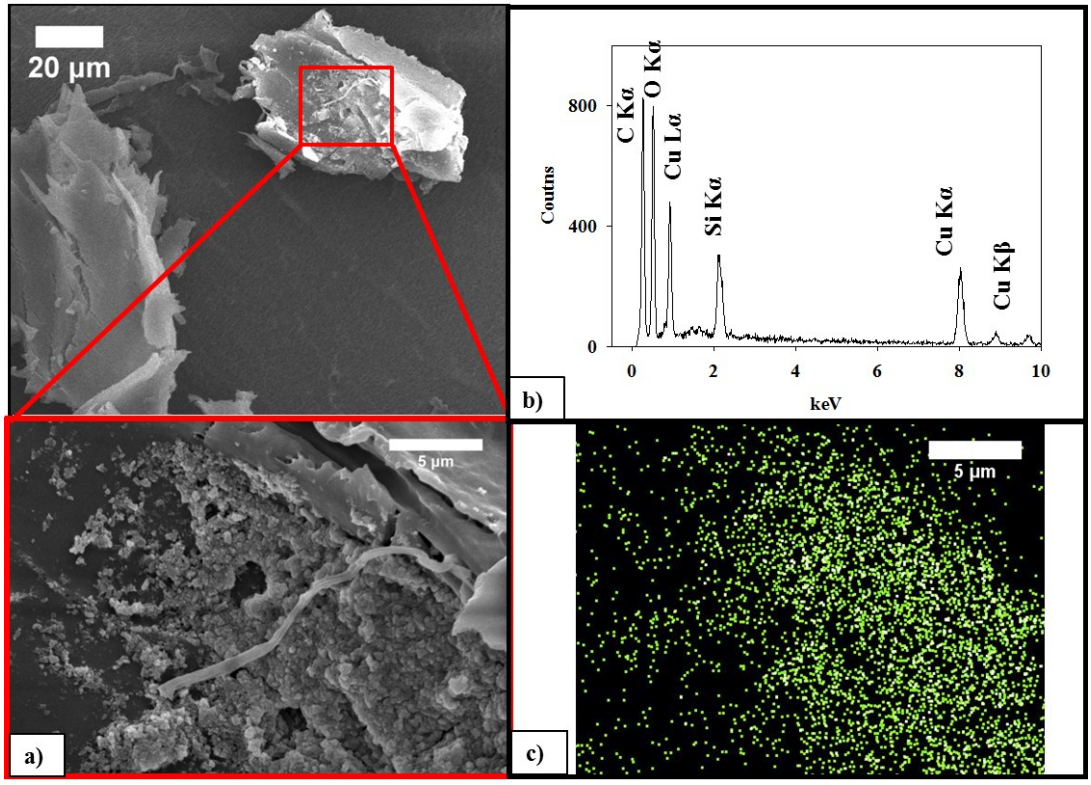


**Figure 4-11**: The presence of copper on the surface of pressure treated wood samples is visualized and confirmed via a) SEM imaging, b) EDX spectroscopy and c) EDX copper map

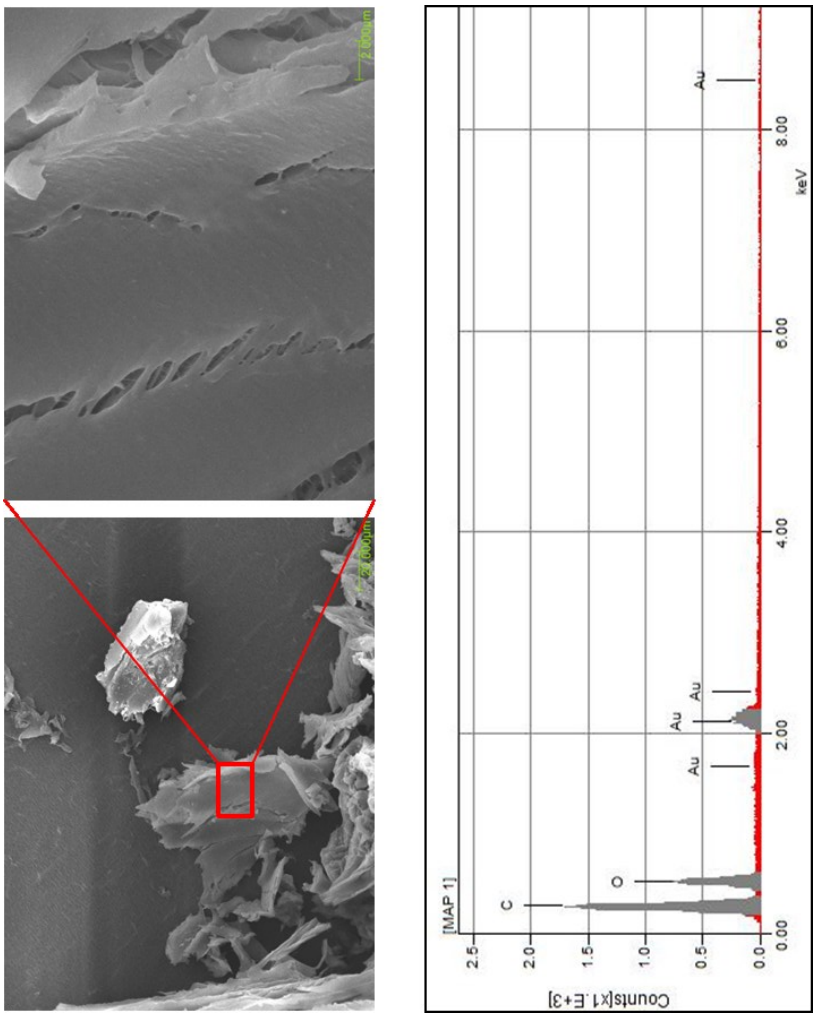


**Figure 4-12**: SEM along with EDX finds that smooth regions of copper saw dust samples are absent of an copper nanoparticles.

spICP-MS was utilized to directly and explicitly characterize the form of copper released from MCA wood samples in well controlled laboratory conditions. Samples for spICP-MS were prepared in lab, as opposed to collected from rainwater runoff, to allow for explicit control over sampling time and released copper exposure to water. Figure 4-13 shows the results from spICP-MS analysis of the MCA-wood leachate produced following the brief submersion of GC wood in milliQ water. The raw spICP-MS data is shown in Figure 4-13a-e and the average copper concentration (and standard deviation) measured from triplicate leachate solutions is shown in Figure 4-13f. Immediately after removal of the MCA sample from solution, aliquots of the leachate solution was analyzed following: no filtration (Figure 4-13a), filtration through a 0.45μm filter (Figure 4-13b), and filtration through a 0.02μm filter (Figure 4-13c).

The unfiltered solution appears to have a high intensity (> 1000 Cu counts) of detection events – this indicates the presence of copper particles (either as clusters bound to wood fragments or suspended freely in solution). Filtration with a 0.45μm filter removed all high intensity pulses and resulted in an average measured signal of ~150 Cu counts for all detection events with few particles above the background, indicative of dissolved copper and particles <450nm in size. Filtration with a 0.02μm filter further reduced the measured signal intensity to ~100 Cu counts, indicating that the filter removed particulate copper greater than 20nm in size. The copper that passed through the 0.02 micron filter was considered dissolved although it is possible some particles less than 20nm are still present. This data alone suggests that the unfiltered MCA release-submersion solution is constituted either of copper > 450nm in size or that the copper is

associated with wood particles > 450nm in size (and therefore could not pass through the 0.45μm filter).

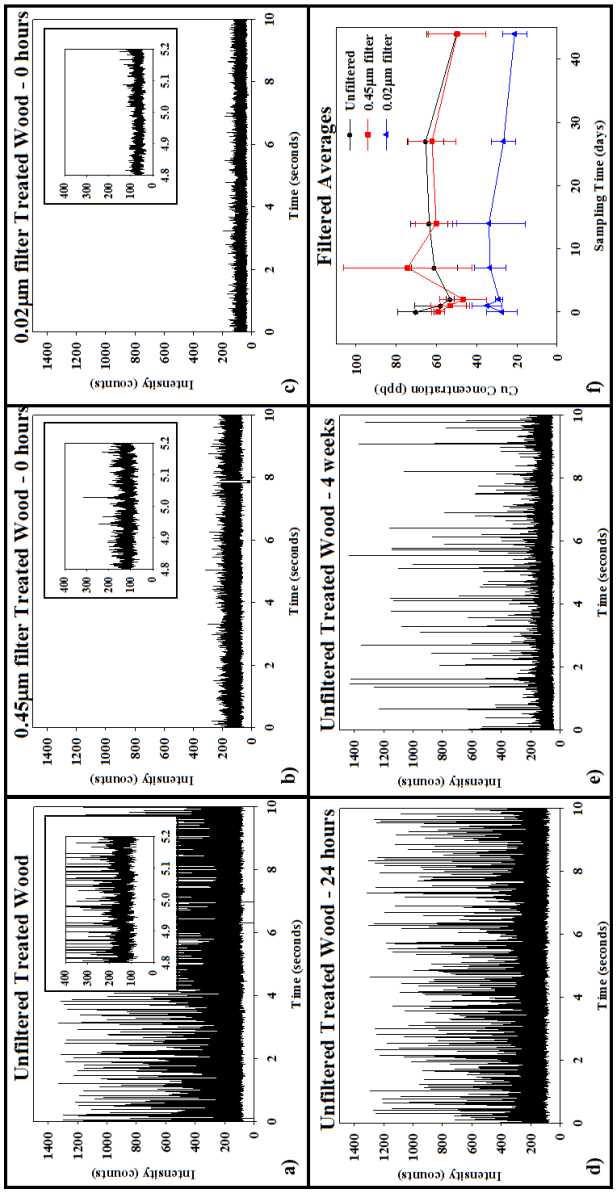


**Figure 4-13**: Single-particle inductively coupled plasma mass spectrometry (spICP-MS) characterization data of treated wood soaking solutions sampled immediately following approximately 180 seconds of wood submersion in water subjected to: a) no filtration, b) 0.45µm filtration, and c) 0.02µm filtration. spICP-MS characterization data of unfiltered soaking solutions collected after d) 24 hours and e) 4 weeks. f)Summary of measured Cu concentrations (ppb) remaining in solution, after filtration, at increasing sampling times following initial 180 second submersion.

Integration of the measured copper signal was used to calculate copper mass remaining in solution following filtration and provided greater insight into the nature of released copper (Figure 4-13f). The measured copper concentration of the unfiltered copper release-submersion solution was 70 (+/- 9) ppb, while the 0.45µm and 0.02µm filtered solution was found to be 59 (+/- 3) ppb and 27 (+/- 8) ppb, respectively (Figure 4-13f). Comparing these concentrations, it becomes clear that while the unfiltered solution (Figure 4-13a) is dominated visually by high intensity pulses, copper removed by a 450 nm size filter composed just ~16% of all copper present in solution. Immediately after the MCA wood is exposed to water, the plurality of copper present in solution, 45%, is between 20-450nm in size, with the remaining 39% of copper measured smaller than 20nm in size, or dissolved.

Shown in Figure 4-13d and Figure 4-13e are the spICP-MS data collected of the unfiltered MCA-wood leachate solutions after 24 hours and four weeks. It is observed that the number of high intensity pulses decreased only slightly after 24 hours and to a much greater extent after four weeks. A cursory visual inspection of the spICP-MS pulse data alone suggests that the copper released into solution transformed to a smaller size (i.e. dispersed and/or dissolved). However, the measured copper concentration remaining in solution following filtration indicates the copper form remained largely unchanged (Figure 4-13f). Specifically, after 44 days of exposure to water, the copper concentration measured following no filtration, 0.45µm filtration, and 0.02µm filtration after 44 days was found to be 50 (+/- 15) ppb, 50 (+/- 14) ppb, and 21 (+/- 6) ppb, respectively. The similarity in copper concentration measured before and after filtration through a 0.45µm filter indicates that CuNPs previously affixed to larger wood fragments (> 450nm) may

have detached and were suspended freely to pass through the 0.45μm filter. More definitively, that the copper concentration present in a form smaller than 20nm did not increase indicates that the copper released from the MCA wood is largely stable and resistant to dissolution for up to 44 days of continual exposure to water– this also observed by the 0.02μm filter plot not increasing in concentration over 44 days in Figure 4-13f.

*Improved particle size characterization with spICP-MS*

It is noted that because the filter cannot preferentially remove CuNPs vs. wood fragments, some of the copper removed during filtering could have been CuNPs smaller than the filter pore size, but affixed to wood fragments larger than the filter. spICP-MS is uniquely adapt at discerning this distinction. Evidence of this occurrence is suggested when the copper carbonate nanoparticle spherical size (i.e. diameter) is calculated from measured peak intensity using the mass percentage of copper and the bulk density of copper carbonate to determine volume assuming the particle was pure copper carbonate as has been done with other particles in previous spICMS work.[19, 27] This calculation was done (calibration curve shown in Figure 4-14) for the unfiltered and 0.45μm filtered samples collected at 0 hour, 24 hour, and 4 weeks, as summarized in Table 4-4.

Calculated particle sizes for samples collected at all three exposure times and passed through a 0.45μm filter prior to spICP-MS analysis are shown in the right hand column of Table 4-4. It was found that despite the filter size being 0. 45μm in size, the largest measured copper nanoparticle size was on the order of 237nm. That the particles were not nearer to the 450nm filter size suggests some of the released copper is associated with wood particles larger than 450nm in size, and therefore large enough to be removed by filtration. Additionally, it is observed that the calculated particle size of

the filtered leachate samples did not decrease; this suggests that the released copper nanoparticles less than 450nm in size are largely stable and will not readily dissolve once released.

For unfiltered samples, it is observed that the 0 hour, 24 hour, and 4 week samples all possess copper nanoparticles with similar size distributions (150nm -580nm). The slight decrease in the largest copper nanoparticle size measured for the unfiltered samples, with increasing exposure time (608nm – 580nm over 44 days), does suggest that some of the larger nanoparticles are either dissolving or de-aggregating, resulting in the measured decrease in size. However, because this is only a slight decrease, it indicates that the larger released nanoparticles are largely stable and resistant towards dissolution and/or de-aggregation. This observation is in agreement with the constant concentration measured for the 0.02μm filtered samples (i.e. the dissolved copper concentration) following 44 days of exposure (Figure 4-13f).

From the filter studies, it is posited that when MCA wood is exposed to precipitation, nearly half of the initially released copper will be in particulate form between 20-450nm in size with the next largest fraction of copper releasing as ions. spICP-MS determined that the largest size of released copper was found to be upwards of 600nm. From the spICP-MS calculations paired with no observed free copper particles in SEM images, it is believed that the majority of released undissolved copper is on the order of 135-237nm in size, either as individual particles or aggregates and associated/affixed to larger wood particles. Additionally, if the copper remains in solution following its release the particulate copper will remain relatively stable and persist in the environment, at least up to 6 weeks, in its particulate form. Local water composition and

chemistry (i.e. concentration of NOM, dissolved salts, pH) could impact release copper nanoparticle stability, however it was not assessed in this study.

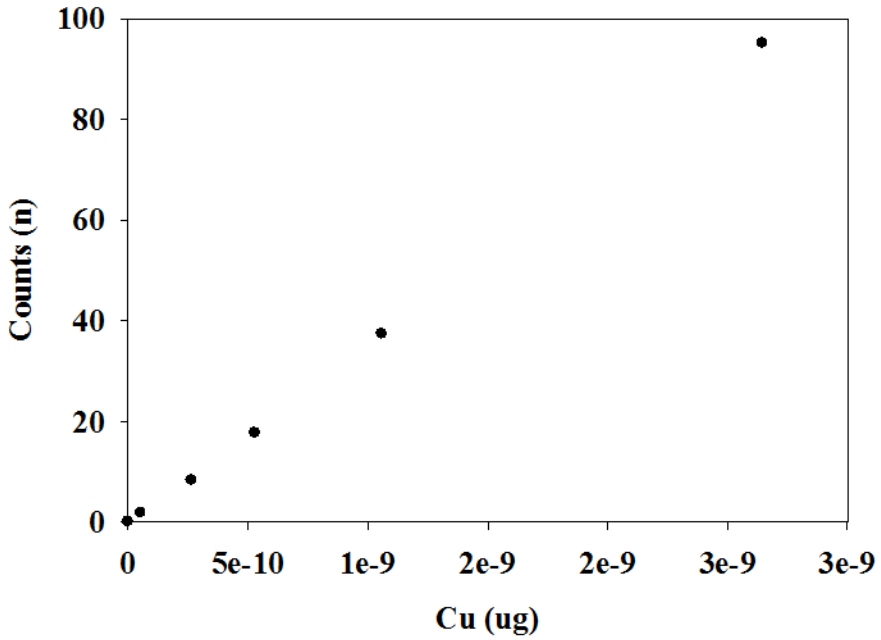


**Figure 4-14**: Calibration curve for spICP-MS analysis of copper established the systematic relationship between measured copper signal and copper nanoparticle mass

| | Particle diameter (nm) | |
|---|---|---|
| | unfiltered | 0.45µm filter |
| 0 hours | 153 - 608 | 134 - 232 |
| 24 hours | 152 - 591 | 136 - 217 |
| 4 weeks | 144 - 560 | 137 - 261 |

**Table 4-4**: Released copper nanoparticle size distribution for unfiltered and filtered samples collected following increasing periods of water explosurefrom integration , calculated with integration of spICP-MS pulse data.

*End of Life*

To complement monthly copper release measurements, a toxicity characteristic leaching procedure (TCLP) was performed on tall-sized samples from each location to identify the extent to which weathering in various climates will impact copper release following MCA use and disposal to a landfill. As seen in Table 4-5, approximately 6.5 mg of copper was extracted from unweathered tall MCA samples (error bars indicate standard deviation of extracted copper measured from triplicate samples). This corresponds to ~5.5% of total copper present in the wood sample, indicating that simulated landfill conditions generated during TCLP testing will only remove a small fraction of the copper present from an unweathered MCA sample. It is believed that this copper is most likely the readily available copper at or near the surface of the wood samples and not the copper within the interior/bulk of the wood.

Following weathering in Baltimore, Pittsburgh, Corvallis, and Golden, the amount of copper extracted following TCLP testing decreased to 3.1 (+/- 2.8) mg, 3.9 (+/- 1.8)mg , 5.4 (+/- 2.9) mg, and 5.3 (+/- 3.4) mg, respectively. Alternatively, samples weathered in Tempe released more copper following TCLP testing, 10.9 (+/- 6.9) mg. These findings indicate that for most climates tested across the continental United States, the release of copper during weathering will deplete the amount of copper available to be released following MCA wood disposal to a landfill. For MCA wood weathered in a uniquely dry and hot climate (Figure 4-3), such as Tempe, AZ, the macroscopic wood fracturing enabled greater access to copper embedded within the bulk of the wood and therefore leads to an increase in the mass of copper leached following disposal. Overall, however, TCLP testing found that both unweathered and weathered MCA wood is largely resistant to leaching extensive amounts of copper (< 10% of initially embedded Cu) in a landfill

scenario. Meaning that following disposal, copper will remain in MCA wood for an extended period of time, with the potential to slowly but continuously leach copper into the environment.

| | Cu release (mg) | stdev |
|---|---|---|
| **Unweathered** | **6.6** | **(± 0.0)** |
| **Baltimore, MD** | **3.1** | **(± 2.8)** |
| **Pittsburgh, PA** | **3.9** | **(± 1.8)** |
| **Corvallis, OR** | **5.4** | **(± 2.9)** |
| **Golden, CO** | **5.3** | **(± 3.4)** |
| **Tempe, AZ** | **10.9** | **(± 7.0)** |

**Table 4-5**: TCLP (i.e. simulated landfill) testing was performed on triplicate tall sized samples before and after weathering to assess copper release (mg) during the product's end-of-life phase.

*Implications for Life Cycle Analysis*

Information on quantity and form of released materials from nano-enabled products will determine the potential human and ecological effects caused by direct exposure to these materials, during the use and at end-of-life of the product. This type of data has the potential to be fed directly into Life Cycle Assessment (LCA), a systems-level tool used to assess the life cycle environmental implications of a product or process. In a comprehensive survey of the LCA studies of nanoparticles and nano-enabled products, Salieri, *et al.* recognized a relative dearth of literature on emissions during product use and end-of-life (general and nanoparticulate);[28] a surprising fact considering that copper nanoparticles are one of the ten most used nanoparticles in the world, in terms of Global Flow (metric tons/year).[29] The authors also highlighted in their conclusions that such emissions can have a completely different physico-chemical form than in the primary application. Consequently, as is the case when assessing emissions during the production phase, nanomaterial released to air, water, and soil during the use phase must be reported as precisely and comprehensively as possible in order to describe such environmental flows for future impact assessments.[28] Given the ubiquity of pressure-treated lumber in American construction, the above study of the natural weathering of MCA treated wood can add to the body of knowledge on consequences of copper release to the environment, providing much needed information on the use phase and end-of-life of the wood, necessary to complete an LCA.

It has been recognized that information on ENM release is a necessary underpinning of nano-LCA.[30] Knowing the magnitude and form of released ENMs is essential for quantifying their environmental impacts, especially in categories with potential for direct exposure to these materials, such as human health and ecotoxicity. In this present study,

the major factor effecting release of MCA from wood was shown to be the regional climate. This is contrary to the results of previous weathering analysis of nanosilver- and carbon nanotube-enabled polymer composites in which the magnitude of release was found to be unrelated to weather patterns,[22] indicating the importance of the product matrix and embedding technology when accounting for ENM release.[31] For an application like MCA treated wood, predicting the release of copper over the application life time requires information on future climate data, as extreme weather conditions can promote the amount of copper release. Geographical location not only affects the amount of copper release, but it is also a key factor in determining the potential effects of copper to the surrounding environment, as illustrated by the difference in ecotoxicity characterization factor (a measure of how much a unit of emission contributes to an impact category) of nano-copper derived for seventeen different subcontinental freshwaters.[32] Therefore, it is imperative to account for the geographical location of application when performing an LCA of the MCA treated wood.

## Conclusions

Commercially available lumber, pressure treated with micronized copper azole (MCA wood) was weathered in five locations across the continental United States for 20 months. Rainwater runoff was collected on a monthly basis, as well as location specific weather data to examine the role of local climate in regulating the release of copper from MCA wood; additionally, lab-based spICP-MS studies were carried out to characterize the form of copper released from MCA wood.

It was found that while copper release from MCA wood is mainly driven by exposure to precipitation, other climate factors that impact physical properties of the wood (i.e. heat, sunlight, and the overall absence of moisture) play a large role in dictating the persistence and extent of copper release. Specifically, two patterns of release were observed in this study: The first is that in wetter climates that experienced great amounts of precipitation (Baltimore, MD and Pittsburgh, PA), the MCA wood remains largely intact (i.e. crack-free) and copper is released primarily from the surface/near surface region of the MCA wood. Following a year of weathering, copper was depleted from that outer region of the wood weathered in these locations and copper release abated. Alternatively, in dryer climates with less precipitation (Golden, CO and Tempe, AZ), the MCA wood dried and cracked, resulting in increased exposed surface area of copper impregnated wood. It was this generation of new copper surface area that facilitated these samples' sustained release of copper into the second year of weathering. Ultimately, MCA wood samples weathered in Baltimore, MD, Pittsburgh, PA, Golden, CO, and Tempe, AZ released approximately 1 mg $Cu/m^2$, 1.5 mg $Cu/m^2$, 3 mg $Cu/m^2$, and 2 mg $Cu/m^2$, respectively, following 18 month of natural weathering.

Laboratory based spICP-MS studies found that copper releases from MCA wood primarily in a particulate form that is 20nm-450nm (45%) and as dissolved/ particles smaller than 20nm (39%). SEM imaging of unweathered MCA wood samples leached in ultrapure water confirmed the presence of nanoparticulate copper affixed to the wood surface as large, micron sized aggregates. Following release into solution, the form of copper is largely stable. Following 6 weeks in solution, spICP-MS did not find evidence of particle dissolution to ionic form.

End of life TCLP testing found that unweathered MCA wood is largely resistant to releasing embedded copper, with less than 6% of initially impregnated copper releasing from an unweathered sample. Following weathering, copper available to leach during TCLP testing was for the most part was slightly diminished, however, weathering in Tempe, AZ did lead to an increase in the copper extracted.

Results of this study are essential for a cradle-to-grave LCA, as it provides the amount of copper release during the use phase and end-of-life of the MCA treated wood, which are necessary for assessment of the overall environmental burden of the product. An LCA for this application can identify the direct and indirect factors contributing to various impact categories throughout the product life cycle and recognize areas for future improvement to promote sustainable product design.

**Acknowledgments**

Work described in the above chapter reflects the combined efforts of a diverse group of researchers: method development, sample characterization was coordinated and carried out by the author of this text, Ronald S. Lankone. Monthly sample analysis and spICP-MS analysis was performed by Katie Challis. SEM imaging was performed by Ben Frank and Katie Challis. TCLP testing was performed by Frank Brown. LCA considerations were developed by Leila Pourzahedi. AAS analysis was performed by David Durkin.

## References


1. Unger, A.; Schniewind, A. P.; Unger, W., History of Wood Conservation. In *Conservation of Wood Artifacts: A Handbook*, Unger, A.; Schniewind, A. P.; Unger, W., Eds. Springer Berlin Heidelberg: Berlin, Heidelberg, 2001; pp 3-7.
2. William E. Platten, I.; Luxton, T. P.; Gerke, T.; Harmon, S.; Sylvest, N.; Bradham, K.; Rogers, K. *Release of Micronized Copper Particles from Pressure-treated Wood Products*; EPA Report No. EPA/600/R-14/365 2014.
3. Thomas, T. A.; Levenson, M. S.; Cobb, D. G.; Midgett, J. D.; Porter, W. K.; Saltzman, L. E.; Bittner, P. M., The Development of a Standard Hand Method and Correlated Surrogate Method for Sampling CCA (Pressure)-Treated Wood Surfaces for Chemical Residue. *Journal of Children's Health* **2005,** *2* (3-4), 181-196.
4. Lebow, S. T. In *Alternatives to chromated copper arsenate (CCA) for residential construction*, Environmental Impacts of Preservative-Treated Wood, February 8-11, Orlando, Florida, USA Orlando, Florida, USA 2004.
5. Lebow, S. T.; Lebow, P. K.; Foster, D. O.; Brooks, K. M. *Environmental Impact of Preservative-Treated Wood in a Wetland Boardwalk*; NTIS/02922892_a; CR-89-316: Madison, Wisconsin 2000; p 126.
6. Civardi, C.; Van den Bulcke, J.; Schubert, M.; Michel, E.; Butron, M. I.; Boone, M. N.; Dierick, M.; Van Acker, J.; Wick, P.; Schwarze, F. W., Penetration and Effectiveness of Micronized Copper in Refractory Wood Species. *PLoS One* **2016,** *11* (9), e0163124.
7. Evans, P.; Matsunaga, H.; Kiguchi, M., Large-scale application of nanotechnology for wood protection. *Nat Nano* **2008,** *3* (10), 577-577.
8. Civardi, C.; Schubert, M.; Fey, A.; Wick, P.; Schwarze, F. W. M. R., Micronized copper wood preservatives: efficacy of ion, nano, and bulk copper against the brown rot fungus Rhodonia placenta. *PLoS ONE* **2015,** *10*, 15.
9. Limbach, L. K.; Wick, P.; Manser, P.; Grass, R. N.; Bruinink, A.; Stark, W. J., Exposure of Engineered Nanoparticles to Human Lung Epithelial Cells: Influence of Chemical Composition and Catalytic Activity on Oxidative Stress. *Environmental Science & Technology* **2007,** *41* (11), 4158-4163.
10. Civardi, C.; Schwarze, F. W. M. R.; Wick, P., Micronized copper wood preservatives: An efficiency and potential health risk assessment for copper-based nanoparticles. *Environmental Pollution* **2015,** *200*, 126-132.
11. Civardi, C.; Schwarze, F. W.; Wick, P., Micronized copper wood preservatives: an efficiency and potential health risk assessment for copper-based nanoparticles. *Environ Pollut* **2015,** *200*, 126-32.
12. Lebow, S.; Lebow, P.; Foster, D., Estimating preservative release from treated wood exposed to precipitation. *Wood and fiber science* **2008,** *40* (4), 562-571.
13. Lebow, S., Effect of precipitation pattern on leaching of preservative from treated wood and implications for accelerated testing. *Maderas. Ciencia y tecnología* **2014,** *16*, 423-434.
14. Lebow, S.; Lebow, P.; Hirth, K., Technical Note: Comparison of accelerated methods for evaluating leaching from preservative-treated wood. *Wood and Fiber Science* **2017,** *49* (1), 93-104.
15. Laborda, F.; Bolea, E.; Jimenez-Lamana, J., Single particle inductively coupled plasma mass spectrometry: a powerful tool for nanoanalysis. *Anal Chem* **2014,** *86* (5), 2270-8.
16. Mitrano, D. M.; Ranville, J. F.; Bednar, A.; Kazor, K.; Hering, A. S.; Higgins, C. P., Tracking dissolution of silver nanoparticles at environmentally relevant concentrations in laboratory, natural, and processed waters using single particle ICP-MS (spICP-MS). *Environ. Sci.: Nano* **2014,** *1* (3), 248-259.
17. Navratilova, J.; Praetorius, A.; Gondikas, A.; Fabienke, W.; von der Kammer, F.; Hofmann, T., Detection of Engineered Copper Nanoparticles in Soil Using Single Particle ICP-MS. *Int J Environ Res Public Health* **2015,** *12* (12), 15756-68.
18. Montano, M. D.; Olesik, J. W.; Barber, A. G.; Challis, K.; Ranville, J. F., Single Particle ICP-MS: Advances toward routine analysis of nanomaterials. *Anal Bioanal Chem* **2016,** *408* (19), 5053-74.
19. Pace, H. E.; Rogers, N. J.; Jarolimek, C.; Coleman, V. A.; Higgins, C. P.; Ranville, J. F., Determining transport efficiency for the purpose of counting and sizing nanoparticles via single particle inductively coupled plasma mass spectrometry. *Anal Chem* **2011,** *83* (24), 9361-9.

20. Service, I. E., ICC-ES Evaluation Report ESR-2240. 2018.
21. Health, I. f. V. P. World Maps of Koppen-Geiger Climate Classification. http://koeppen-geiger.vu-wien.ac.at/usa.htm (accessed August 22).
22. Lankone, R.; Challis, K.; Bi, Y.; Hanigan, D.; Reed, R. B.; Zaikova, T.; Hutchison, J.; Westerhoff, P.; Ranville, J. F.; Fairbrother, H.; Gilbertson, L., Methodology for Quantifying Engineered Nanomaterial Release from Diverse Product Matrices Under Outdoor Weathering Conditions and Implications for Life Cycle Assessment. *Environmental Science: Nano* **2017**.
23. EPA., U. S., Method 3051A (SW-846): Microwave Assisted Acid digestion of Sediments, Sludges, Soils, and Oils Washington, D.C., 2007; Vol. Revision 1.
24. Adams, R. P.; Wright, J. W., Alkanes and Terpenes in Wood and Leaves of Pinus jeffreyi and P. sabiniana. *Journal of Essential Oil Research* **2012,** *24* (5), 435-440.
25. Mitsui, K., Acetylation of wood causes photobleaching. *Journal of Photochemistry and Photobiology B: Biology* **2010,** *101* (3), 210-214.
26. Dietsch, P., Effect of reinforcement on shrinkage stresses in timber members. *Construction and Building Materials* **2017,** *150*, 903-915.
27. Pace, H. E.; Rogers, N. J.; Jarolimek, C.; Coleman, V. A.; Higgins, C. P.; Ranville, J. F., Correction to Determining Transport Efficiency for the Purpose of Counting and Sizing Nanoparticles via Single Particle Inductively Coupled Plasma Mass Spectrometry. *Analytical Chemistry* **2012,** *84* (10), 4633-4633.
28. Salieri, B.; Turner, D. A.; Nowack, B.; Hischier, R., Life cycle assessment of manufactured nanomaterials: Where are we? *NanoImpact* **2018,** *10*, 108-120.
29. Keller, A. A.; McFerran, S.; Lazareva, A.; Suh, S., Global life cycle releases of engineered nanomaterials. *Journal of Nanoparticle Research* **2013,** *15* (6), 1-17.
30. Gilbertson, L. M.; Wender, B. A.; Zimmerman, J. B.; Eckelman, M. J., Coordinating modeling and experimental research of engineered nanomaterials to improve life cycle assessment studies. *Environmental Science: Nano* **2015,** *2* (6), 669-682.
31. Pourzahedi, L.; Vance, M.; Eckelman, M. J., Life Cycle Assessment and Release Studies for 15 Nanosilver-Enabled Consumer Products: Investigating Hotspots and Patterns of Contribution. *Environmental Science & Technology* **2017,** *51* (12), 7148-7158.
32. Pu, Y.; Tang, F.; Adam, P.-M.; Laratte, B.; Ionescu, R. E., Fate and Characterization Factors of Nanoparticles in Seventeen Subcontinental Freshwaters: A Case Study on Copper Nanoparticles. *Environmental Science & Technology* **2016,** *50* (17), 9370-9379.

**Chapter 5.** Appendix

**Supplemental Figures for Photodegradation of polymer-CNT nanocomposites: Effect of CNT loading and CNT release characteristics**

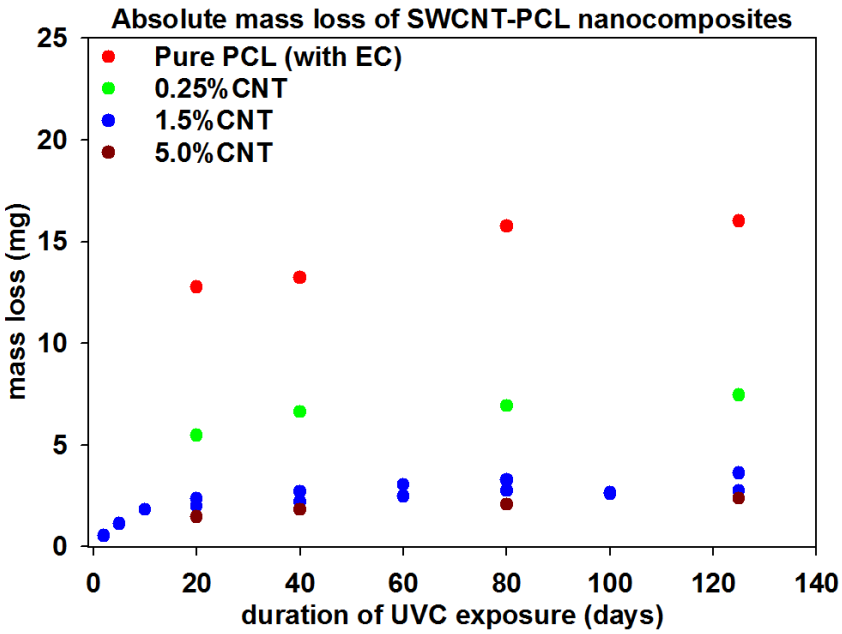


**Figure 5-1**: Absolute mass loss, in mg, of each nanocomposite sample irradiated with 254nm light. Also shown is the mass loss for the Pure PCL containing ethyl cellulose irradiated with 300nm light.

**Supplemental Text for Methodology for Quantifying Engineered Nanomaterial Release from Diverse Product Matrices under Outdoor Weathering Conditions and Implications for Life Cycle Assessment**

Nanocomposite Preparation

All nanocomposites used in this study were prepared with solution blending with nanoparticle loadings designated as a percent by mass (%w/w). Solution blending produces PNCs with a high degree of nanoparticle dispersion and excellent reproducibility and scalability on the lab scale. Solution blending requires, for both AgNPs and CNTs, that the NPs be first dispersed in an organic solvent. Upon formation of a stable dispersion, a polymer of choice was then added. Following a period of mixing, the NP-polymer suspension was then poured into Fisher aluminum weigh dishes (Cat. Number 08-732-105) and allowed to dry overnight. Prior to characterization and weathering, all nanocomposites are further dried for at least one additional night in a desiccator.

Nanomaterials

AgNPs were provided by Dune Sciences and CNTs were purchased from Carbon Solutions Inc., where they were synthesized by electric arc discharge over Ni/Y nanoparticle catalyst. Samples were used as received unless otherwise described. Comprehensive material characterization was conducted on the raw material and data, including TEM, XPS,ATR-FTIR, and SEM.

1.5% SWCNT-poly-ε-caprolactone (1.5%CNT-PCL)

Samples were prepared by first weighing out single-walled CNTs (SWCNTs, Mettler Toledo XS20) and adding them to a 50 mL Erlenmeyer flask filled with 21 mL of THF

and 21 mL of chloroform. Ethyl cellulose (EC, 31.5 mg) was weighed out and also added to the flask. EC was added to act as a natural surfactant for the SWCNTs and facilitates uniform dispersion. This mass of EC does not significantly impact the chemical composition of the surface of the nanocomposites, as confirmed by both XPS and ATR-FTIR (data not shown) The SWCNT and solvent mixture are then capped with septa, clamped in place, partially submerged in a bath sonicator (70W, Branson 1800), and sonicated for three hours. Following sonication, 420 mg of PCL was added to this solution and sonicated for an additional hour. The final solution was then poured, in 6 mL portions, into 7 separate Fisherbrand Disposable Aluminum Dishes. The dishes were then covered, dried overnight and circular nanocomposite samples, referred to as coupons, were formed by evaporation.

1.5% SWCNT-polystyrene (1.5%CNT-PS)

1.5% CNT-PS samples were prepared by weighing and adding 12.6mg SWCNTs to a 50 mL Erlenmeyer flask filled with 42 mL of ortho-dichlorobenzene (O-DCB) and 0.42 mL of ethanol, added to quench sonopolymerization. This mixture was then sonicated (Branson 1800) into suspension for three hours. PS (840 mg) was then added to the flask and sonication continued for another three hours. The suspension was then poured, in 6 mL portions, into 7 separate Fisherbrand Disposable Aluminum Dishes. To ensure complete evaporation of O-DCB, the dishes were placed on a hot plate set for 100 $^{0}$C. The dishes were then covered and allowed to dry overnight at 100$^{0}$C.

2% AgNP-polystyrene (2%AgNP-PS), 2% AgNP-poly (methyl methacrylate)(2%AgNP-PMMA), 0.04% AgNP-poly (methyl methacrylate)(0.04%AgNP-PMMA)

AgNP nanocomposites were prepared from an aqueous suspension of 20 nm AgNPs (Tween 20, NS20D_06062014B) provided by Dune Sciences, at an initial concentration of 1000 ppm; referred to hereafter as AgNP/$H_2O$. To disperse the NPs in a polymer matrix, an aliquot was first added to a 25 mL Erlenmeyer flask, placed in an oil bath, and gently stirred as it was heated at $70^0$C for 20 hours. 2% AgNP samples required 8 mL of AgNP/$H_2O$ and 0.04%AgNP samples required 160 μL of AgNP/$H_2O$. Following 20 hours of heating, all the water was removed and only the AgNPs remained. The particles are then re-suspended in 20 mL of chloroform (Figure 5-2). Following the addition of chloroform, the solution is stirred vigorously (1200 rpm) for 1 minute with a magnetic stir bar on a stir plate. At this time 400 mg of either polystyrene or poly (methyl methacrylate) were added. The flask was then capped and stirred for an additional 60 minutes at 1200 rpm. The suspension was then poured, in 6 mL portions, into aluminum weigh dishes, covered, and dried overnight at ambient temperature. To ensure stirring in chloroform resuspended most, if not all, of the original AgNPs present in the AgNP/$H_2O$. UV-Vis measurements taken of the as received suspension as well as the resuspended material showed that the characteristic SPR peak at 420 nm did not change significantly in profile or intensity before and after resuspension (Figure 5-12).

Sample Characterization

*X-ray photoelectron spectroscopy (XPS)*

XPS was performed with a PHI 5400XPS, MgKα X-ray (1253.6eV) on PNC samples prior to weathering. Samples were sufficiently dry before analysis and bound to a metal sample stub using copper tape. Quantitative analysis of elemental regions of interest

(C(1s), O(1s), and Ag(3d)), were collected on samples using a pass energy of 58.7eV, a step size of 0.125eV, and with 10 sweeps. Survey scans, that measure signal from all elements present, were performed as well to ensure samples were free of contamination. All data processing was carried out using CasaXPS. For each PNC type analyzed, spectra were collected on three samples from a given batch to assess uniformity in surface composition. The Ag-PNCs were produced in three batches, denoted by date of production (7-29-15, 8-4-15, and 8-11-15); three samples from each batch were analyzed with XPS, giving a total of 9 spectra for each Ag-PNC type. The average Ag composition on the surface of each PNC type (2%Ag-PS, 2%Ag-PMMA, 0.04%Ag-PS) was calculated from the mean average of concentrations measured for each of the 9 scans; the standard deviation was calculated from the 9 scans as well.

*Scanning electron microscopy (SEM)*

SEM imaging was conducted with a Jeol 6700F, FESEM. Ag NP and CNT nanocomposites samples were dried prior to imaging. All samples were bound to a conductive metal stub using copper tape and sputter-coated with platinum nanoparticles for 300 seconds, at a rate of 2nm/minute. This was done to minimize charging of the sample during imaging. Samples were imaged in two or three randomly selected locations across the surface to ensure uniformity of surface morphology. All images were processed using ImageJ.

*Attenuated Total Internal Reflectance Fourier Transform IR (ATR-FTIR)*

ATR-FTIR was performed with a Nicolet iS5 FT-IR Spectrometer, equipped with a diamond window; a sampling depth of 2 μm is reported by the manufacturer. Samples were dried prior to analysis and analyzed with resolution of 0.482$cm^{-1}$, with 32 scans collected; the background of the instrument was set to ambient atmosphere.

*ICP-MS and Digestion – instrument and digestion procedure*

Preweighed unweathered 2%Ag-PMMA and 2%Ag-PS were acid digested to determine original Ag content. Samples were transferred into a Teflon™ digestion vessel and 10 mL of ACS grade Nitric acid (67-70% $HNO_3$, Macron Fine Chemicals) was added to the vessel. The vessels were sealed and microwave digested (ramped to 200 C, held for 5 minutes)[1-3]. Following digestion, samples were quantitatively transferred (microwave containers were rinsed 3 times with MilliQ water, with each rinse volume contributed to the total volume) into 50 mL Falcon™ tubes and diluted to total volume of 50 mL using 18 MΩ ultrapure water (Millipore). Digestate was diluted 100x in ultrapure water prior to analysis by a quadrupole ICP-MS (NexION 300D series, Perkin Elmer). Total Ag was measured using mass 106.905 amu. Indium (114.116 amu) was used as an internal standard throughout the analysis. Perkin Elmer's Syngistix™ for ICP-MS software was used to collect data and calculate concentration.

Standard curves are established (R-squared values of >0.998) for both elements with six data points ranging from 0.1 to 30 µg/L using the SPEX CertiPrep standards (Metuchen, NJ).

A mixing t-piece was employed to introduce 10 ppb indium as an internal standard throughout the entire analyses as well as standard quality assurance and quality control measures. The internal standard is used to monitor and account for instrumental drift. Check standards and ultra-pure water blanks are analyzed approximately every fifteen samples. After about the 9$^{th}$ month of sampling NIST SRM 1640a for natural waters is included as a check as well. The standards are monitored for accuracy (within 10% variation from certified value) and blanks are used to ensure there is no sample carryover, as well as establish limits of detection for each analysis.

Each month, an instrumental limit of detection (LOD) is determined by quantifying the average intensity in at least three ultrapure water blank and adding 3σ (3 times the standard deviation). From each control blank, 5 mL are separated and used as matrix spikes. A standard solution of Ag and Y) is spiked into the blank to a concentration of 1ppb and analyzed to determine if the matrix is causing any interference. Recoveries of Ag and Y between 80-120% are considered acceptable.

Quantifying ENM release by ICP-MS

ICP-MS analysis is carried out on monthly release samples to determine total ENM release from products (here, Ag and SWCNT from PNCs). Yttrium (Y) is used to indicate SWCNT concentration due to the presence of Y nanoparticles in the SWCNT (~5 wt%) used in the PNCs. The Y nanoparticles are incorporated into SWCNTs during synthesis and have been previously used to quantify SWCNT particles.46-48 The acid rinse of the collection jars and acid digestion prior to ICP-MS results in AgNP dissolution and release of Y from CNTs. Since atmospheric dusts are also collected and can clog the ICP-MS introduction system, it is removed from the suspension by either settling (up to two days) or centrifugation prior to analysis. Ag and Y concentrations of each sample are analyzed using a Nexion300D ICP-MS (Perkin Elmer, Toronto, ON). Instrument settings are compiled in Table S1 and a detailed description of the analytical procedures are provided in the SI.

Data management

A coordinated data consolidation and management protocol/system is required given the volume and diversity of data collected. Every month data is collected from each location, including release values of 9 – 29 samples and the weather data collected from

the weather station. A standardized spreadsheet is provided to each location that contains all sample names and corresponding columns to record the collected final volume. Upon completion of sampling, each location completes this file and sends, along with the weather station data (in .csv format) to the data center (Baltimore, MD) for processing. Following ICP-MS analysis, a single spreadsheet containing measured release values for all samples (all locations) is generated by the analytical center (Golden, CO) and sent to the data center for processing and compilation.

## References


1. Besecker, K. D.; Rhoades Jr, C. B.; Jones, B. T.; Barnes, K. W., Closed-Vessel Nitric Acid Microwave Digestion of Polymers. *Atomic Spectroscopy* **1998,** *19* (2), 55-59.
2. Sun, Y.-C.; Ko, C.-J., Evaluation of closed-vessel microwave digestion method for the determination of trace impurities in polymer-based photoresist by inductively coupled plasma mass spectrometry. *Microchemical Journal* **2004,** *78* (2), 163-166.
3. Tsai, T.-L.; Lin, C.-C.; Guo, G.-L.; Chu, T.-C., Effects of microwave-assisted digestion on decomposition behavior of polymethyl methacrylate (PMMA). *Materials Chemistry and Physics* **2008,** *108* (2–3), 382-390.

**Supplemental Figures for Methodology for Quantifying Engineered Nanomaterial Release from Diverse Product Matrices under Outdoor Weathering Conditions and Implications for Life Cycle Assessment**

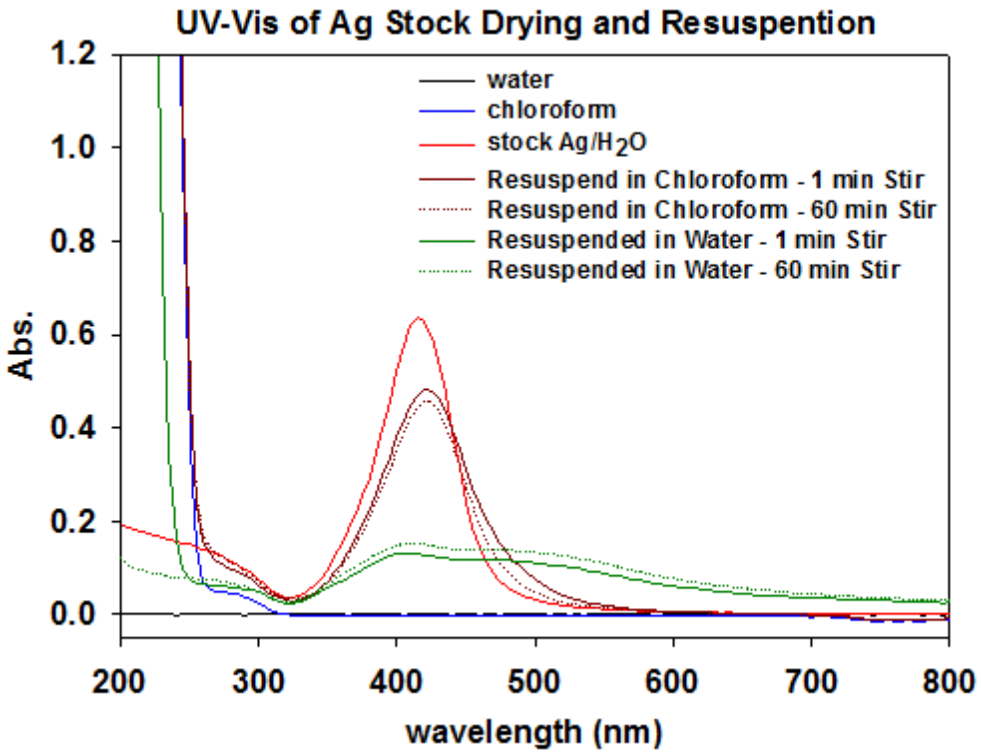


**Figure 5-2**: UV-Vis demonstrates effective resuspension of AgNPs in chloroform following drying of their as received aqueous suspension.

| Parameter | Setting |
|---|---|
| Nebulizer Gas Flow | 0.88-1.0 mL/min |
| Auxiliary Gas Flow | 1.2 ml/min |
| Plasma Gas Flow | 16 or 18 ml/min |
| ICP-RF Power | 1600 V |
| Analog Stage Voltage | -1712 |
| Pulse Stage Voltage | 1250-1375 |
| Deflector Voltage | -6.5 or -10 |
| Cell Ent | -1.0 or -5.0 |
| Cell Exit | -1.0 or -5.0 |
| Cell Rod Offset | -15.0 |

**Table 5-1**: ICPMS Settings, shifts in setting occurred after some troubleshooting by Perkin Elmer technician and resulted in improved instrument performance.

**Supplemental Test for Characterizing copper release and transformation following natural weathering of nanoenabled products**

Acid rinse control studies

The following experiment was performed to determine the copper recovery from rain collection jars. An aqueous copper solution was prepared by soaking a venti size of AG MCA wood in 1.5L of deionized water for one month. The wood was removed and the copper concentration of the remaining leachate solution was measured with ICP-OES. Six jars containing 200ml of this solution were set out on the rooftop (without any wood in the jars). Three jars were capped and sealed and three were uncapped. Following one month of weathering, the solution in all six samples was collected following the collection procedure described above and analyzed for copper content with ICP-OES. The copper recovery for each jar was determined by comparing the recovered copper mass to the expected copper mass from 200mL of the initial solution.

Material Characterization

Copper concentration distribution

Wood samples for copper concentration analysis from various regions along unweathered and weathered wood using the following procedure: Four 3/16" holes were drilled 0.2" into the top of the wood, along the sample edges, and the saw dust from these four holes was collected, combined, and weighed for subsequent digestion in a known volume of concentrated nitric acid. Another 0.2" depth was drilled into the wood through the existing drill holes and the saw dust was also collected, combined, and weighed for digestion. This procedure was repeated on the bottom of the wood samples as well. Wood was also drilled out so that a 0.2" depth of wood could be collected from the center height

of the block (1.65" – 1.85"). This height specific drilling approach was repeated in the center of the block as well so that the copper content along the edges could be compared to the copper content in the center of the wood. This approach was also followed for weathered wood samples to determine if there was a profile of copper concentration, as a function of depth, remaining in the wood following weathering.

Following wood collection and digestion, all samples were analyzed with Atomic Absorption spectroscopy (AAS), performed on an AAnalyst200 (Perkin Elmer), with a Cu Lumina Hollow Cathode Lamp (324.75 nm wavelength, 2.7/0.8 slit_mm) using 2wt% HNO3 (trace metal grade) solution (in ultrapure 18 MOhm water) as the blank and the rinse. Each sample test was completed in triplicate and performed four times, with all data averaged for reporting. In between sample runs, a blank solution was run three times through the column to remove any residual copper – in total, 1055 tests were performed. The range of copper concentrations used in for standard (calibration) solutions was 0.5ppm, 1ppm, 5ppm, 10ppm.

Copper single particle ICPMS

All single particle ICPMS data was acquired with a PerkinElmer NexION 300D using the fast scan method. [1] The nano module of PerkinElmer's Syngistix™, was used to collect all spICPMS data. The instrument utilized a glass high-solids nebulizer (Meinhard Type C 50psi) and cyclonic spray chamber with ( Pyrex via Meinhard, Golden, CO) with a quartz ball joint injector. Sampler and skimmer cones are nickel with an aluminum hyperskimmer cone. The instruments torch position, nebulizer gas flow, and Quadrople Ion deflectors were tuned daily for optimum performance. Nebulizer gas flow was usually between 0.72-0.80 L/min.

Transport efficiency of the instrument was determined daily using the mass-based method described in Pace et.al 2011 paper: a four standard dissolved gold curve (1-20ppb) was analyzed and a triplicate analysis 60 nm gold NP (NIST RM 8013) was used to determine the transport efficiency [2-3]. Dissolved standard curves for copper with five standards ranging from 1-50ppb were prepared daily in MilliQ water, to matrix match samples, and analyzed to determine copper concentration and copper mass in copper particle pulses.

Due to prior issues with drifting copper baseline, all analysis was performed with short tubing and direct aspiration, skipping of the sample peristaltic pump, and allowing the argon gas flow over the nebulizer into the spray chamber to suction the sample into the system. Any variation to nebulizer gas flow results in different sample introduction rates so sample uptake rate was determined on the day of each analysis by measuring the amount of MilliQ water taken up over 2 minutes.

Conversion of ICPMS Pulse data into Particle Size

Determination of transport efficiency and conversion of pulse data into nanoparticle mass or size data is thoroughly explained in Pace et.al 2011 and its correction.2-3 In brief, the standard curve is converted from a intensity to concentration curve to an intensity to ug/event using equation 1. Each pulse is considered an event and the mass of the analyte ( in this case Cu) is determined.

$$W = [\eta_n * q_{liq} * t_{dt} * C]$$

Eq 1. W is the mass observed per event (µg/event). Where ηn is the transport efficiency, qliq is the flow rate (ml/ms) and C is the analyte concentration (µg/ml). The transformed standard curve may be used to calculate the mass per particle event. A

correction for the analyte, or copper, percentage in the particle composition is also necessary. From there, if we assume the particle is spherical and has the same density as bulk copper carbonate we then use the trigonometric equation 2 to calculate the size of particle from particle mass.

$$d = \sqrt[3]{\frac{6 * m_p}{\rho * \pi}}$$

Equation 2: Spherical diameter (d) is calculated from the equation for a sphere and particle dentisity (ρ) and particle mass (mp).

Minimum and maximum sizes are tabulated in Table 4-4. The minimum size is limited by the background or the ability to define a pulse above background. This ability is decreased when there is a lot of background signal, as in our samples. The higher the background signal, the larger the smallest detectable size. Therefore, the minimum size detected is larger in unfiltered samples than in filtered samples. Some of the background is contributed to particles which are removed in the filter process, likely due to the fact that filtration is a imperfect process and sometimes removes particles smaller than its pore size. Also, a filter could be removing large particles of wood with trace amounts of copper which contributes to the background. Perkin Elmer Syngistix software identified the pulses and applied these calculations to the particles, based on the density, flow rates, percent copper, and transport efficiency determined and input by the instrument operator.

Electron Microscopy and Energy-dispersive X-ray spectroscopy

Leachate prepared as described above for spICPMS was also filtered onto a 0.05µm polycarbonate filter for imaging with scanning electron microscopy (SEM) using a JEOL JSM IT100. Samples were sputter coated with gold for 300 seconds prior to imaging. Images were collected using an acceleration voltage of 10keV. Energy-

dispersive X-ray spectra (EDX) were collected as well, utilizing an acceleration voltage of 20keV. Additional SEM images of unweathered MCA wood were also acquired with an FEI Quanta 600 with a tungsten cathode under low vacuum (0.98 torr) with backscatter imaging and acceleration voltage of 20kV. Samples were small slices of MCA wood no more than 3 cm across and less than 2mm thick without coating. EDX was used to identify elements present on sample.

ICP-OES Analysis

Copper concentrations present in collected rainwater runoff samples were determined with ICP-OES analyses. Samples were filtered with 0.45µm filters prior to analysis. A PerkinElmer Optima 5300DV was used for the first portion of the study until the lab acquired a PerkinElmer Optima 8300 in July of 2017. Results lower than the detection limit were reported as BDL and graphed as zero . A cyclonic spray chamber with a high solids Meinhard nebulizer was used for sample introduction on both instruments. For the Optima 5300DV the nebulizer gas flow rate was set to 0.65 L/min and a sample uptake rate of 1.2 ml/min was used. Argon flow to the plasma was 16mL/min with an RF power of 1.5kW to keep conditions robust. Optima 8300 settings: nebulizer gas flow 0.68 L/min, plasma gas flow 12L/min, RF Power 1.5kW and pump flow rate 1.2ml/min. The analysis method was based on EPA method 200.7, but excluded silver. The instrument was calibrated daily. All analysis included a 10ppm Sc solution that is mixed in with a mixing T prior to nebulization. CCV checks were run every ten samples to monitor instrument performance.

Attenuated Total Internal Reflectance-FTIR

Spectra were collected with a Nicolet iS5 FT-IR spectrometer, equipped with a diamond window. The manufacturer reports a sampling depth of approximately two microns for the diamond window. Samples were analyzed at a resolution of 0.482 cm−1, with 32 scans. Each ATR-FTIR was referenced to the ambient atmosphere.

End-of-life Testing

Before performing the modified TCLP on the regionally weathered samples, the preliminary analysis and TCLP of an unweathered sample was performed per the USEPA Test Methods for Evaluating Solid Waste: Physical/Chemical Methods (SW-846 method 1311). This included phase(s) determination of sample (assumed 100% solid), prescribed particle reduction requirements of passing a 9.5 mm sieve or surface area to mass ratio greater than 3.1 cm2/g, and extraction fluid determination (EF #1). The results from the preliminary analysis were used in identifying appropriate extraction fluid and most realistic testing conditions for the weathered samples.

No sample preparation was applied for all weathered pressure treated lumber samples for size reduction, this was to more accurately represent the condition of the samples in real world environments. All samples had relative dimensions of 2” x 1.5” x 2.25” with masses ranging from ~40 – 80 grams. Extraction fluid #1 was prepared by using the method listed in SW-846 method 1311 section 5.7.1 with reagent grade Glacial Acetic Acid (99%) and a 1N solution of Sodium Hydroxide. Each sample was weighed before being placed into separate 2L HDPE extraction vessels. Once weighed the mass of EF needed per sample was determined using the following formula from SW-846 method 1311 section 7.2.11, where: EF Weight=(20*percent solid*sample mass)/100 , and added

to the extraction vessel. Each sample was then closed/labeled and sealed with tamper tape, secured in rotary agitator, and agitated for a duration of 18 + 2 hrs.

Upon completion of agitation all samples were filtered with acid washed borosilicate fiber filter with a pore size of 0.7 μm (Ahlstrom grade 151-25), using a Kontes Ultraware 300 mL microfiltration assembly. Immediate preservation using ultrapure nitric acid was performed on each sample, acid was added to sample until the measured pH was below 2.0. All samples were stored in refrigerated units until ICP-OES analysis was to be performed.

## Reference


1. Montaño, M. D.; Badiei, H. R.; Bazargan, S.; Ranville, J. F., Improvements in the detection and characterization of engineered nanoparticles using spICP-MS with microsecond dwell times. *Environ. Sci.: Nano* **2014,** *1* (4), 338-346.
2. Pace, H. E.; Rogers, N. J.; Jarolimek, C.; Coleman, V. A.; Higgins, C. P.; Ranville, J. F., Correction to Determining Transport Efficiency for the Purpose of Counting and Sizing Nanoparticles via Single Particle Inductively Coupled Plasma Mass Spectrometry. *Analytical Chemistry* **2012,** *84* (10), 4633-4633.
3. Pace, H. E.; Rogers, N. J.; Jarolimek, C.; Coleman, V. A.; Higgins, C. P.; Ranville, J. F., Determining transport efficiency for the purpose of counting and sizing nanoparticles via single particle inductively coupled plasma mass spectrometry. *Anal Chem* **2011,** *83* (24), 9361-9.

**Chapter 6.** Curriculum Vitae

**Education**

*The Johns Hopkins University*
**Baltimore, MD**
Ph.D., Chemistry — Anticipated Completion 2018
M.A., Chemistry — 2014

*Tulane University*
**New Orleans, LA**
B.S., Chemistry — 2012
Mathematics & Jewish Studies (Minor)

**Research Experience**
Graduate Research Student, Dept. of Chemistry, Johns Hopkins University
2012 – Present
Undergraduate Research Student, Dept. of Chemistry, Tulane University
2011 – 2012

**Teaching Experience**
Head Teaching Assistant, General Chemistry, Johns Hopkins University
2013 – 2014
Teaching Assistant, General Chemistry, Johns Hopkins University
2012 – 2013

**Research Interests & Skills**
Production and characterization of nanoparticle – polymer nanocomposites (PNCs) for both accelerated and natural weathering studies, functionalization and purification of carbon nanotubes, chemical derivatization of carbonaceous materials, characterization of nanomaterial release from nano-enabled materials via single particle ICP-MS, functionalization of nanocellulose. Materials characterization via: X-ray photoelectron spectroscopy, Scanning electron microscopy, Energy dispersive X-ray spectroscopy, Attenuated total internal reflectance FT infrared spectroscopy, Transmission infrared spectroscopy, Ultraviolet – visible spectroscopy, Transmission electron microscopy, Dynamic light scattering, Thermogravimetric analysis

**Presentations and Conferences**

- American Chemical Society National Meeting & Exposition (Oral Presentation)
  - 2014 & 2018
- Environmental Nanotechnology, Gordon Research Conferences (Poster)
  - 2015 & 2017
- Environmental Nanotechnology, Gordon Research Seminar (Oral Presentation)
  - 2017
- Tech Connect World Innovation Conference & Expo (Oral Presentation)
  - 2017
- International Conference on the Environmental Effects of Nanoparticles and Nanomaterials (Oral Presentation, 2nd Place)
  - 2016
- 88th ACS 2014 Colloid & Surface Science Symposium (Oral Presentation)
  - 2014

**Publications**

1. Lankone, R. S.; Challis, K. E.; Bi, Y.; Hanigan, D.; Reed, R. B.; Zaikova, T.; Hutchison, J. E.; Westerhoff, P.; Ranville, J.; Fairbrother, H.; Gilbertson, L. M., Methodology for quantifying engineered nanomaterial release from diverse product matrices under outdoor weathering conditions and implications for life cycle assessment. *Environmental Science: Nano* **2017**, *4* (9), 1784-1797.

2. Lankone, R. S.; Wang, J.; Ranville, J. F.; Fairbrother, D. H., Photodegradation of polymer-CNT nanocomposites: effect of CNT loading and CNT release characteristics. *Environmental Science: Nano* **2017,** *4* (4), 967-982.

3. Nosaka, T.; Lankone, R. S.; Bi, Y.; Fairbrother, D. H.; Westerhoff, P.; Herckes, P., Quantification of carbon nanotubes in polymer composites. *Analytical Methods* **2018**, *10* (9), 1032-1037.

4. Wang, J.; Lankone, R. S.; Reed, R. B.; Fairbrother, D. H.; Ranville, J. F., Analysis of single-walled carbon nanotubes using spICP-MS with microsecond dwell time. *NanoImpact* **2016,** *1*, 65-72.

5. McGeachy, A. C.; Olenick, L. L.; Troiano, J. M.; Lankone, R. S.; Melby, E. S.; Kuech, T. R.; Ehimiaghe, E.; Fairbrother, D. H.; Pedersen, J. A.; Geiger, F. M., Resonantly Enhanced Nonlinear Optical Probes of Oxidized Multiwalled Carbon Nanotubes at Supported Lipid Bilayers. *The Journal of Physical Chemistry B* **2017,** *121* (6), 1321-1329.

6. Reed, R. B.; Zaikova, T.; Barber, A.; Simonich, M.; Lankone, R.S.; Marco, M.; Hristovski, K.; Herckes, P.; Passantino, L.; Fairbrother, D. H.; Tanguay, R.; Ranville, J. F.; Hutchison, J. E.; Westerhoff, P. K., Potential Environmental Impacts and Antimicrobial Efficacy of Silver- and Nanosilver-Containing Textiles. *Environmental Science & Technology* **2016,** *50* (7), 4018-4026.

7. Barber, A.; Kly, S.; Lankone, R. S.; Gao, C.; Fairbrother, D. H.; Moffitt, M.; Ranville, J., Single Particle ICP-MS Combined with Field-flow Fractionation for Characterizing Nanoparticles in Composite Particles. *Submitted to Analytical Chemistry*

8. Lankone, R.S.; Challis, K.; Bi, Y.; Wang, Y.; Garland, M.; Pourzahedi, L.;Tanguay, R.; Gilbertson, L.; Westerhoff, P.; Fairbrother, H.; Ranville, J. F., Characterizing copper release and transformation following natural weathering of nanoenabled products. *In Preparation for submission to Science of the Total Environment*